Quantum Memories at Finite Temperature

Benjamin J. Brown,[1, *] Daniel Loss,[2] Jiannis K. Pachos,[3] Chris N. Self,[1, 3] and James R. Wootton[2]

[1]*Quantum Optics and Laser Science, Blackett Laboratory, Imperial College London, Prince Consort Road, London, SW7 2AZ, United Kingdom*
[2]*Department of Physics, University of Basel, Klingelbergstrasse 82, CH-4056 Basel, Switzerland*
[3]*School of Physics and Astronomy, University of Leeds, Leeds LS2 9JT, United Kingdom*

To use quantum systems for technological applications we first need to preserve their coherence for macroscopic timescales, even at finite temperature. Quantum error correction has made it possible to actively correct errors that affect a quantum memory. An attractive scenario is the construction of passive storage of quantum information with minimal active support. Indeed, passive protection is the basis of robust and scalable classical technology, physically realized in the form of the transistor and the ferromagnetic hard disk. The discovery of an analogous quantum system is a challenging open problem, plagued with a variety of no-go theorems. Several approaches have been devised to overcome these theorems by taking advantage of their loopholes. Here we review the state-of-the-art developments in this field in an informative and pedagogical way. We give the main principles of self-correcting quantum memories and we analyze several milestone examples from the literature of two-, three- and higher-dimensional quantum memories.

Contents

*Electronic address: benjamin.brown09@imperial.ac.uk

I. INTRODUCTION

Quantum mechanics holds the potential for performing computational simulations (Feynman, 1982) and information processing tasks (Deutsch, 1985; Shor, 1994) much faster than classical technologies. To outperform modern classical machines, a quantum computer must manipulate hundreds of qubits to follow a program of millions of quantum logical operations (Hastings *et al.*, 2014b; Poulin *et al.*, 2014; Wecker *et al.*, 2014). To realize such a feat using a real physical system, we must preserve a vast entangled quantum state over a long duration, while computations are executed. Recognizing that any device exists at non-zero temperature, we see that probabilistic errors will continually disrupt experimental efforts to coherently control quantum states. It

is widely understood that the problem of decoherence is among the largest obstacles impeding the realization of quantum technologies.

The breakthrough that validated the practical possibility of quantum computation was the discovery of quantum error correction (Lidar and Brun, 2013; Shor, 1996; Steane, 1996). The principle behind this is to use a redundancy of physical quantum systems to encode a small number of logical computational qubits. We are then able to realize error-correcting protocols by measuring auxiliary physical systems of the code to identify and correct errors affecting the encoded information. Provided the incident noise is suitably low, we can achieve arbitrarily robust quantum states for an arbitrarily long time by using a suitably large redundancy of ancillary systems (Preskill, 1998). Unfortunately, quantum error-correcting protocols present an uphill technical challenge for both engineering complex entangled error-correcting codes, and for reducing incident laboratory noise below a threshold value when compared with current experimental achievements (Barends *et al.*, 2014; Nigg *et al.*, 2014; Reed *et al.*, 2012). A novel alternative to active error correction would be the discovery of physical systems that are able to reverse the effects of errors themselves.

A particularly elegant approach to realizing fault-tolerant quantum technologies would be the discovery of a *self-correcting quantum memory* (Bacon, 2006; Kitaev, 2003). A self-correcting memory stores information in a degenerate subspace of a Hamiltonian system, while the interactions of the Hamiltonian are passively defending the information from induced errors. This is indeed the principle behind current classical information storage media, where bits of information are encoded in the magnetic orientation of ferromagnetic materials. Classical information stored in this manner is robust due to the collective behavior of some Avogadro's number of magnetically oriented atoms that make up the media.

It is an exciting and fundamental question of nature, and indeed the topic of this Review, as to whether we can find macroscopic quantum systems to maintain coherent quantum information while simultaneously equilibrating with its surrounding environment. The discovery of such a system will provide a beautiful solution for one of the largest puzzle pieces required to achieve scalable quantum computation. In addition to the remarkable practical applications, the realization of a self-correcting universal quantum computer is also of significant fundamental interest. A macroscopic system that is capable of simulating arbitrarily complex quantum phenomena would provide a powerful demonstration that quantum mechanics is not restricted to the microscopically accessible parts of the Universe (Farrow and Vedral, 2014).

We are currently able to encode qubits for significant timescales (Schoelkopf and Girvin, 2008) using ground states of ions (Harty *et al.*, 2014), solid state devices (Fuchs *et al.*, 2011; Saeedi *et al.*, 2013), or using superconducting systems (Devoret and Scoelkopf, 2013). Their long coherence times are achieved due to the large energy gap that separates excited states from their ground space. Nevertheless, the finite nature of this timescale places a limit on the computations that can be performed without some error-correction protocol. Ideally, we would like to construct a quantum memory that can store quantum states for times that can be tuned arbitrarily using a variable parameter, such as the macroscopic size of the memory. This would allow the execution of arbitrarily long quantum algorithms given sufficient quantum resources. Furthermore, interacting atoms together to create entanglement necessitates the presence of a coupling bus, for example, vibrational modes for the case of ions or an optical cavity in the case of neutral atoms. These additional structures are subject to thermal errors and are therefore prone to decoherence. The ability to perform the computation within the protected space of states without having to employ additional noisy coupling systems are therefore also necessary to realize quantum computation.

Topologically ordered many-body systems (Wen, 2004) play an important role in the study of passive quantum error correction. Their ground space cannot be accessed by local operations. In this feature lies the appeal of topological models as candidate systems for quantum memories; if quantum information is locally inaccessible, then the effect of local decoherence must also be negligible with respect to globally encoded information.

In addition to their locally inaccessible degrees of freedom, topological quantum systems are of further interest due to their amenable features for realizing fault-tolerant quantum computation. This has been the subject of intense study (Nayak *et al.*, 2008; Pachos, 2012) for two-dimensional anyonic systems where computational operations are performed by braiding anyonic quasiparticles. Braid operations, the fundamental operations involved in topological quantum computation, are naturally insensitive to faults. This is because computational operations achieved by braiding depend only on the topology of the anyonic trajectories, and are thus insensitive to minor changes in the paths of traveling anyons that may occur as a result of local noise. Models that achieve universal fault-tolerant quantum computation by anyon braiding are well known (Brennen and Pachos, 2007; Freedman *et al.*, 2002; Kitaev, 2003).

The study of topological quantum computation has extended far beyond the study of anyon braiding. Fault-tolerant computational operations are also realized by the manipulation of holes (Bombin and Martin-Delgado, 2009; Raussendorf *et al.*, 2006; Wootton, 2012), twist defects (Barkeshli *et al.*, 2014, 2013; Bombin, 2010a) or by other means (Wootton and Pachos, 2011b). It is also noteworthy that research in the direction of computation using experimentally amenable anyon models (Bravyi, 2006; Zilberberg *et al.*, 2008) that do not support a universal set of topological computational operations have also led to schemes to supplement such systems with non-topological operations to complete their computational gate set (Bravyi and Kitaev, 2005; Wootton *et al.*, 2009).

Consideration of topologically ordered systems as a basis for quantum memories therefore allows us to draw from this wealth of established knowledge to realize a fault-tolerant computational model.

In spite of many known interesting and attractive models, we are yet to rigorously prove the existence of a low-dimensional passively protected quantum memory. It is the purpose of this Review to highlight the challenges involved in finding systems that maintain their quantum character at finite temperatures, and to discuss new models that come towards a solution to this problem. The present Review is separated into two distinct parts. In the first part we introduce the field, and paint a picture that demonstrates the difficulty in discovering a stable memory. We show this by means of explicit introductory examples, as well as discussions of rigorously proved no-go theorems for the finite temperature stability of large classes of systems. In the second part we discuss new models that come some way towards the quantum stability over macroscopic timescales. We offer insights into how such models are discovered and we assess their favorable features, and their drawbacks. In doing so we identify underlying open problems and discover established tools that can be used to approach this actively studied and exciting field.

The present Review takes the following structure. In Secs. II and III we introduce a common notation, concepts in quantum error correction and the analytical and numerical methods for examining finite temperature. We conclude Sec. III with a rigorous set of conditions that we demand of a quantum memory, together with a list of attractive features that would make a model suitable for quantum computation and plausible for experimental realization. In Sec. IV, we review the plethora of no-go theorems established so far with respect to passive error correction. We use this study to chart the landscape of the proposed models. The latter Sections, Secs. V, VI, VII, VIII and IX offer a comprehensive review of current actively studied models that demonstrate favorable properties for self correction. In Sec. X we conclude with an overview of the current state of the field where we discuss open problems that remain to be pursued.

II. HAMILTONIANS AND QUANTUM ERROR CORRECTION

The study of quantum memories at finite temperature lies at the intersection of the fields of quantum error correction, condensed-matter physics and statistical mechanics. We therefore require a unifying language that captures the breadth of physics covered by all of these fields. We find such a language in the *stabilizer formalism*. This formalism, initially introduced as an efficient description of quantum error correcting codes (Gottesman, 2001), provides a natural way of understanding the fault-tolerant nature of the Hamiltonian models considered here.
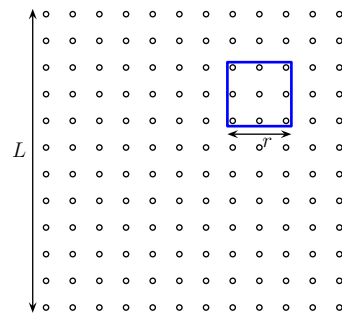

FIG. 1 A regular two-dimensional lattice of qubits with linear size L. All Hamiltonian interactions are contained within a box of linear size r, shown in blue.

The stabilizer formalism efficiently describes quantum error correcting codes using a list of commuting Pauli operators, known as *stabilizers*. We can use this operator description from quantum error correction to write down a large class degenerate Hamiltonians. The Hamiltonians we obtain this way have ground state subspaces that correspond to the code space of some quantum code, and its excited states reflect the errors the code suffers. We remark that while this formalism describes only a small subset of quantum systems, stabilizers provide an analytically tractable class of Hamiltonian models where most of the developments in this field have been based.

In Subsec. II.A we begin by introducing the class of models that we will mainly be concerned with here, namely *commuting Pauli Hamiltonians*. In Subsec. II.B we give a comprehensive overview of the stabilizer formalism that enables us to identify error correcting procedures for the considered Hamiltonians. We review how one might perform error correction on either a quantum code or a commuting Pauli Hamiltonian in Subsec. II.C. We then study an explicit and extensively studied example of a commuting Pauli Hamiltonian in Subsec II.D, namely, *Kitaev's toric code model*. In addition to providing a straight-forward example of a commuting-Pauli Hamiltonian, the toric code model also exhibits topological order and gives rise to anyonic quasi-particle excitations. We discuss at length the topological nature of the toric code in Subsec. II.E. We conclude this Section by discussing zero-temperature gap stability in Subsec. II.F, a feature naturally presented by topologically ordered systems, and an important feature to consider while searching for stable quantum memories.

A. Commuting Pauli Hamiltonians

We first define the Pauli group $\mathcal{P}_n = \mathcal{P}_1^{\otimes n}$ acting on n distinct two-level quantum systems that we refer to as qubits. The Pauli group, $\mathcal{P}_1$, includes, up to phases, the Pauli matrices

$$X = \begin{pmatrix} 0 & 1 \\ 1 & 0 \end{pmatrix}, \ Y = \begin{pmatrix} 0 & -i \\ i & 0 \end{pmatrix}, \ Z = \begin{pmatrix} 1 & 0 \\ 0 & -1 \end{pmatrix}, \quad (1)$$

and identity, $\mathbb{1}$. We will often use indices with elements of $\mathcal{P}_1$ to describe the single qubit support of elements of $\mathcal{P}_n$. For instance, if we wish to act operator $U \in \mathcal{P}_1$ on the jth physical qubit for $1 \leq j \leq n$, we write $U_j \in \mathcal{P}_n$. Written explicitly, we have

$$U_j \equiv \underbrace{\mathbb{1} \otimes \mathbb{1} \otimes \cdots \otimes \mathbb{1}}_{j-1} \otimes U \otimes \underbrace{\mathbb{1} \otimes \mathbb{1} \otimes \cdots \otimes \mathbb{1}}_{n-j}. \quad (2)$$

Having introduced the Pauli group acting on n qubits, we are able to write down Pauli Hamiltonians that describe interactions between the qubits of a regular lattice. Consider a D-dimensional lattices of qubits of linear size L, as shown in Fig. 1. The $n \sim L^D$ qubits of the lattice are arranged in a structure that depends on the model we introduce. We write down Hamiltonians of the type

$$H = -\frac{\Delta}{2} \sum_j S_j, \quad (3)$$

where we sum over a set $\mathcal{I}$ of Hermitian interaction terms $S_j \in \mathcal{I}$ such that $\mathcal{I}$ is a commuting subset of $\mathcal{P}_n$.

We must impose physical constraints on Hamiltonian (3). We demand that the Hamiltonian terms are local. We therefore constrain all elements of $\mathcal{I}$ to have non-trivial support only on the lattice qubits that can be contained within a box of linear size no greater than r, where r is independent of the lattice size. We show a box of linear size $r = 3$ in Fig. 1. Additionally we must bound the interaction strength of the Hamiltonian. We impose that Δ is a constant independent of system size.

In general, Hamiltonians that are the sum of local elements of $\mathcal{P}_n$ are intractable for study. We are able to impose additional restrictions that enable us to find solvable classes of Hamiltonians. We first demand that elements $S_j \in \mathcal{I}$ commute, such that

$$[S_j, S_l] = 0, \quad \forall j, l. \quad (4)$$

In addition to this, we consider only frustration-free Hamiltonians. Specifically, for all Hamiltonian ground states $|\psi\rangle$, elements $S_j \in \mathcal{I}$ satisfy

$$S_j |\psi\rangle = (+1) |\psi\rangle, \quad (5)$$

for all j and ground states. Conditions (4) and (5) enable us to employ the stabilizer formalism that is described in the following Subsection. For convenience, we take the ground states to be described by an orthonormal basis $|\psi_\mu\rangle$,

$$|\psi\rangle = \sum_\mu c_\mu |\psi_\mu\rangle \quad (6)$$

where integers μ parametrize the ground states, with $\sum_\mu |c_\mu|^2 = 1$.

We finally remark on the excited eigenstates of Hamiltonian (3). The Hamiltonian terms $S_j \in \mathcal{I}$ are elements of $\mathcal{P}_n$, and therefore all satisfy the property that $S_j^2 = \mathbb{1}$.

It follows from this that the eigenvalues, M_j, of operators S_j take only values ± 1. We are therefore able to specify excited states of Hamiltonian (3) using the list of eigenvalues M_j. The Hilbert space can then be described completely by the ground eigenspace of H, together with the list of eigenvalues $\{M_j\}$. Ii is often convenient to simply write eigenstates $E |\psi\rangle$ for $E \in \mathcal{P}_n$ and omit any M_j notation. The values M_j are determined by commutation relations $S_j E = M_j E S_j$. The energy eigenvalue ε_E for eigenstate $E |\psi\rangle$ follows immediately from the values M_j such that

$$\varepsilon_E = -\frac{\Delta}{2} \sum_j M_j. \quad (7)$$

B. The Stabilizer Formalism

Many quantum error-correcting codes can be described using the stabilizer formalism (Gottesman, 2001). This formalism shares many parallels with the commuting Pauli Hamiltonians introduced in the previous Subsection. Quantum error-correcting codes describe a subspace of states called the *code space*. We denote an orthonormal basis of states in the code space with vectors $|\psi_\mu\rangle$ for $1 \leq \mu \leq 2^k$. The code space of a stabilizer code are specified by the *stabilizer group*. The stabilizer group $\mathcal{S}$ is an Abelian subgroup of $\mathcal{P}_n$, where we have defined $\mathcal{P}_n$, the Pauli group for n qubits, in the previous Subsection. All of the elements of the stabilizer group $S_j \in \mathcal{S}$ are additionally taken to satisfy

$$S_j |\psi_\mu\rangle = (+1) |\psi_\mu\rangle, \quad \forall \mu, \quad (8)$$

thus specifying the basis states $|\psi_\mu\rangle$.

The stabilizer group can be described using a generating set of $m \leq n$ stabilizers, listed in angle braces

$$\mathcal{S} = \langle S_1, S_2, \ldots, S_m \rangle, \quad (9)$$

where all S_j of the generating set are *independent* elements of the stabilizer group, i.e. the stabilizer generators satisfy the condition that $\prod_j S_j^{n_j} = \mathbb{1}$ with $n_j \in \{0, 1\}$ only for $n_j = 0$ for all j. A code of n qubits that is generated by m independent stabilizer generators will encode $k = n - m$ logical qubits.

Encoded logical qubits are manipulated by the algebra generated by the set of logical operators, $\mathcal{L}$, denoted $\overline{X}_j, \overline{Z}_j \in \mathcal{P}_n$ for $j = 1, 2, \ldots, k$. The logical operators commute with all elements of the stabilizer group, and logical operators $\overline{X}_j$ and $\overline{Z}_j$ will commute with operators $\overline{X}_l \overline{Z}_l$ for $l \neq j$. Operators $\overline{X}_j$ and $\overline{Z}_j$ however anticommute. The logical operators therefore generate the Pauli group over the k encoded logical qubits.

We remark that logical operators are not unique with respect to their action upon the code space, but are only unique *up to multiplication by stabilizer operators*. This is seen using the commutation relation $[S_j, O] = 0$ for all

$S_j \in \mathcal{S}$ with $O \in \mathcal{L}$. It follows from this that

$$S_j O \ket{\psi_\mu} = O S_j \ket{\psi_\mu} = O \ket{\psi_\mu}, \quad \forall \mu. \qquad (10)$$

We finally introduce the definition for the weight of an operator, and the distance of a quantum error-correcting code. These are useful terms when comparing different error correcting codes. The *weight* of operator O, denoted wt(O), is the number of qubits that O has non-trivial i.e., non-identity, support over. For instance, the operator $P = X_2 X_3$ has wt$(P) = 2$, as it acts non trivially on qubits 2 and 3. The definition of weight is used to define the *distance* of a quantum error-correcting code, denoted d. The distance of a code is the weight of the lowest minimum-weight logical operator O over all logical operators $O \in \mathcal{L}$. We write this as an equation

$$d = \min_{S_j \in \mathcal{S}} \min_{O \in \mathcal{L}} \text{wt}(S_j O). \qquad (11)$$

We seek quantum error-correcting codes with high distance as we expect these codes to be robust with respect to local noise models. A well-designed error-correcting code is able to tolerate $d/2 - 1$ errors on distinct physical qubits. For the case of $d/2 - 1$ or fewer physics errors, we should be able to infallibly recover the encoded quantum information. In general a quantum error correcting code can tolerate more than $d/2$ physical errors provided the errors incident to the system do not find an adversarial configuration.

Having introduced the stabilizer formalism, we are now able to explicitly see the correspondence between stabilizer quantum error-correcting codes and frustration free commuting Pauli Hamiltonians. The ground states of Hamiltonian (3) are the common $+1$ eigenspace of the set of commuting local interaction terms, $\mathcal{I}$. We are therefore able to identify the ground space of Hamiltonian (3) with the code space of a stabilizer group $\mathcal{S}$, whose generators are included in $\mathcal{I}$. In general, $\mathcal{I}$ can be an over-complete generating set of $m \geq n - k$ elements. In Subsec. II.A, we specified only that elements of $\mathcal{I}$ are local with respect to the geometry of its underlying lattice.

C. Quantum Error-Correcting Protocol

The stabilizers of a quantum error-correcting code are designed to detect errors suffered by encoded quantum states. Provided incident noise occurs at a suitably low rate, we can identify an error with a probability that increases with the distance of the code. This is due to the celebrated *accuracy threshold theorem* (Aharonov and Ben-Or, 1997; Aliferis and Cross, 2007; Aliferis *et al.*, 2006; Kitaev, 1997; Knill *et al.*, 1998; Preskill, 1998; Shor, 1996). Once we have identified an error, we can subsequently find a unitary operator that reverses the error and thus corrects for the incident noise. Here we briefly elaborate on the procedure of performing quantum error correction.

In general, the encoded states $\ket{\psi}$ can decohere due to arbitrary quantum noise. Given the vast space of realistic noise channels a physical quantum system can suffer, we might suspect that one cannot possibly expect to reverse incident noise. However, if we assume ideal measurements, the act of measuring stabilizer operators projects the decohered encoded state onto the state $E \ket{\psi}$ with some error $E \in \mathcal{P}_n$. This is due to the fact that only states of the type $E \ket{\psi}$ are eigenstates of elements of the stabilizer group. Having measured the stabilizer operators, attempting to determine and correct for the discrete set of Pauli errors E becomes a much more palatable challenge.

Further to this, performing stabilizer measurements furnishes us with information we can use to determine E. The set of stabilizer measurement outcomes, $M_j = \pm 1$, are referred to as the *error syndrome*. The values M_j are determined by the commutation relation

$$S_j E = M_j E S_j. \qquad (12)$$

The syndrome information is not enough to uniquely specify error E. Instead, we are able to take the available syndrome information and predict the most-likely value of E with respect to the noise channel. For realistic noise models we typically look for the most-likely error based on the assumption that E is a low-weight operator. Assuming that we can find the most probable error that is consistent with the given syndrome, we can obtain a correction operator, $C \in \mathcal{P}_n$, that maps the state $E \ket{\psi}$ back to the code space. In the case that $CE \in \mathcal{S}$, i.e. $CE \ket{\psi} = \ket{\psi}$, we successfully recover the encoded state. Otherwise, the correction operator we obtain will return the encoded state to the code space having suffered a logical error, such that $CE \in \mathcal{L}$.

We attempt to determine E using a *decoding algorithm*. A decoding algorithm uses the error syndrome to estimate the most-likely incident error to the code state that is consistent with the given syndrome. We remark that, in general, it is not always an efficient task to find the most probable error. In App. A we describe in detail a specific implementation of an efficient decoder, namely, the clustering decoder, which is commonly used throughout this Review. The clustering algorithm is very versatile for decoding the quantum error-correcting codes defined by commuting Pauli Hamiltonians.

The correspondence between the syndrome of a quantum error-correcting code and the excited states of commuting Pauli Hamiltonians means that all the error-correction procedures explained here are trivially adapted to correct errors suffered by a commuting Pauli Hamiltonian model.

D. The Toric Code

We illustrate the concepts introduced above using *Kitaev's toric code model* (Kitaev, 2003). A comprehensive study of the toric code model from the point of quantum
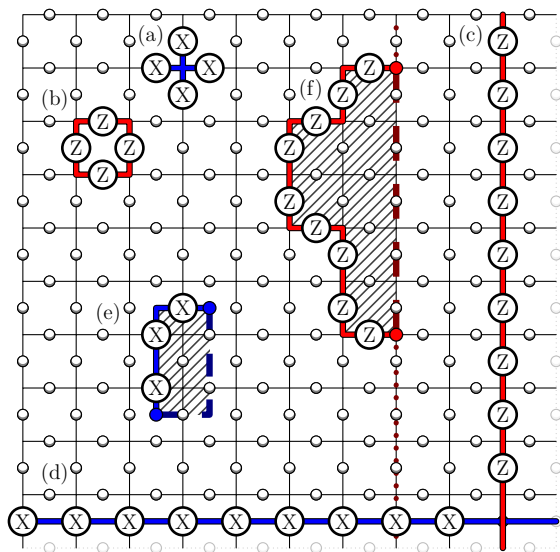
FIG. 2 The toric code lattice. Qubits, shown by white points, are arranged on the edges of a square lattice. The left and dotted right boundary are unified and similarly the top and dotted bottom edges are unified. (a) and (b) show a star and plaquette operator in blue and red, respectively. (c) and (d) show logical operators $\overline{Z}_1$ and $\overline{X}_1$, respectively. The Pauli operator in the bottom right corner of each operator is omitted to show the crossing point. (e) A small error that is easily corrected. The error syndromes are marked by points at the end of the error string. (f) An string-error with syndromes separated by over half the code distance. We cannot reliably correct this error as there are two available correction operators with equal weight, one of which will lead to a logical error on the code space.

error correction can be found in Ref. (Dennis *et al.*, 2002). Qubits are arranged on the edges of a two-dimensional square lattice of linear size L with periodic boundary conditions, i.e. a torus, as shown in Fig. 2. The stabilizer group is generated by star, A_v, and plaquette, B_p, operators for each vertex, v, and face, p, of the lattice. The star and plaquette operators are defined such that

$$A_v = \prod_{\partial j \ni v} X_j, \quad B_p = \prod_{j \in \partial p} Z_j. \tag{13}$$

Written colloquially, a star operator A_v is the tensor product of Pauli-X operators supported on the edges j that include vertex v in its boundary, ∂j, and the plaquette operator is the tensor product of Pauli-Z operators acting on the edges that bound a face p, where the boundary of face p is denoted ∂p. We show examples of such operators in Fig. 2(a) and (b). Star and plaquette operators share either zero or two common qubits and therefore commute. The set of all the star and plaquette operators generate the stabilizer group.

When defined on a torus, the toric code model encodes two logical qubits. The logical operators of the model correspond to extensive strings of Pauli-X and Pauli-Z operators that wrap around non-trivial cycles of the torus.

We show two such operators in Fig. 2(c) and (d), respectively. One can see from the digram that these logical operators have distance $d = L$, the linear size of the system. It is easily checked that these operators commute with all the stabilizers of the code, but mutually anti commute, as they overlap at a single edge of the lattice, where, in the diagram, the Pauli operators are omitted.

Error correction for the toric code is particularly intuitive as its syndromes follow a simple geometrical structure. Errors can be regarded as 'strings' on the lattice. We show two such errors composed of Pauli-X and Pauli-Z operators in Fig. 2(e) and (f) respectively. We cannot detect the positions of the string-like errors. Instead, the syndrome measurements identify the end points of the string-like errors. The decoding procedure then consists of using the known end points of the strings and trying to determine the least-weight operator E that may have caused all the syndromes. The decoder subsequently returns a string-like correction operator C, that corresponds to a string that reconnects all the syndromes. If the errors are very few and error strings are very short with respect to the size of the lattice, it is straight forward to identify the shortest error path. This path connects pairs of syndromes that will likely correspond to a stabilizer operation with high probability, i.e. $CE \in \mathcal{S}$. In Fig. 2(e) we show a dotted line that supports a suitable correction operator.

In general, the product of an error and its corresponding correction operator will form closed loops on the toric code lattice. The action of these operators will trivially affect the code space *only if* the loop they form bounds a region or a set of disjoint regions on the lattice. We shade the region bounded by CE in Fig. 2(e).

In the case that either the error strings are very long, such as those shown in Fig. 2(f), or there are many error strings scattered over the lattice it becomes too hard to unambiguously determine a set of strings that trivially connect all the point syndromes. For the example given in Fig. 2(f), there are two possible low-weight correction operators of weight $d/2$, labelled C' and C'', whose trajectories are marked by red dashed and dotted lines, respectively. Operator C' is such that $C'E \in \mathcal{S}$. In the diagram we shade the region enclosed by $C'E$. The action of $C''E \in \mathcal{L}$ on the other hand does not enclose a region of the lattice. Instead, as we see, the correction has non-trivial support with the logical operator shown in blue at Fig. 2(d). Such a correction will therefore cause a logical error on the code space. It is with this example that we see we cannot correct errors once their weight becomes too large.

Error correction on the toric code and the structure of its stabilizers can be understood at the fundamental level of homology. This topic goes beyond the scope of the present Review, but the interested reader is advised to (Nakahara, 2003) or Appendix A of Ref. (Anwar *et al.*, 2014) to find a discussion of homology in the context of quantum error correction.

We briefly summarize a quantum error correcting pro-

(a) Initiation of system in specific logical state by performing a certain logical operation.

(b) Thermal error induced by the environment.

(c) Syndrome measurement by measuring stabilizers.

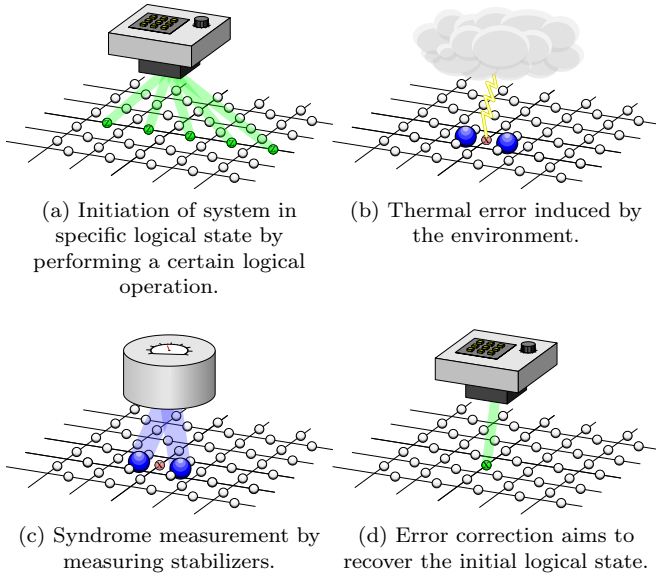(d) Error correction aims to recover the initial logical state.

FIG. 3 The error correcting protocol for the toric code model. (a) the initialization of the system, (b) the error due to the coupling with the environment, (c) and (d) the decoding algorithm that aims to recover the initially encoded state.

tocol. The system is initialized in a code state by applying appropriate operations, Fig. 3(a). While the quantum information is stored, errors will occur on the system, as shown in Fig. 3(b). To identify these errors, stabilizer measurements are performed to obtain syndrome information. Non-trivial syndromes are identified in Fig. 3(c). A decoder subsequently uses the syndrome information to attempt to find a correction operator. A suitable correction operator that successfully corrects the incident error is applied in Fig. 3(d), thus enabling the reliable readout of encoded quantum information.

E. Topological Order and Anyons in the Toric Code

The Hamiltonian realization of toric code model (Kitaev, 2003) supports a $\mathbb{Z}_2$ lattice gauge theory (Kitaev, 2003; Kogut, 1979; Nussinov and Ortiz, 2009a,b; Wegner, 1971; Wen, 2003). Here, we consider the model as a prototypical example of a *topologically ordered lattice model* with *anyonic quasiparticle excitations* (Leinaas and Myrheim, 1977; Wilczek, 1982). Its Hamiltonian

$$H_{\text{toric}} = -\frac{1}{2} \sum_v A_v - \frac{1}{2} \sum_p B_p, \qquad (14)$$

has degenerate ground states $|\psi_\mu\rangle$ as defined previously. We take interaction strength $1/2$ such that quasiparticles have unit mass. Its anyonic excitations are a special class of particles that exist in two-dimensional systems. Anyons are of particular interest due to their exchange statistics that are neither fermionic nor bosonic. Interestingly, the concept of quantum error correction and of

anyons is intrinsically connected, as it will become apparent from the toric code example. For a comprehensive explanation of the general theory of anyons we advise the reader to see Appendix E of Ref. (Kitaev, 2006), or alternatively (Brennen and Pachos, 2007; Nayak *et al.*, 2008; Pachos, 2012; Preskill, 2004) for an introductory overview. In this Subsection we review the anyonic picture of the excitations of the toric code as it provides an efficient description of the dynamics of certain models presented in this Review.

The toric code has four types of quasiparticle excitations. The first, known as the *vacuum particle*, is denoted 1. The vacuum particle describes no anyons. All models, topologically ordered or otherwise, support the vacuum particle. Excited eigenstates of Hamiltonian (14), $|\phi\rangle = E |\psi\rangle$, have electric charges, labelled e, on vertices v that satisfy $A_v |\phi\rangle = -|\phi\rangle$. Similarly, the toric code supports magnetic charges, m, on faces p whenever $B_p |\phi\rangle = -|\phi\rangle$. The fourth particle of the toric code is known as the *dion*, labelled ϵ, that is the combination of an e and an m particle.

Anyonic systems have *fusion rules* to describe the combination of pairs of particles. We write the fusion product of particles a and b as $a \times b$. The fusion product is commutative and associative. For the toric code we have

$$e \times m = \epsilon, \qquad (15)$$
$$a \times a = 1, \qquad (16)$$
$$a \times 1 = a, \qquad (17)$$

for all $a = 1, e, m, \epsilon$. In full generality, we can define *non-Abelian* anyon models, where anyons can have multiple fusion outcomes. These are beyond the scope of this Review, but are discussed in the context of quantum error correction in (Brell *et al.*, 2014; Wootton *et al.*, 2014).

Interestingly, quasiparticle excitations of the toric code are created in pairs. At the microscopic level of the lattice this is witnessed as anyons are created at the two endpoints of string-like operators. This feature is reflected by the fusion rule (16), which shows that we require two anyons to recover the vacuum state. Conversely we can only create anyons in pairs of particle-antiparticles from the vacuum state.

By using the anyonic description of error operators we find an alternative understanding of the logical operators of the toric code. As described in the previous Subsection, the logical operators are string-like operators that wrap around non-trivial cycles of the torus. In the anyonic picture string-like operators correspond to the trajectories of anyons. A logical operator corresponds to the creation of a pair of anyonic particles. One such particle then follows some non-trivial trajectory around the torus and subsequently annihilates with the other pair-created anyon that remained at its initial point. With this point we can define a natural basis for the ground space of the toric code, where orthogonal ground states correspond to different particle fluxes that pass around some arbitrarily selected non-trivial cycle of the torus. We show such a

cycle in Fig. 4(a), where the flux of anyon a wraps around the torus along the red line. In the case that many anyonic excitations move around the torus, the ground state is well defined according to the fusion rules of the different particle types. If we change the number of handles, or *genus*, g, of the surface where Hamiltonian (14) is embedded, then we change its degeneracy to 2^{2g} and we are able to encode $2g$ qubits there. This is attributed to the extra non-trivial cycles that can be traversed by anyons on the topologically deformed surface.

As an aside remark, the non-trivial braiding statistics between anyons can be obtained from the commutation relations of logical operators (Einarsson, 1990) of the toric code, as the commutation relations between crossing logical operators that follow different non-trivial cycles of the torus correspond to the braiding of anyonic quasiparticles.

Errors can also be interpreted in the anyonic picture. Errors occur when energy is introduced to the system which then creates anyons. Two such anyons are shown in Fig. 4(b). Anyons that propagate around non-trivial cycles on the torus introduce logical errors to the ground space of the system. Unfortunately, once anyons are created on the toric code, it is possible for them to propagate across the system via some suitable mechanism with no additional energy cost. We find this by observing that string-like operators can be introduced to a ground state of Hamiltonian (14) at constant energy, independent of the length of the string. This insight is the underlying problem that makes it very difficult to design two-dimensional topologically ordered passive quantum memories.

The low-energy excitations of the toric code is an example of a *topological quantum field theory* (Witten, 1988). Models that support topological field theories can be identified by their anyonic statistics, non-trivial ground state degeneracy, or by means of order parameters such as topological entanglement entropy (Kitaev and Preskill, 2006; Levin and Wen, 2006) that developed from earlier studies of entanglement entropy in topologically ordered lattice models (Hamma *et al.*, 2005a,b). Topological quantum field theories, and extensions thereupon (Haah, 2011; Hamma *et al.*, 2005c; Walker and Wang, 2012; Yoshida, 2013) give rise to classes of models that are of interest in the field of quantum memories. In the following Subsubsec. we discuss the stability of the gap that is exhibited by topologically ordered systems at zero temperature in the presence of stray perturbations.

F. Zero-Temperature Stability

In addition to considering the stability of memories against thermal noise, which is the subject of this Review, we must also be mindful of the effects of perturbations when designing quantum memories. Any deviation of a Hamiltonian from our idealized expectations will cause differences in energies as well as dynamics. This can have
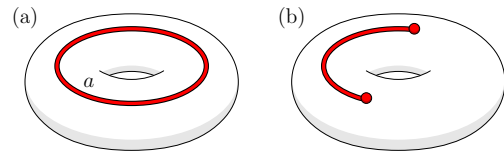

FIG. 4 (a) The ground space is naturally described with a basis labeled by anyonic charges, a, wrapping around a non-trivial cycle of the torus and then annihilating with its antiparticle, such as that shown in red. (b) Two anyonic excitations created that can propagate at no energy cost to affect the ground space of the system.

deleterious effects for any quantum information stored and processed in the system. Fortunately, topologically ordered systems are naturally adept at suppressing the effects of such perturbations. Even so, for arbitrary suppression we require systems of arbitrarily large size, so we will be interested in the thermodynamic limit for true stability.

Probably the most well known, but also most misinterpreted result regarding perturbations in topological ordered systems is that of (Bravyi *et al.*, 2010a). In that work gapped Hamiltonians made up of local, frustration-free and commuting terms are considered for which the degenerate ground state space is topologically ordered. Local perturbations of general form with finite but sufficiently low strength with respect to the unperturbed Hamiltonian gap are then introduced. It is shown that the splitting of the topologically originated ground state degeneracy is at most exponentially small with the system size. It is further shown that the gap between the ground state space and its excited states is also stable against small local perturbations. The topologically ordered phase is then preserved in the thermodynamic limit, and any given degree of suppression can be efficiently realized. The explicit example of the toric code Hamiltonian perturbed by magnetic fields has been well studied in Refs. (Dusuel *et al.*, 2011; Trebst *et al.*, 2007; Tupitsyn *et al.*, 2010; Vidal *et al.*, 2009).

This result suggests that the timescale at which decoherence by dephasing is induced will diverge exponentially with system size. However, this result is too quickly adopted. It is very likely that the system will typically not be in the ground state of the perturbed Hamiltonian. One reason is that, for an arbitrarily large system, it will become a certainty that localized excitations will exist somewhere. Another reason is that the ground state may need to be prepared rather than achieved by cooling. Since the perturbations are not known in general, and since the ground states they result in may be too complex to prepare, we would expect to use the ground state of the unperturbed Hamiltonian. Finally, perturbations will be time-dependent in general.

Since the state of the system will not typically be an eigenstate of the Hamiltonian, the effects of dynamics must be considered. For the case of the toric code, it has been shown that the coherence time will be at

most $\mathcal{O}(\log L)$ in the presence of certain local perturbations, including a simple magnetic field (Kay, 2011). Much of this is due to the perturbations enabling anyons to hop across the lattice. It has been shown that this effect can be suppressed by randomizing the couplings of the toric code Hamiltonian, thus introducing Anderson localization (Stark *et al.*, 2011; Wootton and Pachos, 2011a). The lifetime then improves to $\mathcal{O}(\text{poly}(\text{L}))$ (Kay, 2011). These dynamical effects are also studied in (Bravyi and König, 2012; Kay, 2009; Pastawski *et al.*, 2010; Röthlisberger *et al.*, 2012; Tsomokos *et al.*, 2011).

Properties such as these are not necessarily limited to topologically ordered systems. In principle, other types of order may possess equal or perhaps better ground state stability against unknown perturbations. However, topologically ordered phases are currently the only known means for such suppression, and thus forms the backbone of current proposals for self-correcting memories.

III. MEMORIES AT FINITE TEMPERATURE

In this Section we consider the physics of a quantum memory interacting with a thermal environment. We introduce the mathematical and numerical tools to analyze the effects of finite temperature on models where the energy spectrum is well understood, such as the commuting Pauli Hamiltonians we introduced previously. As a concrete example we analyze the toric code coupled to a finite temperature environment. We conclude with a list of criteria we demand of an experimentally amenable quantum memory.

A. Modeling a Finite Temperature Environment

Formally, a thermal environment is modelled as a quantum system, that we call the thermal bath, which is coupled to the Hamiltonian system describing the memory of interest. This interaction entangles the memory to the bath such that some information of the encoded system cannot be recovered by measurements of the system alone. The overall effect of the thermal interaction is that the reduced state of the memory thermalizes towards the *Gibbs state*

$$\rho = \sum_j \frac{e^{-\beta\varepsilon_j}}{Z} |e_j\rangle \langle e_j| , \tag{18}$$

where $Z = \sum_j \langle e_j| e^{-\beta H} |e_j\rangle$ is the canonical partition function and $\{|e_j\rangle\}$ is a complete set of energy eigenstates of H, each with energy $\{\varepsilon_j\}$. We denote by $\beta = 1/T$ the inverse temperature of the system and take Boltzmann's constant equal to one.

In general the evolution of a many-body quantum system interacting with a thermal bath is very complicated. In fact it is unknown if the model describing the full thermal evolution is analytically solvable (Terhal and Burkard, 2005). To model the coupled system we assume that the weakly interacting bath acts locally and independently on individual physical systems. We also assume that the thermal bath is *Markovian*, i.e. that information transferred from the quantum system to the bath is quickly lost and forgotten by the environment.

We model the thermal environment such that each qubit is independently coupled to a bath of harmonic oscillators. We assume that the bath can only introduce single physical qubit errors to the memory system. To simplify the problem we will also often assume that the noise model will introduce either Pauli-X or Z errors, as such errors act like hopping operators between eigenstates of the commuting Pauli Hamiltonians introduced in the previous Section. Master equation methods can be applied to study this interaction (Alicki *et al.*, 2009; Viyuela *et al.*, 2012), which is closely related to the spin-boson model (DiVincenzo and Loss, 2005; Leggett *et al.*, 1987; Weiss, 2012). Consider the energy cost to introduce an error $U = X_j$, Z_j at qubit j is $\omega_U = \varepsilon_i - \varepsilon_f$, where ε_i and ε_f are the energies of the system before and after the application of U, respectively. Then we model the rate at which the lattice suffers error U with the equation

$$\gamma(\omega_U) = \frac{\omega_U}{1 - e^{-\beta\omega_U}} . \tag{19}$$

This expression for the error rate acting on each qubit is motivated by the thermalization of a spin coupled to a Markovian Ohmic bath in the weak-coupling limit (DiVincenzo and Loss, 2005; Leggett *et al.*, 1987; Weiss, 2012). Importantly, Eqn. (19) describes a model where high-energy processes, i.e., processes that increase the energy of the system, are exponentially suppressed with respect to processes that do not involve the exchange of energy. To guarantee that the final state is the thermal state we require detailed balance

$$\gamma(\omega) = e^{\beta\omega}\gamma(-\omega), \tag{20}$$

for large β (Robert and Casella, 2004). It is easily verified that Eqn. (19) satisfies the detailed balance condition. Further, $\gamma(\omega)$ is normalized such that $\gamma(0) = 1/\beta$.

The transition rates we use to describe thermal dynamics reproduce a well-known rule of thumb for estimating the timescale at which thermal processes occur, namely *Arrhenius' law*. This heuristic estimate predicts that energetic processes occur over timescales like

$$\tau \sim e^{\beta E}, \tag{21}$$

where the process occurs with energy cost E. A first order approximation of rate Eqn. (19) in the low temperature limit gives the reciprocal of Arrhenius' law.

B. Coherence Time of Memories

To determine how well a candidate memory performs at finite temperature we introduce a suitable figure of

merit. To this end, we define the *coherence time*, τ. The coherence time is the typical amount of time required for a ground state of the considered system to evolve such that we are no longer able to recover encoded quantum information with suitably high probability. The system evolves according to the dynamics we introduced in the previous Subsection, and we allow the use of active error correction techniques *at the time of readout*. Naturally, the coherence time depends on the physical characteristics of the system, like the natural units that describe its couplings. We overlook these details as they are fixed by Eqn. (19). We are primarily interested in the dependance of the coherence time on the parameters that we can vary, such as the system size and inverse temperature of the bath.

Let us consider the smallest possible example of a toric code and estimate its coherence time. This is defined on four qubits by Hamiltonian

$$H_{4\text{Qu. toric}} = -\frac{\Delta}{2}(A + B), \qquad (22)$$

with stabilizers

$$A = X_1 X_2 X_3 X_4, \quad B = Z_1 Z_2 Z_3 Z_4. \qquad (23)$$

The code states are given by the four-qubit GHZ states with an even number of qubits in the 1 state. Logical operators for this code act on only two qubits. For example, we can choose $\overline{X} = X_1 X_2$. The thermal error model defined above applies single qubit Pauli operators one at a time. To implement a logical $\overline{X}$ it must therefore first apply X_1 and then X_2 (or vice-versa). The first operator anticommutes with B, and so costs an energy Δ as dictated by Hamiltonian (22). According to Arrhenius' law this process will take a time of around $e^{\beta\Delta}$. The next flip required for the logical operator allows the release of energy, and so occurs much more quickly. The coherence time of this small toric code is then $\tau \sim e^{\beta\Delta}$. Exponential coherence time scaling with inverse temperature and gap size, determined by the interaction strength is common to all memories of small size.

To protect the degenerate ground states against coherent perturbations, the topological memory needs to be large, $L \gg 1$, as discussed in Subsec. II.F. Hence, we must look toward the thermodynamic limit. We must therefore ask, what happens to the coherence time of the memory against thermal noise as we increase the system size? It is useful to compare with the benchmark $\tau \sim e^{\beta\Delta}$ for small systems obtained from Arrhenius' law, Eqn. (21). The worst possible case for a memory would be sub-Arrhenius scaling of coherence time with β. This would mean that large system sizes have entropic effects that causes the memory to fail faster than for small system sizes. A memory with Arrhenius scaling allows the same protection as one would get against thermal errors for a small system size to co-exist with arbitrarily high suppression of perturbations. Finally, larger system sizes might have the beneficial effect of allowing a greater gain in coherence time as temperature is lowered by resulting

in super-Arrhenius scaling, such as $\tau \sim e^{a\beta^2}$ for some $a > 0$.

C. Energetic and Entropic Considerations

A useful concept in quantum memories is that of energy barriers. The four-qubit toric code discussed in the previous Subsection gave an example where Arrhenius' law can be applied simply to find that the lifetime of the memory is correlated to its gap, Δ. However, the corresponding process for larger many-body systems is much more complicated. Thermal errors act locally, and so it is not possible to transition between ground states via a single excited state. Instead, errors must navigate a highly degenerate landscape of excited states to transit between ground states. For this reason there is typically no simple generalization to find the energy E that can be used to estimate the lifetime via Arrhenius' law. Nevertheless, in order to gain some intuition about the thermalization process, we can still attempt to find such an energy scale.

Consider the case that the system is initially in a logical ground state $|\psi\rangle$. We wish to determine how easy it is for thermal errors to rotate the encoded state to, for instance, $\overline{X}|\psi\rangle$, by performing the logical operator $\overline{X}$. As we consider physically motivated local noise models, the logical error operator $\overline{X}$ is decomposed into a sequence of the single qubit operators U_t that the thermal bath can apply, such that

$$\overline{X} = \prod_{t=1}^{N} U_t. \qquad (24)$$

Here U_t denotes the t-th operator to be sequentially applied, and N is the total number of operators required to construct $\overline{X}$. Note that this decomposition of the logical operator into single qubit operators is not unique. A permutation of the U_t will result in the same action $\overline{X}$ upon state $|\psi\rangle$. We remark that in general a different sequence of U_t with different N can yield the same logical operator.

Unlike the initial and final states, the state after $0 < t < N$ steps have been applied will be an excited state. Let us use E_t to denote its energy. For each decomposition of $\overline{X}$ into U_t operators we can consider the energy $\max_t E_t$, the maximum energy cost incurred during the sequence. This may be artificially high simply due to a badly chosen sequence. We therefore minimize this over all possible sequences to obtain the energy barrier of the model, E_B. This is the minimum energy that the thermal errors must pay in order to perform a logical error.

For the toric code Hamiltonian (14), a logical operator can be applied by first creating a pair of anyons, and then transporting them around a non-contractible loop. The first operation incurs the energy cost for creating a single pair but no subsequent operation will, $\max_t E_t = 2$. One could also apply a logical operator by first creating a pair on every other qubit around a non-contractible

loop, and then annihilating them all using the remaining qubits around the loop. After the creations and before the annihilations the energy is that for $L/2$ pairs, $\max_t E_t = 2(L/2)$. Clearly the former method is energetically favorable, and so will be preferential for thermal errors at low temperature. It is therefore the energy cost in that case that we take to be the energy barrier, $E_\mathrm{B} = 2$.

Much of the study of finite-temperature quantum memories look to find complex systems that achieve E_B that scales logarithmically or even as a power law with the size of the system. For such systems we should expect the coherence times of such models to scale favorably with system size according to Arrhenius' law. Such models are studied in Sec. VII.

We further remark that due to significant entropic effects during thermalization, we cannot necessarily estimate the coherence time using Arrhenius' law. The resulting time scale, $\tau \sim e^{\beta E_\mathrm{B}}$, is often considered as a widely applicable (Laidler, 1972) rule of thumb, to which counter examples can be found (Yoshida, 2014).

As a counter example to Arrhenius' law, consider a toric code whose Hamiltonian assigns an energy cost $E \sim 1$ to the creation of a single pair of anyons, but then an infinite energy to the creation of any further excitations. Clearly the energy barrier is simply $E_\mathrm{B} = 1$, and any logical error will be caused by only a single pair that walks around the code. This walk takes at least $\mathcal{O}(L)$ sequential steps and so at least $\mathcal{O}(L)$ time. For a typical error model the walk will be diffusive, and so will take a longer time of $\mathcal{O}(L^2)$. In either case, the lifetime is at least linear with L, despite its constant energy barrier. This model is obviously based on an unrealistic Hamiltonian, but similar effects are observed with more reasonable system in Sec. VI. This counter example paints a picture to indicate that it is possible to obtain better lifetimes than Arrhenius suggests by consideration of the dynamics of a system. However, we can also get worse. Examples of entropic effects leading to lifetimes that do not scale as well as Arrhenius' law predicts will be considered in Subsec. III.E.

D. Simulating Finite Temperature Effects

Monte Carlo methods are frequently used to numerically analyze the evolution of a system where analytical methods are intractable, or to find data that supports theoretical conjecture. Here we give an overview of a general method to conduct finite-temperature Monte Carlo simulations for commuting Pauli Hamiltonians (Bortz *et al.*, 1975; Chesi *et al.*, 2010b).

The noise model approximates the thermal evolution of an eigenstate $|\psi(t)\rangle$ with respect to commuting Pauli Hamiltonian H when interacting with a thermal bath of inverse temperature β. As we have mentioned in Subsec. II.A, eigenstates of commuting Pauli Hamiltonians are easily described using a list of eigenvalues, M_j. We simulate the noise model as a sequence of discrete events that map between eigenstates of H. At each event we look to obtain some U and δt such that $|\psi(t + \delta t)\rangle = U |\psi(t)\rangle$. We simulate the thermal evolution up to some time t_max and at $t = 0$ we typically initialize the state to a ground state of H.

For commuting Pauli Hamiltonians the random incident errors U are of the type X_j, Y_j or Z_j, that act on qubit j of the state. Importantly, Pauli-type errors ensure that $|\psi(t + \delta t)\rangle$ is an eigenstate of H. The relative probability of error event U is determined using Eqn. (19). Rates $\gamma(\omega_U)$ are evaluated with respect to H and $|\psi(t)\rangle$. Explicitly, we select error event U by calling from the distribution

$$p_U = \frac{\gamma(\omega_U)}{R}, \tag{25}$$

where we normalize using the total rate $R = \sum_U \gamma(\omega_U)$. and the summation is over all qubits and errors.

The time δt that passes between each step as U is applied is determined using R. Since each U occurs as a random process at rate $\gamma(\omega_U)$, the time step δt is a random variable distributed as an *exponential* distribution with parameter R, the total rate. We numerically generate values of δt such that

$$\delta t = -\frac{\ln(\texttt{rand})}{R}, \tag{26}$$

where $\texttt{rand}$ is a random variable chosen uniformly from the interval $(0, 1]$. We thus obtain the new eigenstate after a time δt, which passes during the event, such that $|\psi(t + \delta t)\rangle = U |\psi(t)\rangle$.

At the end of each event, we check the total time of the system. If $t + \delta t < t_\mathrm{max}$ we perform another event using the new eigenstate $|\psi(t + \delta t)\rangle$. Otherwise we stop the simulation and use $|\psi(t + \delta t)\rangle$ and incident error U to collect sample data.

By averaging over many trials of this process we can obtain estimates of many non-equilibrium thermal quantities, in particular the coherence time τ. We use two different methods to estimate τ in this Review. In the first we apply the decoder repeatedly as we evolve the system and define τ as the average time the decoder first fails. Alternatively we define τ as the time that the decoder success rate falls below some threshold e.g. 99%. These values will numerically differ by a constant factor, but ultimately reveal the coherence-time dependence on system size and temperature that we seek to obtain.

E. Toric Code at Finite Temperature

In this Subsection we analyze the finite-temperature coherence-time scaling of the toric code. The thermal dynamics of the toric code have received extensive study both numerically Ref. (Freeman *et al.*, 2014; Hutter and Loss, 2014) and analytically (Alicki *et al.*, 2009). Here, we give numerical simulations that closely agree with the heuristic description we have described at low temperatures for the toric code model. We also consider the

high-temperature regime of the toric code model to illustrate the interplay between energetic and entropic contributions to the coherence time.

The energy cost, or mass, of a single anyon equates to the Hamiltonian interaction strength, Δ, which we set to $\Delta = 1$ as in Hamiltonian (14). We expect an average density of anyons in the toric code to scale like $\rho \sim e^{-\beta\Delta}$ in thermal equilibrium state. From this it follows that the number of anyon pairs present in a thermalized system of size L is

$$\langle N \rangle \sim \frac{L^2 \rho}{2} = \frac{L^2 e^{-\beta\Delta}}{2}. \tag{27}$$

For finite system sizes at sufficiently low temperature we expect $\langle N \rangle \lesssim 1$, meaning the probability that there is more than a single pair of anyons on the lattice is negligible. The thermal decoherence of encoded information will occur as the result of the behavior of just a single pair of anyons. This regime is quite different to high temperatures, or very large system sizes, where $\langle N \rangle \gg 1$. For the case where there are many anyon pairs present we expect the interaction of the separate pairs to dominate the coherence time of the system. Similar to the four-qubit toric code discussed in Subsec. III.F, we will demonstrate that in the low-temperature regime the coherence time can be estimated by Arrhenius' law applied to the gap of the system with an entropic correction. This contrasts with the high-temperature regime where we observe that entropic effects act to speed up the decoherence, and the true lifetime is much less than Arrhenius' law estimates. We illustrate the different temperature regimes of the toric code in Fig. 5.

1. The Toric Code at Low Temperature

In the low-temperature regime we typically expect a single pair of excitations to cause the toric code memory to fail. We show such a configuration in Fig. 5(b). We estimate the coherence time $\tau_{\text{low}} = \tau_c + \tau_m$, where τ_c is the time it takes for this pair to be created and τ_m is the time it takes for the anyons to diffuse across the lattice up to a separation $L/2$ such that encoded information is irrecoverable by quantum error correction. Since we are only interested in the displacement between a single pair of anyons we can treat a single anyon as fixed with the other moving relative to it. When the anyons are not neighbors they move independently as an unbiased random walk. Using this description we can estimate the diffusion time τ_m. The typical number of steps required for a two-dimensional random walker to reach a distance $L/2$ from its starting point is $(L/2)^2$. The timescale of random walk steps is $(8\gamma(0))^{-1}$, where the factor of 8 counts the number of processes on the lattice that move anyons. We thus obtain

$$\tau_m \simeq \frac{1}{8\gamma(0)} \left(\frac{L}{2}\right)^2 = \frac{\beta L^2}{32}. \tag{28}$$

(a) At low temperature the system contains only a single pair of anyons.

(b) Decoder fails when the single pair is separated by more than $L/2$.

(c) At high temperature the system contains many anyon pairs with average spacing $\Lambda = \rho^{-1/2}$.

(d) Decoder begins to mismatch pairs, failing when an error chain percolates.
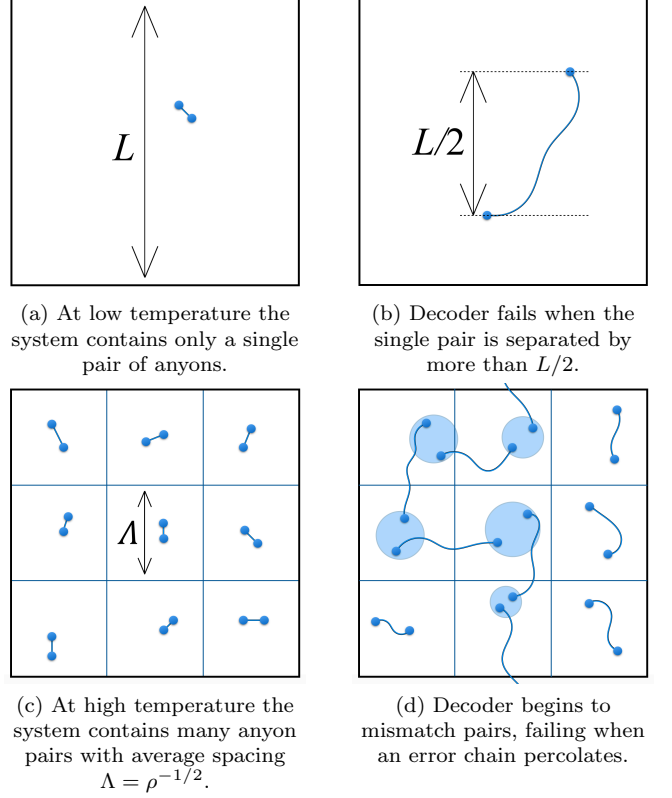
FIG. 5 Typical string-like error configurations from the different temperature regimes of the toric code at finite temperature. Configurations that cause the decoder to fail are also depicted.

To approximate τ_c we note that the energy cost of pair creation is 2Δ. Using the noise model discussed in Subsec. III.D, pairs are created from the vacuum at rate $R_0 = 2L^2\gamma(-2\Delta)$. This implies the time we wait to see a creation event is $1/R_0 \sim e^{2\beta\Delta}/L^2$. However, not all pairs diffuse to the required distance. Some creation pairs will fuse back to the vacuum, self-annihilate, at some point later in the simulation, which we next take into account.

We denote by $\Pi(L, \beta)$ the probability that a pair does not self-annihilate before reaching separation $L/2$. When the anyons do not neighbor each other their motion is an unbiased random walk. It is a standard result for a two-dimensional random that the probability a walker will not return to the origin in the first n steps scales as $1/\ln(n)$. On average we need the walker to avoid self anihilation for $(L/2)^2$ steps. We therefore expect a factor of $[2\ln(L/2)]^{-1}$ in Π. Additionally, when the anyons neighbor each other there is a temperature dependent bias towards self-annihilation since $\gamma(2\Delta)/\gamma(0) \sim \beta$. The probability that they separate rather than annihilate should then include a factor $\sim 1/(1 + A\beta)$ to account for this bias, where A is some constant and $A\beta$ is the relative chance the anyons annihilate when they are nearest
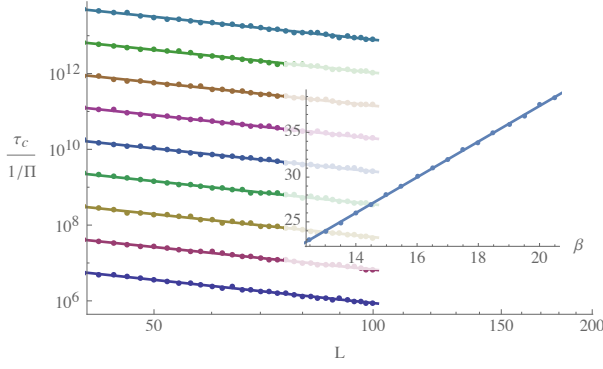
FIG. 6   Log-log plot of the contribution to the coherence time from pair creation τ_c as a function of L for a range of β. We expect τ_c to include a factor of $1/\Pi(L, \beta)$, which we have separately found numerically, so we divide this off. Estimates are obtained over 1000 simulation runs. The fits are linear and all have similar gradient with mean gradient -2.01. Inset is the intercept of the linear fits shown as a function of β. Overall we see a dependence $\tau_c = 0.150(e^{1.99\beta}/L^{2.01})(1/\Pi)$, which is in excellent agreement with the theoretically predicted behavior given in Eqn. (29).

neighbors. The factor $\Pi(L, \beta)$ then takes the form

$$\Pi(L, \beta) \sim \frac{1}{1 + A\beta} \frac{1}{\ln(L/2)}. \tag{29}$$

Combining these elements, we expect a creation timescale

$$\tau_c \simeq \frac{1}{R_0} \frac{1}{\Pi} \sim \frac{e^{2\beta\Delta}}{L^2}(1 + A\beta)\ln(L/2). \tag{30}$$

The total coherence time is $\tau_{\text{low}} = \tau_c + \tau_m$. In the low-temperature limit time τ_c is the dominant contribution to τ_{low} due to its exponential dependence on β.

To test these predictions we rigorously study the system evolving at low temperature using different numerical experiments with various initial conditions where we make variations to the physical noise model. Key technical calculations involved in finding the low-temperature coherence-time scaling are discussed at length in App. B. Here we present the main results concerning the most significant contribution to the coherence time. We separately estimate $\Pi(L, \beta)$, τ_c and τ_m using numerical simulations. We find good agreement with the predicted forms of Eqns. (28), (29) and (30) with the constant $A \sim 5$ for function $\Pi(L, \beta)$. The most significant contribution to τ_{low} comes from τ_c, and the scaling of τ_c is dominated by the factor $1/R_0$. Fig. 6 shows just the $1/R_0$ scaling of τ_c. This observation matches the predicted values of the key parameters very well, demonstrating a dependence on $1/L^2$ and an exponential growth with $2\beta\Delta$.

The minimum energy barrier of the toric code is $E_{\text{B}} = 2\Delta$, giving an Arrhenius' law estimate of the coherence time $\tau \sim e^{2\beta\Delta}$. We have shown that in the low-temperature regime the leading contribution to the coherence time is τ_c, given by Eqn. (30). If we ignore the

sub exponential β dependence inside $1/\Pi$, we can approximate the coherence time by

$$\tau_{\text{low}} \sim e^{2\beta\Delta}\frac{\ln(L/2)}{L^2}. \tag{31}$$

We see that as $\beta \to \infty$ the coherence time for a given system size grows exponentially with β in exactly the way Arrhenius' law predicts. The factors of L^2 and $\ln(L/2)$ are entropic contributions. The L^2 term allows for the freedom of choice in start positions of the anyons; the volume of qubits of the lattice introduce more pathways for decoherence to occur, and decreases the lifetime. The $\ln(L/2)$ term accounts for the increasing probability that random walks lead to self-annihilation with increasing system size. This suppresses the likelihood of the dynamics completing a decoherence process and boosts the lifetime. A naïve interpretation Eqn. (31) suggests that as L becomes large the coherence time vanishes. However, by rearranging Eqn. (27) we see that the definition of low temperature implies that $e^{2\beta\Delta} \gg L^4$ and so the $1/L^2$ factor is negligible with respect to the exponential dependence on inverse temperature. In fact, given the L dependence in our definition of the low-temperature regime, we must reduce the temperature to remain in such a limit. Indeed, a consequence of this definition is that in the thermodynamic limit there are no non-zero temperatures that give rise to low-temperature coherence-time scaling for the toric code model.

2. The Toric Code at High Temperature

We next consider the high-temperature regime where thermalization creates many anyons. In this regime the equilibrium density of anyons is $\rho \sim e^{-\beta\Delta}$. For simplicity we concern ourselves with the density of excitation pairs, $\rho/2$, but where we also absorb the $1/2$ factor into ρ. On average, anyon pairs are created uniformly throughout the system and each occupy an area of approximately $1/\rho$. We approximate the area as a square of linear size $\Lambda = \rho^{-1/2} \sim e^{\beta\Delta/2}$ as shown in Fig. 5(c). In this regime, the probability the decoder fails becomes appreciable once some fraction of pairs separate a distance Λ, as shown in Fig. 5(d).

Within a single $\Lambda \times \Lambda$ region, the evolution approximates the low-temperature case where we need only consider a single anyon pair, i.e. there will be a creation event and the anyons subsequently diffuse apart. We say that a single region fails once its anyons move close to other anyons from neighboring regions. We assume that each region evolves independently. Given that each region contains a single anyon pair we can assume that each region behaves like a small lattice of linear size Λ in the low-temperature regime, where we can estimate the time that the system decoheres, τ_{high}, using Eqn. (31) where we take $L = \Lambda$. Applying Eqns. (28) and (30) to a single region gives estimates for the diffusion and creation
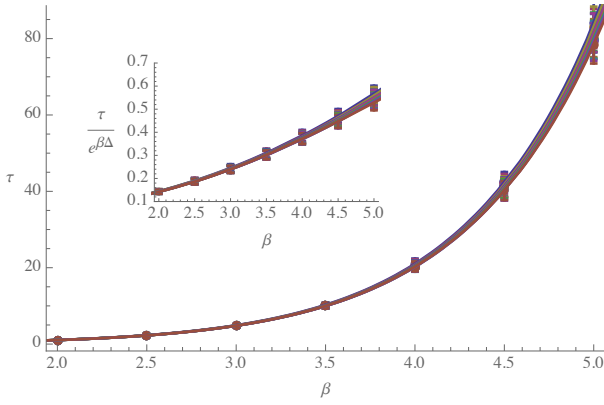
FIG. 7 Coherence time of high temperature toric code as a function of β for a range of large system sizes $L =$ 100, 120, ... 200. Estimates are averages over 1000 simulations. Shown are fits to the form of Eqn. (34). We observe only small variations in the fit parameters between system sizes and their averages give: $\tau_{\text{high}} = 0.56 \, e^{1.01\beta}(1 + 0.28\beta + 0.31\beta^2)$. The inset shows just the non-exponential part of the fit.

timescales $\tau_{m,\Lambda} \sim \beta\Lambda^2 \simeq \beta e^{\beta\Delta}$ and

$$\tau_{c,\Lambda} \sim \frac{e^{2\beta\Delta}}{\Lambda^2}(1 + 5\beta)\ln(\Lambda). \tag{32}$$

To get an expression in terms of β we write $\Lambda = C \, e^{\beta\Delta/2}$, where C accounts for the constants absorbed into ρ. Then substituting Λ into Eqn. (32) and rearranging

$$\tau_{c,\Lambda} \sim e^{\beta\Delta}(1 + r\beta + s\beta^2), \tag{33}$$

where r and s are new constants related to those already introduced. In contrast to the low-temperature case, the timescales for creation and diffusion have the same exponential dependence on β, and so we expect them both to contribute appreciably to the coherence time. Combining terms we obtain high-temperature coherence time

$$\tau_{\text{high}} \simeq \tau_{c,\Lambda} + \tau_{m,\Lambda} \simeq e^{\beta\Delta}(1 + r'\beta + s\beta^2), \tag{34}$$

where r' also includes the motion contribution. This simple modeling ignores high-temperature thermal effects such as pair fusion, where two anyons from different pairs fuse to vacuum combining their strings to form a longer string. Processes such as these will alter both the diffusion speed and the pair self-annihilation probability. As a result we do not expect this model to give good predictions of the values of r' and s. However, we do expect it to correctly predict the general features of the high temperature dynamics. In particular, the altered exponential dependance on β, and the system size independence of the lifetime.

We simulate the system evolving at high temperature in order to test our assumptions and verify predictions about the high-temperature dynamics. Here we present the key results, a thorough discussion of our methods and results is given in App. B. We verify that anyon

densities at the time the decoder fails obey $\rho \sim e^{-\beta\Delta}$ and that for the parameters we consider the typical number of anyons $\langle N \rangle \gg 1$. The average separation between anyon pairs that were either created together or joined by a fusion is seen to scale as $e^{\beta\Delta/2} \sim \Lambda$ as expected. In addition we see that the maximum separation between any pair is always much less than $L/2$ confirming that the decoherence results from the average motion of anyons on a local scale. We give numerical data showing the exponential component of τ predicted in Eqn. (34) in Fig. 7. Our results clearly demonstrate coherence time scaling independent of the system size of the toric code.

If we ignore its sub-exponential β dependence the high temperature coherence time is approximated by

$$\tau_{\text{high}} \sim e^{\beta\Delta}. \tag{35}$$

This is also exponentially growing with β but at a much slower rate than Arrhenius' law predicts, $\tau \sim e^{2\beta\Delta}$. We see that in the high-temperature case entropy accelerates the decoherence process so that the memory fails much faster than its energy barrier alone implies.

F. Characteristics and Conditions of Self-Correcting Memories

To properly compare and classify the different models that have been proposed as self-correcting memories, we must have a clear idea of what a self-correcting quantum memory is. We conclude this Section by presenting the general characteristics we require from a finite temperature quantum memory.

As a quantum memory we would like to have a physical system where quantum information can be initially encoded by external control. The encoded information should then remain coherent without the application of any control for an arbitrary amount of time while the system is exposed to thermal errors or spurious perturbations. Finally, the stored information is extracted. At this point the decoding of the stored information takes place, where a single error correction protocol can be applied. If the employed system is a good quantum memory then we are able to recover the encoded state with high fidelity after a desired amount of time that we are free to tune with system parameters.

Given that we have these conditions, we ultimately seek a many-body quantum system whose coherence time, τ, increases with the system size, L, in the presence of thermal noise. Ideally, we would like to have τ depend exponentially on L. In this case, τ can be made arbitrarily large such that we can run a quantum algorithm of any length using resources that scale efficiently with respect to the problem size. Nevertheless, such memories may be too hard to implement, and as such we take interest in weaker notions of self correction, with perhaps a polynomial dependence on system size.

It is understood that the increase in coherence time, as the system size increases, coincides with super-Arrhenius

coherence time scaling. Memories with sub-Arrhenius or Arrhenius scaling of the coherence time with β are not regarded as self correcting as they are no better than what we expect to achieve with a small quantum memory. Those with super-Arrhenius scaling are said to be at least 'partially self-correcting', as discussed in Subsec. VII.A. The term 'self-correcting' is reserved for the unimpeded increase of coherence time with system size. Memories with either one of these are said to exhibit self-correcting behavior.

To achieve self-correction, we will encode qubits in degenerate subspaces where encoded states are separated from excited eigenstates by an energy *gap*. In general, we cannot expect for a memory engineered in a laboratory to be truly isolated from local coherent noise such as, for instance, a stray magnetic field. To achieve coherence times necessary to complete the tasks demanded of a memory, we are typically interested to scale the system to large sizes. In general, it is not obvious that the gap does not vanish as we scale the system in the presence of small perturbations. We therefore require a system with a *stable gap*, i.e. a system whose gap does not vanish in the large system-size limit, even in the presence of stray perturbations.

We similarly require that the encoded subspace remains at least approximately degenerate in the presence of a stray field in the large system limit. Without such a property, quantum information will not evolve coherently and encoded states will rapidly become mixed. We refer to such a system as having a *stable degeneracy*.

We also require the ability to decode a candidate quantum memory efficiently when we wish to read information from the system. Indeed, given a memory that is capable of storing quantum information for the duration of a quantum circuit, the problem-solving benefits we attain from a quantum computer are rendered useless if we cannot read information from the computation in an amount of time that scales efficiently with the size of the memory, which must scale with the depth of the computation. Given a quantum memory then, we must also develop the classical software to interpret syndrome information thus enabling the correction of small errors to the system.

Of course we also demand physical constraints when designing a memory. We require the system to interact locally within three or fewer dimensions, and we also require that Hamiltonian interactions do not increase in strength with system size. Combining these arguments with the limitations of what is in principle possible to achieve experimentally, we can define the following list of necessary criteria as well as a list of desirable criteria for a system to efficiently behave as a memory. The *required conditions* for a finite temperature memory are listed below

1. Encodes a qubit in a stable degenerate subspace.

2. Encoded states are separated from the excited spectrum by a stable gap.

3. Local in three or fewer dimensions.

4. Bounded strength of interactions.

5. Constant-weight Hamiltonian interactions.

6. Efficiently decodable in polynomial time.

7. Coherence-time against thermal noise that scales as a power law with system size up to a cutoff.

8. Given a cutoff, demonstrates super-Arrhenius inverse-temperature coherence-time scaling at the thermodynamic limit.

Finding systems that satisfy these required features are certainly exciting, and provide a proof of principle that a finite temperature quantum memory can be designed. However, the required conditions do not guarantee that the proposed memories are feasible to implement with respect to the level of quantum control we can currently achieve in a laboratory. For instance, we may consider a Hamiltonian with constant, but high-weight interaction terms. Similarly, we do not require that Hamiltonian terms take bounded eigenvalues, but only that the interaction strength is bounded. This allows, for example, for bosonic interaction terms. We therefore append to the list of required criteria a list of desirable features we might wish to develop into a quantum memory to accelerate the experimental amenability and scalability of such a system. We propose finding quantum memories with the following *desirable features*

1. Coherence time against thermal noise that increases exponentially with system size.

2. Translational invariance.

3. Locally embeddable in two or fewer dimensions.

4. Bounded Hamiltonian operators.

5. Low-weight (ideally two-body) Hamiltonian interactions.

6. No system size cutoff point where self-correcting properties cease to exist.

7. Compatible with a fault-tolerant universal quantum gate-set.

Imposing translational invariance is particularly exciting with respect to scalability, as we could potentially engineer such a system by designing simple repeating units of the many-body system. We may even expect to find such a system in a strongly interacting crystal. We additionally consider fault-tolerant computational abilities in our wish list of desirable features. Indeed, while finding systems capable of preserving coherent quantum states at finite temperature presents already a considerable challenge we may also wish to directly use such a system to perform interesting computational tasks. Such properties will help reduce computational overhead when we consider the application of a memory to a quantum circuit. We use these conditions as a comparative tool to guide us through the presentation of a wide variety of models discussed in the following.

IV. NO-GO THEOREMS

Before starting the search for a quantum memory over the vast space of possible realizations with many-body lattice Hamiltonians, it is wise to rule out systems which we cannot expect to maintain quantum information at finite temperature. For this purpose we now consider no-go theorems that identify broad classes of models with physical characteristics that cannot lead to passively protected memories.

The study of finite-temperature quantum memories requires a breadth of technical aspects, from the abstract mathematical theory of coding, to the more physically motivated field study of finite temperature effects on lattice Hamiltonians. To this end, no-go results can be broadly separated into two types. We label these *general no-go theorems* and *physically motivated no-go results*. The distinction is the following; general no-go theorems seek to exclude large classes of systems from possessing important properties that we expect to be necessary for self correction. Physically motivated no-go results take into consideration dynamics and microscopic thermal effects to show specific models that will fail to behave well as a quantum memory. Both approaches have complementary advantages, and are ultimately of equal importance.

The general no-go theorems typically eliminate the possibility of *energy barriers* in certain broad classes of systems. Macroscopic energy barriers between degenerate ground states are the basis of our current understanding of finite-temperature stability in classical models. The prototypical case of a classical stable model is the two-dimensional Ising model, which is presented in Subsection V.A. It is therefore very unlikely that we can expect to find a passive quantum memory with a model that does not support a macroscopic energy barrier. We remark at this point that although we know systems where an energy barrier is sufficient to obtain a quantum memory, it may not be a necessary feature to realize self correction as discussed in the conclusions of Ref. (Landon-Cardinal and Poulin, 2013).

Physically motivated results lose the generality of their counterpart class of no-go theorems. Instead, they model thermal effects acting on specific models. This approach offers new intuition to show that under physical considerations certain models fail to perform well as a quantum memory. Such results are typically obtained by studying the relevant order parameters that correspond to logical operations acting on the code space of quantum memories. Order parameters are then studied with respect to the dynamics of quantum system when interacting with an auxiliary environmental system, or in its Gibbs thermal equilibrium state. These results give strong support to known general no-go theorems for models where it is believed that finite-temperature stability cannot exist.

Known no-go theorems are most limiting in two dimensions. It has been shown that two-dimensional stabilizer models cannot support a macroscopic energy barrier that

will scale with the size of the system. It was shown by Bravyi and Terhal (Bravyi and Terhal, 2009) that local two-dimensional stabilizer states, which include the toric code model, cannot support a macroscopic energy barrier. Indeed, the best energy barrier we can hope for is constant with respect to the size of the system. This result is generalized to two-dimensional topologically ordered commuting Hamiltonians by Landon-Cardinal and Poulin (Landon-Cardinal and Poulin, 2013). These results are supported by a wealth of physical no-go results, typically obtained using Kitaev's toric code model, where various order parameters are shown to rapidly decay at finite temperature.

Three-dimensional no-go theorems have a significantly limited power (Haah, 2013; Yoshida, 2011). These results leave more promise for the discovery of new models with a macroscopic energy barrier. Indeed, the assumptions necessary to prove the discovered three-dimensional no-go theorems cover a significantly restricted set of models than the theorems known in two dimensions. Supporting these results, we also have various physical results showing that topological entanglement entropy (Castelnovo and Chamon, 2008), and the correlation functions of string-like logical operators (Alicki *et al.*, 2010) decay rapidly for the three-dimensional toric code model. This is consistent with the aforementioned general results that rule out the possibility of it supporting a macroscopic energy barrier. We see in Sec. VII, that there are many known physically feasible three-dimensional models that avoid the no-go assumptions we describe here, and present favorable properties for finite temperature stability.

In this Section we begin by reviewing no-go theorems in two dimensions. We reproduce the proof of Bravyi and Terhal to show that two-dimensional stabilizer models cannot support a macroscopic energy barrier, and we discuss the supporting physically motivated no-go results. We follow the discussion by considering the no-go theorems in three dimensions. We conclude with possible avenues for avoiding the known no-go theorems. The final Subsection serves as motivation for the positive results that we will discuss later on, which include the various models that have been proposed as stable quantum memories.

A. No-Go Results in Two Dimensions

In this Subsection we review no-go results in two dimensions. We consider in detail the general no-go theorem due to Bravyi and Terhal (Bravyi and Terhal, 2009), and we discuss the physically motivated no-go results. We motivate this no-go theorem by first considering the toric code, the prototypical model for quantum error correction. We have seen in Sec. II.D that the logical operators of the toric code are one-dimensional string-like operators. Models with logical operators of this type have a constant energy barrier. To understand this from the
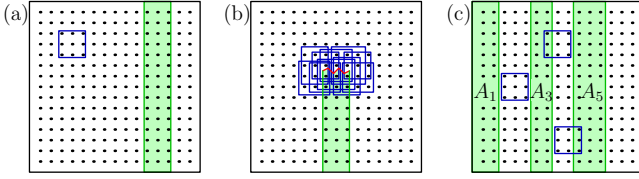
FIG. 8 Square lattices where qubits are displayed as black points. (a) Local stabilizer generators are confined to small square of size r shown in blue for size $r = 3$. For such a code there exists a logical operator supported on a quasi one-dimensional strip of width r, shown in green. (b) An error that forms part of a logical operator, supported on the green region, need not violate more than a constant number of local stabilizers, marked in blue, that extend to a distance of $r - 1$ away from the end point of the green strip. (c) A high weight logical operator can be cleaned onto region $A = \bigcup_k A_k$, where each stabilizer generator, examples of which are supported inside of the blue squares, have common support with no more than one strip. The proof concludes with an argument showing that a logical operator must be supported on a single A_j region.

anyonic picture of two-dimensional topologically ordered memories, these logical operations correspond to the creation of a pair of anyonic excitations, at a constant energy cost, which are then free to walk across the lattice at no additional energy penalty. This is discussed in detail in Refs. (Alicki *et al.*, 2009; Nussinov and Ortiz, 2008), but ultimately follows from the fact that one can find a sequence of single qubit error operations that will realize a logical operator without increasing the energy of the system beyond a constant value that is independent of the system size. With the toric code in mind it becomes interesting to see if we can find a two-dimensional system with logical operators that are not supported along a one-dimensional line. In this Subsection we follow the proof of Bravyi and Terhal (Bravyi and Terhal, 2009) to show that local two-dimensional stabilizer models necessarily have one-dimensional logical operators which are expected to be incompatible with finite temperature stability. In the exposition we show how a local noise model can construct a logical operation over its code space at no more than a constant energy cost with respect to the size of the lattice, thus completing the proof.

We consider a two-dimensional square lattice of size $L \times L$. The qubits interact via the local Hamiltonian

$$H = -\sum_a S_a, \qquad (36)$$

where S_a are in general an over-complete set of local generators for stabilizer group $\mathcal{S}$. The ground space of H is the code space of $\mathcal{S}$. Without loss of generality, each local stabilizer generator that acts on a small subset of qubits on the lattice can be contained in a square box no larger than constant linear size r. We show such a box in blue in Fig. 8(a). Moreover, each box can contain no more than a bounded constant number of interaction terms. Hamiltonians with these properties are physically

well-motivated as described in Subsec. II.A. We will observe that for the described stabilizer group with local generators S_a, there must exist a logical operator that is supported on a one-dimensional strip of width r, as shown in green in Fig. 8(a).

We now elaborate on the noise model that introduces a one-dimensional logical error without increasing the energy of the system above a constant independent of its size. The noise model of interest can introduce Pauli errors to single qubits of the lattice. We consider 'segments' of a Pauli logical operator supported on the highlighted in green region in Fig. 8(b) which is of variable length $1 \leq l \leq L$, cutoff along the horizontal red zigzag line. Importantly, the minimum energy cost associated to this segment is upper bounded by $E \sim \mathcal{O}(r^2)$, independent of the system size or l. The part of the Pauli logical operator supported on the green region will only violate, i.e. anti-commute with, stabilizer generators of the physical Hamiltonian that are within a radius $\sim r$ from the cutoff point, shown by the blue area on the lattice. Violated stabilizers correspond to the energy cost of the error on the segment with respect to the Hamiltonian.

Given that we have shown that the energy cost of a logical operator segment is upper bounded by energy cost E independent of l, it suffices to demonstrate that the energy barrier associated to a unit transportation of the cutoff for a generic two-dimensional stabilizer model is constant. Indeed, we can change segment length from l to $l + 1$ by overcoming an energy barrier that does not exceed a constant energy cost, $W \sim \mathcal{O}(r^3)$, independent of system size, before returning to its energy minima E once the logical segment achieves length $l + 1$. We bound W firstly by considering the introduction of a single qubit Pauli error on the lattice. Due to the locality of the terms of the physically constrained Hamiltonian, introducing a new Pauli error can only increase the energy of the system by a constant at most $\sim r^2$. To increase the logical operator segment from length l to length $l + 1$ the noise model introduces a specific set of r single Pauli errors close to the red zig-zag line in Fig. 8(b). This requires the addition of no more than r single qubit Pauli operators, whose energy cost can be no more than r^2. We are therefore able to bound $W \sim r \times r^2$. The described argument holds in the generality of creating a logical segment from the ground space of the lattice by considering the increase of the size of a segment from $l = 0$ to $l = 1$.

We have shown that a logical operator segment of length l has energy at most E, and that we can increase the length of the logical operator segment with energy cost no greater than W. It follows from this that the single Pauli error noise model can introduce a logical error to the ground space of the model using a logical operator segment with length $l = L$ with energy never greater than $E + W$. This demonstrates that a commuting Pauli Hamiltonian with one-dimensional logical operators have a constant energy barrier.

It only remains to show that a stabilizer group generated locally in two dimensions necessarily has one-

dimensional logical operators. The technical proof makes use of *the cleaning lemma*, proved in Ref. (Bravyi and Terhal, 2009). This lemma simply states that, given some subset of qubits of a stabilizer group $\mathcal{S}$, which we label A, one of the two following statements are true; either, there exists at least one logical operator supported entirely on the qubits of A, or, alternatively, that all logical operators $\overline{L}$ can be deformed by a stabilizer $S \in \mathcal{S}$, such that $\overline{L}S$ is not supported on A. We now complete this proof using the cleaning lemma. We separate the lattice into an even number of strips of width either r or $r-1$. We can check that a lattice of size $L = a(r-1) + br$ can be decomposed into some even number of $a + b$ strips for $L \geq 2(r-1)^2$, for proof, see footnote [1]. We index the strips in order, and we consider the region of odd strips $A = \cup_{k \in \mathrm{odd}} A_k$, as shown in Fig. 8(c).

We now obtain this proof by contradiction. We assume that there exists a logical operator whose minimum support cannot be contained on a vertical strip of width r. Due to the width of the strips, such a logical operator cannot be deformed by stabilizers away from region A. Therefore, by the cleaning lemma, it must be possible to support the logical operator entirely on region A. As the logical operator support is wider than a single strip, it must be supported on multiple odd strips A_k. Accordingly, we decompose the logical operator $\overline{L} = \bigotimes_{k \in \mathrm{odd}} \overline{L}_k$, where $\overline{L}_k$ is the support of $\overline{L}$ on strip A_k for odd k.

To complete the argument, we consider operators $\overline{L}_k$. A logical operator will commute with all elements of $\mathcal{S}$. Given the choice of strip width, we observe that the support of any stabilizer overlaps with no more than one odd strip. We show examples of the supports of stabilizer generators within blue squares in Fig. 8(c). It follows from this fact that, in addition to the logical operator $\overline{L}$, all operators $\overline{L}_k$ must also commute with the stabilizer group. Operators that commute with the stabilizer group are one of two types of operators. Either, they are elements of the stabilizer group, such that $L_k \in \mathcal{S}$, or, they themselves are logical operators. Given that $\overline{L}$ is a logical operator, there must be one $\overline{L}_k$ that is a logical operator with width less than or equal to r, providing the desired contradiction. With the observation that we necessarily have at least one logical operator with a one-dimensional support for a stabilizer group which is generated by local two-dimensional stabilizer generators, we conclude the proof that there exists a constant energy barrier between two orthogonal ground states of commuting Pauli Hamiltonian in two-dimensions.

The discussed work of Bravyi and Terhal has been extended in a number of different directions. In Ref. (Landon-Cardinal and Poulin, 2013), it is shown that given a local *topologically ordered* commuting Hamiltonian, that there always exists a noise model that can locally create a logical operation on the ground space of the model at no more than a constant increase in system energy, thus extending the result of Bravyi and Terhal to a more general class of systems. We remark also on the work due to Haah and Preskill in Ref. (Haah and Preskill, 2012) where it is shown that two-dimensional stabilizer models cannot even support *partial self correction*, a weaker notion of self correction that we discuss later in Subsec. VII.A. This result is obtained by consideration of the lattice geometry of the one-dimensional support of the logical operators of two-dimensional commuting Pauli Hamiltonian models.

Supporting the discussed general results in two dimensions, there is also a plethora of physically motivated results in the literature that typically consider the prototypical case; the toric code model. Among the approaches include a study of topological entanglement entropy (Kitaev and Preskill, 2006; Levin and Wen, 2006) for the toric code model in the thermal equilibrium state, see Refs. (Castelnovo and Chamon, 2007; Iblisdir *et al.*, 2009, 2010). In Refs. (Iblisdir *et al.*, 2009, 2010) it is identified that in realistic systems the topological entanglement entropy vanishes in the large system size limit at finite temperature for the general class of Kitaev quantum double models (Kitaev, 2003). Further physically motivated study includes the rigorous proof of instability in the toric code model using the Liovillian open dynamics to show that the expectation values of the logical operators of the toric code model decay rapidly when weakly coupled to a Markovian environment (Alicki *et al.*, 2009). These results are generalized in Ref. (Chesi *et al.*, 2010a), and are considered for the toric code with higher-dimensional spins in Ref. (Viyuela *et al.*, 2012).

In addition to the physically motivated no-go results we also remark on the result due to Hastings (Hastings, 2011) which shows that commuting two-dimensional models are unable to support topological order at finite temperature. Similar conclusions were derived by Nussinov and Ortiz by consideration of lattice models in Refs. (Nussinov and Ortiz, 2008, 2009a,b) using methods that were later improved in Ref. (Chesi *et al.*, 2010a). Results such as these are particularly important with respect to finite-temperature perturbative stability, which we regard as a required condition for a stable quantum memory. The results of Hastings are supported numerically as discussed by Wootton in Ref. (Wootton, 2013), where he compares the topological order of unstable memories at finite temperature with stable interacting models. These numerical results are discussed later in Subsec. VI.D.

---

[1] Proof by induction. We obtain $L = 2(r-1)^2$ with solution $a = 2(r-1)$ and $b = 0$. Assume true for $L = a(r-1) + br$ for all $L \geq 2(r-1)^2$. In the case that $a > 0$ we obtain $L + 1 = a'(r-1) + b'r$ with values $a' = a - 1$ and $b' = b + 1$. If $a = 0$ we choose $a' = 2r - 1$ and $b' = b - 2(r-1) + 1$, which satisfies $a' + b' =$ even, since b is even.

B. No-Go Results in Three Dimensions

Thus far we have seen that no-go theorems are very restrictive against energy barriers in two-dimensional systems. It is shown that both commuting topologically ordered Hamiltonians, and commuting Pauli Hamiltonians in two dimensions necessarily support at most a constant energy barrier. In this Section we discuss known results in three dimensions. Here, the landscape of local Hamiltonians is much more rugged. Indeed, we will observe that no-go theorems for three-dimensional models are often superseded by models that avoid the assumptions of a given theorem in a physically sound way.

The first general no-go result in three dimensions is given in Ref. (Yoshida, 2011). Here, the methods of (Kay and Colbeck, 2008) and (Yoshida and Chuang, 2010) are used to show that three-dimensional Pauli Hamiltonians that are translationally invariant, and have a constant ground state degeneracy, must have a one-dimensional logical operator, which can be produced with energy cost independent of the system size.

The work of Yoshida has been supported by physically motivated results that study the three-dimensional toric code model (Hamma *et al.*, 2005c) following various approaches. Castelnovo and Chamon study the topological contributions to the entanglement entropy of the three-dimensional model in its Gibbs equilibrium state in Ref. (Castelnovo and Chamon, 2008). They find that, while some topological order parameters remain robust up to a critical temperature, a qubit cannot be stored in the three-dimensional toric code at finite temperature because loop-like order parameters decay rapidly in the large system size limit. Similar results are anticipated using the methods of Alicki *et al.* in Ref. (Alicki *et al.*, 2010), where they study the thermal dynamics of the three-dimensional toric code model by considering the model weakly coupled to a Markovian thermal reservoir.

Pleasingly, it has been explicitly shown that one can surpass the no-go theorem of Yoshida. In Ref. (Haah, 2011), Haah constructs a translationally invariant three-dimensional Pauli Hamiltonians with a macroscopic energy barrier. The model, commonly known as the cubic code, does not have a constant ground state degeneracy, and thus avoids the no-go theorem of Yoshida. We discuss this model in detail in Sec. VII.B.

Following the discovery of the cubic code, Haah succeeded Yoshida's no-go theorem in Ref. (Haah, 2013). He uses an elegant representation of the Pauli group to show that translationally invariant three-dimensional commuting Pauli Hamiltonians can support at best an energy barrier that scales logarithmically with the size of the system. Subsequently, Michnicki demonstrated an explicit example of a Pauli Hamiltonian model that supports a power-law energy barrier, which is not translationally invariant, known as the welded toric code model (Michnicki, 2012, 2014). In this model the energy barrier of the non-commuting logical operators are varied by changing the size of the system over different length scales. No-

tably, the welded code has a constant two-fold ground state degeneracy, and only violates the translational invariance assumption of the Yoshida proof. We discuss the welded toric code in Sec. VII.C.

Finally, we remark on a recent result given in Ref. (Pastawski and Yoshida, 2014). There the authors show that there is a trade off for three-dimensional commuting Pauli Hamiltonians between their capability to support an energy barrier and the fault-tolerant quantum gates that can be achieved by local operations within the ground space of the Hamiltonian. Specifically they considered commuting Pauli Hamiltonians that can perform a fault-tolerant non-Clifford logical operation by local operations. They show Hamiltonians with such a property cannot support a macroscopic energy barrier. This result is obtained by extending the results of Ref. (Bravyi and König, 2013). An example of such a code which performs a non-Clifford gate, namely the $\pi/8$-gate, by applying the $\pi/8$-gate locally to each of the physical qubits, is the three-dimensional color code (Bombin and Martin-Delagado, 2007b). Indeed, this model is not expected to support finite temperature stability, as it falls into the class of models described by the no-go theorem due to Yoshida.

C. On No-Go Results

In this Section we have considered several no-go results. Known no-go theorems identify two large classes of two-dimensional models that cannot support a macroscopic energy barrier; commuting Pauli Hamiltonians, and topologically ordered commuting Hamiltonians. In addition we have discussed no-go theorems showing three-dimensional commuting Pauli Hamiltonians are constrained in their ability to support a power law energy barrier if they are translationally invariant. These results are summarized in the Venn diagram shown in Fig. 9. Importantly, we provide specific models as examples of the general categories that demonstrate the corresponding behavior.

The no-go results significantly restrict the models we might consider in two-dimensions for finite temperature quantum memories. In particular, it is shown that commuting two-dimensional models cannot support topological order at finite temperature (Hastings, 2011), and conversely that commuting topologically ordered models cannot support a macroscopic energy barrier (Landon-Cardinal and Poulin, 2013). These are very restrictive findings given that we demand perturbative stability for a quantum memory, which is assured with the condition of topological order. Nevertheless, it is not known that topological order is necessary for perturbative stability. As such, there may exist perturbatively stable models that are not topologically ordered that can support a macroscopic energy barrier (Landon-Cardinal and Poulin, 2013). With this in mind, there may still exist commuting two-dimensional models that are suitable as
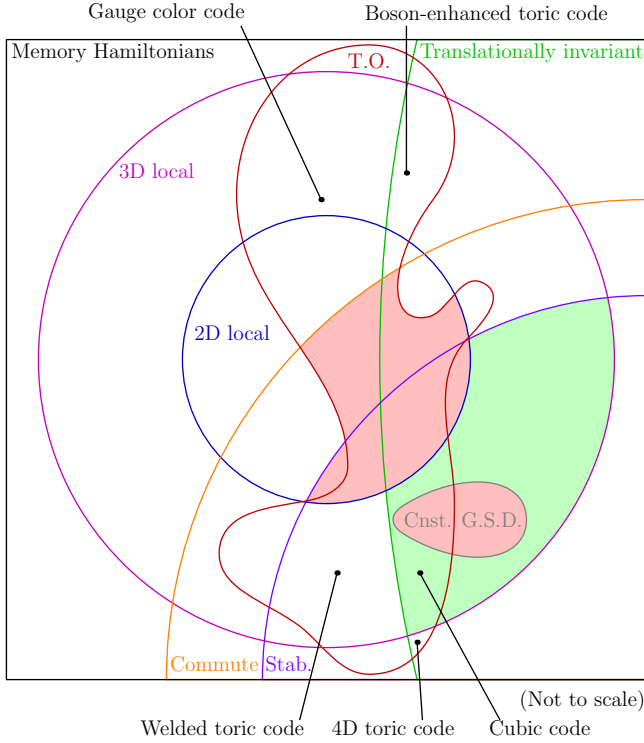
FIG. 9 The landscape of no-go theorems in the space of candidate memory Hamiltonians. Two- and three-dimensional models are shown in magenta and blue circles. Commuting and stabilizer models are shown inside the orange and purple circles. Translationally invariant models are within the green circle. Models satisfying topological order conditions are inside the region enclosed by the red line. Three-dimensional models with a constant ground state degeneracy lie inside the grey circle. Regions shaded red have been proven to support an energy barrier that does not scale with the size of the system. Areas shaded in green correspond to models that have energy barriers that scale at best logarithmically with system size. We mark some specific examples of models that we will discuss later in the Review.

quantum memories.

Another approach to overcoming no-go results in two-dimensional topologically ordered systems is to simply violate their physical assumptions. One area of stable quantum memories that has attracted notable interest are *interacting anyon models*. In general, achieving such systems requires the violation of the locality assumption of the discussed no-go theorems. Considerable work has been conducted to find condensed-matter systems that give rise to an effective interacting anyon theory in a local setting. Interacting anyon models are the topic of Sec. VI.

Further, as we have touched upon in this Section, we can obtain positive results for macroscopic energy barriers in three-dimensional commuting Pauli Hamiltonians. In Sec. VII we review three-dimensional models including *the cubic code model*, a translationally invariant model with logarithmic energy barrier, and the *welded*

toric code model, that obtains a power law energy barrier by breaking translational invariance.

Curiously, we see in Sec. VII that the power-law energy barrier of the welded toric code does not provide any practical macroscopic protection as we might had expected given its favorable properties. Results such as these that contradict our best understanding of stability provide an opportunity to achieve deeper insights into what physical features could ensure stability at finite temperatures. These model require further study and may be helpful to refine our existing no-go results.

Beyond commuting Pauli Hamiltonians there may exist stable quantum memories based on two- or three-dimensional non-commuting Hamiltonians. Due to the difficulty in analytical and numerical calculations for such models, these classes of systems are less well understood compared with their commuting counterparts. However, interesting results have emerged in the field of *subsystem codes*, see for instance Refs. (Bacon, 2006; Bravyi, 2011; Bravyi and Terhal, 2009). A subsystem code of particular recent interest is the gauge color code (Bombin, 2013, 2014). We discuss Subsystem codes in Sec. IX.

Finally, we note that the presented general no-go theorems only rule out the possibility of energy barriers in certain classes of models. One might try to sidestep these no-go theorems by finding an alternative method to prevent a finite temperature environment from corrupting information in the ground space of a quantum memory. We discuss work towards finding such alternatives in Sec. VIII.

In the next Section we give consideration to both classical and quantum systems that are known to be thermally stable. Unfortunately, known quantum systems that are proven to be thermally stable are local in dimensions larger than three. Nevertheless, such analysis gives constructive insights into the properties that give rise to a finite temperature quantum memory.

V. THERMAL STABILITY IN HIGH DIMENSIONS

Thermal stability in classical systems became well-understood with the discovery of Peierls' argument (Peierls, 1936). It shows us that in statistical mechanics stability increases with dimensionality. In this Section we follow this trend in the quantum realm. We consider high-dimensional generalizations of well-studied quantum memories to arrive at systems that support finite-temperature stability. Disappointingly, this approach has not yet uncovered a stable model with dimensionality smaller than four. However, to take a positive outlook on the results summarized in this Section, it is demonstrated that finite-temperature stability is not fundamentally inhibited by quantum mechanics. Furthermore, the consideration of high-dimensional quantum models that support finite-temperature stability may enable us to develop a new intuition of thermal stability, and, may inspire the discovery of a stable quantum mem-

ory in lower dimensions.

In this Section we review the seminal case of finite-temperature stability by studying the famous two-dimensional classical Ising model. We go on to describe the four-dimensional toric code model; the first quantum model that is provably stable at finite temperature. We conclude this Section with a further high-dimensional generalization, namely, the six-dimensional color code model. This model supports both finite-temperature stability, and a set of fault-tolerant operations that can implement universal quantum computation.

A. Stability in Classical Models

In this Subsection, we review the Peierls argument of stability in the two-dimensional classical Ising model (Ising, 1925). The Peierls' argument (Peierls, 1936), later refined by Griffiths (Griffiths, 1964), shows that the critical phenomena of the Ising model are dependent on its dimensionality. For a modern overview of the Peierls' argument, and other important topics relating to the Ising model, we refer the reader to Ref. (Huang, 1987). A comprehensive numerical study of this model as a classical memory is presented in Ref. (Day and Barrett, 2012).

While we have more sophisticated methods of extracting the phase diagram of the two-dimensional Ising model due to its exact solution by Onsager (Onsager, 1944; Yeomans, 1992), the intuition developed from Peierls' original argument is a very useful tool for understanding the stability of models where no exact solution is known, see, for instance, Refs. (Bonati, 2014; Lebowitz and Mazel, 1998). Indeed, Peierls' argument is used to demonstrate the stability of the high-dimensional quantum systems. It is therefore instructive to give a detailed discussion of Peierls' argument applied to the simplest case.

We consider the Ising model defined on an $L \times L$ periodic square lattice of $V = L^2$ spins on its vertices, as shown in Fig. 10. The spin variables σ_j take two values, ± 1, and interact via nearest-neighbor interactions described by the classical Hamiltonian

$$E(\boldsymbol{\sigma}) = -\frac{1}{2} \sum_{\langle j,k \rangle} \sigma_j \sigma_k, \qquad (37)$$

where $\langle j, k \rangle$ denote pairs of vertices that are connected by edges of the square lattice, and $\boldsymbol{\sigma}$ is a configuration of all lattice spins. The model behaves as a classical memory that stores a single bit in its two-fold degenerate ground space, where the bit is encoded in the magnetization of the system, $\overline{\sigma} \equiv \sum_j \sigma_j / V$. The ground states of the model are $\overline{\sigma} \pm 1$, such that the state $\overline{\sigma} = \pm 1$ corresponds to the configuration where $\sigma_j = \pm 1$ for all j, respectively.

In practice, the Ising model exists at finite temperature. At non-zero temperature the probability of finding the system in the ground state vanishes in the thermodynamic limit. However, for the purpose of storing a
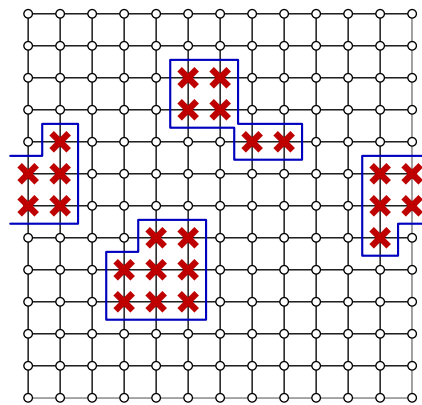

FIG. 10 A configuration of the periodic two-dimensional Ising lattice. Spins lie on vertices, and interactions are represented by the edges of the square lattice. Initially, the spins are oriented along the same direction indicated. Flipped spins are marked by red crosses. In general, patches of flips occur in 'droplets'. The energy penalty introduced by flipped droplet scales like its boundary, marked in blue.

bit of information, it is sufficient to measure the sign of the magnetization provided it remains non-zero. It is expected that the magnetization will maintain the correct sign in the ordered phases of the system. To this end, we must check that the thermal average of the absolute value of the magnetization, $\langle |\overline{\sigma}| \rangle$, remains non-zero in the thermodynamic limit for some suitably low but finite temperature.

The argument begins by considering a spin configuration with respect to Hamiltonian (37). In Fig. 10 we have a lattice of spins that are mostly in the $+1$ state, shown by white circles, with regions, or 'droplets', of flipped spins in the $\sigma_j = -1$ state. We show three such droplets in the example configuration by patches of red crosses. The Hamiltonian will impose a unit energy cost for each pair of nearest-neighbor spins that have opposite states. As such, the energy cost of a droplet is proportional to the length of its boundary. These boundaries are known as *Peierls contours*, indexed by b, and are marked in blue in Fig. 10. We note that a contour is a *single closed droplet boundary* and that in general a given configuration can contain many contours. The probability then that a state is in a given configuration from a thermal Gibbs distribution is $p(\boldsymbol{\sigma}) = \exp(-\beta E(\boldsymbol{\sigma}))/\mathcal{Z}$, where $\mathcal{Z} = \sum_{\boldsymbol{\sigma} \in C} e^{-\beta E(\boldsymbol{\sigma})}$ is the partition function and C is the set of all possible configurations.

To determine $\langle |\overline{\sigma}| \rangle$, we begin by finding an approximation to the simpler value $\langle N_- \rangle$; the thermal average of the number of spins in the -1 state, for configurations where spins in the $+1$ state are dominant, i.e. $\overline{\sigma} > 0$. We refer to regions of $\sigma_j = -1$ as lying 'inside' the boundary. In order to evaluate $\langle N_- \rangle$, we first estimate the number of spins found inside a given contour. Consider a contour with a single trivially closed loop of length l. Here, the upper bound on flipped spins is $l^2/16$. This is because the largest number of flipped spins for a given fixed contour

length occurs when the droplet is square with sides of length $l/4$. For the more general case on the lattice with periodic boundary conditions, one can find droplets that span the lattice with a disjoint boundary of two parts with $l \sim 2L$. In this case, we find an upper bound of $l^2/8$ flipped spins before the number of spins in state -1 become dominant. We use this approximation to rewrite the operator

$$N_-(\boldsymbol{\sigma}) \leq \sum_b \frac{l_b^2}{8} \delta_b(\boldsymbol{\sigma}), \tag{38}$$

where operator $\delta_b(\boldsymbol{\sigma}) = 1$ if $\boldsymbol{\sigma}$ contains contour b, and 0 otherwise, and l_b denotes the length of contour b.

For Eqn. (38) to be meaningful, we must bound the number of contours b that have length l. A boundary must be a closed loop. However, we can find a crude estimate for the number of closed loops by calculating the number of random walks of length l can occur on a lattice of volume V that start at any initial position. A walk can begin from one of V possible points. The first step moves in one of four possible directions, and subsequently, to avoid moving backwards, we choose from only one of three possible directions. With these assumptions we find $4 \cdot 3^{l-1} V$ possible paths. This method will count each closed loop l times, as a given contour can begin from any of the l faces that the contour crosses. We therefore arrive at an upper bound for the number of configurations $4 \cdot 3^{l-1} V/l$. This approximation enables the estimate

$$\langle N_- \rangle \leq \frac{V}{6} \sum_{l=4,6,\ldots} l 3^l e^{-\beta l}, \tag{39}$$

where we have also used that the thermal average for configurations containing contour b of length $l_b = l$ is suppressed by a Boltzmann factor $\langle \delta_b \rangle \sim e^{\beta l}$. We take the infinite volume limit to obtain

$$\langle N_- \rangle \lesssim 27 V e^{-4\beta} \frac{2 - 9e^{-2\beta}}{(1 - 9e^{-2\beta})^2}, \tag{40}$$

for $e^{-2\beta} < 1$. By symmetry we find an equivalent value for $\langle N_+ \rangle$ over configurations where $\overline{\sigma} < 0$.

We return to the initial problem of obtaining $\langle |\overline{\sigma}| \rangle$. We divide the set of all configurations $\boldsymbol{\sigma} \in C$ into two subsets; C_+ and C_-, where $C_\pm$ contains configurations with a greater number of ± 1 spins. Configurations with $\overline{\sigma} = 0$ will not contribute to magnetization, and we therefore neglect them. We then have that

$$\langle |\overline{\sigma}| \rangle = \sum_{\boldsymbol{\sigma} \in C_+} \overline{\sigma} p(\boldsymbol{\sigma}) - \sum_{\boldsymbol{\sigma} \in C_-} \overline{\sigma} p(\boldsymbol{\sigma}). \tag{41}$$

As, by definition, configurations in C_+ have at least $V/2$ spins in the $+1$ state, we can use that $\sum_{\boldsymbol{\sigma} \in C_+} \overline{\sigma} p(\boldsymbol{\sigma}) \geq 1/2 - \langle N_- \rangle/V$. Similarly, we use the relationship $\sum_{\boldsymbol{\sigma} \in C_-} \overline{\sigma} p(\boldsymbol{\sigma}) \leq \langle N_+ \rangle/V = \langle N_- \rangle/V$ to arrive at

$$\langle |\overline{\sigma}| \rangle \geq 1/2 - 2\frac{\langle N_- \rangle}{V}. \tag{42}$$

We see from Eqn. (40) that Eqn. (42) has solutions larger than zero for finite values of β, independent of system size, thus demonstrating stability.

B. Stable Quantum Models of High Dimension

In the previous Subsection we studied suitable conditions for finite-temperature stability by considering the equilibrium state of the two-dimensional classical Ising model. This model is in stark contrast with its one-dimensional counterpart (Ising, 1925), which does not have a finite-temperature phase transition. Instead, it has thermal dynamics akin to those of the two-dimensional toric code model. Indeed, it is a well understood principle of statistical mechanics that the stability of a model will increase with dimensionality.

Following this reasoning, Dennis et al. (Dennis et al., 2002) showed, using a Peierls' argument, that the generalized toric code in four dimensions has a finite critical temperature, below which the model is thermally stable. The four-dimensional toric code is defined on a hypercubic lattice. Qubits are placed on the faces of the lattice, f. The interactions of the model are six-body operators associated to the links l and the cubes c of the lattice. Link operators, A_l, are the tensor product of Pauli-X operators on the faces f which include link l in the boundary of each face ∂f. Similarly, cube operators, B_c, associated to cube c, are the tensor product of Pauli-Z operators on the face qubits that lie on the boundary of the respective cube ∂c. We define the four-dimensional toric code Hamiltonian as

$$H_{\text{4D toric}} = -\sum_l A_l - \sum_c B_c, \tag{43}$$

where the link and cube operators are given by

$$A_l = \prod_{\partial f \ni l} X_f, \quad B_c = \prod_{f \in \partial c} Z_f, \tag{44}$$

respectively. The logical operators of the model are supported in two-dimensional planes which, in four dimensions, intersect at a single point. Each qubit in the model supports four A_l operators, and four B_c operators, such that excitations of the four-dimensional model are not point like particles, but instead are line-like particles created by two-dimensional membrane-shaped operators. These geometric features reproduce the energetics of the two-dimensional Ising model that we have already described. An environment must therefore overcome an $\mathcal{O}(L)$ energy barrier to decohere information encoded in the ground space of the model. The Authors of Ref. (Dennis et al., 2002) used these features of the model and follow a Peierls' argument to show that there is a finite temperature, below which, the model lies in an ordered phase. In this phase quantum information can be maintained for a time that increases exponentially with the size of the system.

As an aside, we remark that the argument of (Dennis *et al.*, 2002) was constructed to show the discussed stable model could be decoded using a local algorithm, i.e. an algorithm that does not require the long-range propagation of classical information. Typically when we consider active error correction, such as the decoder described in App. A, we reasonably assume that the classical computation can propagate messages at an infinite velocity when compared with the velocities associated to the underlying quantum hardware. We are therefore able to design effective decoding algorithms that use syndrome information obtained instantaneously from the entire quantum error correcting code. Realistically, classical computations ultimately can only communicate at a finite rate bounded by the speed of light. The study of thermally stable quantum memories are therefore interesting from the point of view of classical decoding, where benefits might be gleaned from considering quantum error correcting codes that are analogous to thermally stable memories. Interesting new results in the area of local decoding algorithms in low-dimensional systems are found by Herrold *et al.* (Herold *et al.*, 2014). These results may have important applications from the point of view of local thermally stable quantum memories in low dimensions.

While thermal stability is a good indication that we can reliably store quantum information for macroscopic periods of time, as in the case of the two-dimensional Ising model, it is not known by any of the Authors that it has been shown that thermal stability is a sufficient condition for a stable finite-temperature quantum memory. To rigorously prove that a quantum memory has a memory time that grows macroscopically with system size, one must consider the dynamics of a candidate memory with respect to an open environment. Following the result of Dennis *et al.*, Alicki *et al.* rigorously proved the memory time of the four-dimensional toric code grows exponentially with the size of the system when weakly coupled to a Markovian heat bath in Ref. (Alicki *et al.*, 2010). In their work, the Authors develop the open system picture (Davies, 1974) for degenerate many-body quantum systems to measure the decay of correlation functions of the considered models. Their results rely on *quantum dynamical semigroups* (Alicki and Lendi, 2007). The development of their method leading to their result was built over a series of papers (Alicki and Fannes, 2009) and (Alicki *et al.*, 2009), where in the former the abstract dynamical picture is constructed, and the latter Reference shows logical operator correlations for the two-dimensional toric code decay rapidly compared with its higher-dimensional counterpart. These results provide an important extension of the work of Dennis *et al.*, as they rigorously account for the dynamics of the system.

Finally, we remark on extensions to the study of high-dimensional quantum systems. Consideration of Peierls' argument suggests that a phase transition occurs at the temperature where the Peierls contours percolate over the system with high probability. The recent work of Hastings *et al.* (Hastings *et al.*, 2014a) shows, using mean-field arguments and supporting numerical evidence, that as dimensionality increases, the critical temperature of the transition diverges from the temperature at which Peierls contours percolate. This is well understood in the classical case of the D-dimensional Ising model (Lebowitz and Mazel, 1998). The study of high-dimensional quantum memories generalizes known classical results and offers new insights into the physics of phase transitions and critical phenomena.

C. Thermally Stable Quantum Computation

We conclude this Section with a discussion on the more general problem. What is the smallest dimensionality where we obtain both thermal stability and the desirable feature of a gate-set that can be executed fault-tolerantly to realize universal quantum computation? This problem has been approached by Bombin *et al.* (Bombin *et al.*, 2013). The authors consider D-dimensional generalizations of the color code models (Bombin and Martin-Delagado, 2007a). These models are of particular interest due to the extended set of gates they can achieve on their ground states *transversally*. A logical gate on the ground space of the code is executed transversally when one can perform said gate by applying the desired logical operation independently to each of the physical degrees of freedom of the model. This is a favorable approach to performing gates as local operations on individual degrees of freedom do not propagate errors during their application. In general, the available transversal gates of a given model are limited by its microscopic details. Notably, the two-dimensional color code (Bombin and Martin-Delagado, 2006) can perform the Clifford gate-set transversally. Together with the noisy preparation of magic states (Bravyi and Kitaev, 2005), the Clifford gate-set achieves universal quantum computation. It has also been discovered that a three-dimensional color code can achieve fault-tolerant universal quantum computation (Bombin and Martin-Delagado, 2007b). Transversally, this three-dimensional model can achieve a $\pi/8$-gate, and a controlled-not gate. Together with the ability to prepare and measure the ground space in the logical X- and the Z-basis, this model achieves universal quantum computation. Sadly however, the three-dimensional color code does not support finite temperature stability, as it is shown by the three-dimensional no-go theorem due to Yoshida (Yoshida, 2011). To achieve a universal gate-set and have stable excitations akin to those of the two-dimensional Ising model within the color code family of models one needs $D = 6$ (Bombin *et al.*, 2013). Together with preparation and measurement in both the Pauli-X, and Pauli-Z basis, the six-dimensional color code is compatible with the transversal application of the $\pi/8$-gate, and the controlled-not gate, which gives rise to universal fault-tolerant quantum computation.

Six dimensions are by no means a lower-bound on the

system dimensionality where both of these features co-incide. Instead, it is a first estimate on the smallest required dimensionality for a system with both of these properties that is to be improved upon. The result is obtained for the restricted case of models of commuting two-level physical systems. One may indeed be able to reduce the discovered critical dimension by considering many-body systems composed of higher-dimensional spins or fermionic degrees of freedom (Bombin *et al.*, 2013). Moreover, this result is restricted to models that give rise fault-tolerant quantum computation by transversal gates. Indeed, quantum coding theory has shown that universal transversal operations are known to be incompatible with stabilizer error correction (Anderson and Jochym-O'Connor, 2014; Eastin and Knill, 2009; Zeng *et al.*, 2011). The diligent reader may question this remark as to how the stabilizer models the three- or six-dimensional color code achieves a universal set of operations given known restrictions on universal transversal gate sets. Indeed, its transversal gate set is not truly universal, but, as pointed out earlier, its universal set of operations are completed by the ability to prepare and measure in both the Pauli-Z and Pauli-X basis. We finally remark that perhaps we may find stable low-dimensional systems with universal fault-tolerant operations by considering different types of fault-tolerant operations other than transversal gates.

VI. INTERACTING ANYON MODELS

As we have discussed in Subsec. II.E, the syndrome of two-dimensional topological stabilizer codes can be interpreted in terms of point-like anyonic quasiparticles. This leads to some favorable properties, such as the simple structure of the stabilizer space and the intuitive means by which the syndrome may be decoded. However, as explained in Sec. IV, it is precisely this point-like nature that prevents the creation of diverging energy barriers that, by their turn, can lead to self-correcting behavior.

One path towards self-correction is to consider models with all the advantages of two-dimensional topological codes, but which are nevertheless able to realize self-correcting behavior. Interacting anyon models have been proposed to this end. All consider coupling a toric or planar code, the case of toric code Hamiltonian defined with open boundary conditions, to an external system, and then using this to mediate interactions between the anyons. These interactions change the energy landscape of the anyons, and can lead to diverging energy barriers for logical errors. Here we review the different types of anyonic interactions. We go on to review proposals to generate them.

A. Forms of Anyonic Interaction

To understand interacting anyon models, it is useful to first make a distinction between stabilizers and projective anyon number operators. The toric code stabilizers, introduced in Subsec. II.D, are known as star and plaquette operators, denoted A_v and B_p respectively. Star and plaquette operators have eigenvalues ± 1. A state where a vertex v or a plaquette p of the toric code lattice holds an anyon lies in the -1 eigenspace of its corresponding stabilizer. Vacuum states, where no anyon lies within a plaquette or vertex, lie within the $+1$ eigenspace of all the stabilizers.

By convention the stabilizer space corresponds to the $+1$ eigenspace of all stabilizers. We can use stabilizer operators to define projectors onto the common -1 eigenspace of the code, and hence onto anyon states, such that

$$n_v = \frac{1}{2}(\mathbb{1} - A_v), \quad n_p = \frac{1}{2}(\mathbb{1} - B_p). \qquad (45)$$

We call these projectors anyon number operators, as their eigenvalues are the anyonic occupation of vertex v or plaquette p.

For local Hamiltonians, the replacements $A_v \to -n_v$ and $B_p \to -n_p$ defines an equivalent Hamiltonian, up to a constant shift in energy. However, interacting Hamiltonians that use n_j projectors lead to different physics. To illustrate this point, we consider the example of two different Hamiltonians that describe interactions between a single pair of vertices, which we index 1 and 2. These Hamiltonians are

$$H_s = -A_1 - A_2 - \frac{1}{2}A_1 A_2, \quad H_n = -A_1 - A_2 + n_1 n_2. \quad (46)$$

The first two terms ensure that the ground state is that of anyonic vacuum. The remaining term is an interaction.

The A_1 and A_2 terms contribute an energy penalty of 1 for each anyon present in both cases. The $A_1 A_2/2$ term contributes an energy penalty of 1 when there is a single anyon, but nothing when there are two. The $n_1 n_2$ term contributes nothing for a single anyon, but an energy penalty of 1 for a pair of anyons.

The different behavior of H_s and H_n lead to different interpretations about what form the interactions take. For H_n the $n_1 n_2$ only contributes when multiple anyons are present. We therefore call it an anyon-anyon interaction. The $A_1 A_2/2$ term of Hamiltonian H_s contributes only when there is both an anyon on one vertex and vacuum on the other, so we call it an anyon-vacuum interaction. In what follows we consider both of these interaction types extended over the entire lattice.

B. Interacting Anyon Hamiltonians

The first proposals for interacting anyon models considered anyon-anyon interactions of the form

$$H_{\mathrm{AA}} = \Delta H_{\mathrm{toric}} + V \sum_{k} \sum_{k' \neq k} n_k n_{k'} \, U(r_{kk'}), \qquad (47)$$

with H_{toric} defined in Eqn. (14), values Δ and V are arbitrary coupling constants, indices k denote all stabilizers, both vertices and plaquettes, and $r_{kk'}$ is the Euclidean distance between k and k'. The first term here is the standard stabilizer Hamiltonian and the second is the anyon-anyon interaction.

1. Logarithmic Potential

In Ref. (Hamma *et al.*, 2009) the following attractive potential was proposed

$$U(r_{kk'}) = \ln r_{kk'}. \qquad (48)$$

Note that this diverges with distance, leading to a diverging energy barrier of $\mathcal{O}(\ln L)$. This potential has a confining effect for temperatures of $T < V/2$. In this regime, all anyons present in the code will typically be within an $\mathcal{O}(1)$ distance of each other. A logical error is caused when a single anyon breaks free and winds around the torus. This corresponds to a random walk in an $\mathcal{O}(\ln r_{kk'})$ potential formed by the other anyons, from which the typical coherence time $\tau = \mathcal{O}(L^{V\beta})$ can be found. This diverges polynomially with L, and has an exponent that increases as temperature decreases.

For higher temperatures the model continues to have a diverging coherence time. This is due to a different mechanism, described in more detail below. The scaling in this case is $\tau = \mathcal{O}(L^2)$ (Wootton, 2013). Note that, though this remains polynomial, the exponent no longer depends on temperature.

This analysis applies only to the toric code. For the planar code (Bravyi and Kitaev, 1998; Dennis *et al.*, 2002) a single anyon can be created at a boundary. Since this has no other anyons to confine it, it does not experience a $\tau = \mathcal{O}(L^{V\beta})$ coherence time for any temperature. Instead the coherence time scales as $\tau = \mathcal{O}(L^2)$ for all temperatures.

An interaction of this form can be mediated by coupling the anyons to a two-dimensional lattice of hopping bosons. Only local couplings are needed to produce interaction (48). However, the coupling strength must diverge with system size to realize the potential. This violates a requirement for a self-correcting memory; that of bounded interactions. Nevertheless, note that these diverging couplings are not directly responsible for the increasing lifetime, since the physical energy scales remain finite. Moreover, the model needs to be fine tuned. Small perturbations in the hopping couplings of the bosons can cause the long-range interactions to become short-range

and thus stop the effectiveness of the model. The model is an important proof of principle for self-correcting memories with local interactions, even if it is not physically viable.

2. Power-Law Potential

In Ref. (Chesi *et al.*, 2010b) the interactions have the following repulsive potential

$$U(r_{kk'}) = r_{kk'}^{-\alpha}, \; \alpha \geq 0. \qquad (49)$$

At first glance this would appear to be ineffective. The potential does not diverge with distance and in fact it decays in general such that the energy barrier for the creation and separation of a pair is finite. Furthermore, the potential is repulsive, making anyons less likely to annihilate once created than in the non-interacting case. Nevertheless, when the interactions are sufficiently long range, $\alpha < 2$, they have a strong beneficial effect.

The simplest case to consider is that of $\alpha = 0$, where the potential does not decay over distance but remains constant. The energy of the system does not depend on the positions of anyons in this case, only their number N. Every anyon repels every other one with an energy V. The energy above the ground state is then

$$E_N = N\Delta + \frac{V}{2} N(N - 1). \qquad (50)$$

Note that this grows quadratically with N, rather than simply linearly as in the non-interacting case. A similar superlinear scaling of energy with anyon number occurs for other $\alpha < 2$ as well as the logarithmic potential above.

By using simple arguments, it is possible to find a lower bound on the coherence time for the $\alpha = 0$ case. Since we can realistically only expect a finite energy density, i.e. states with $E_N = \mathcal{O}(L^2)$, the system is limited to states with $N = \mathcal{O}(L)$ anyons at most. This would correspond to an infinitely sparse anyon configuration, with a distance of $\mathcal{O}(\sqrt{L})$ between each pair of anyons created by the thermal noise. The time required to cause a logical error is then no less than that required for random walks over this length scale, and so $\tau = \mathcal{O}(L)$.

Using a more careful treatment it can be shown that the number of anyons is suppressed further than the above argument implies. This leads to a longer coherence time which, for general $\alpha < 2$, scales like $\tau = \mathcal{O}(L^{2-\alpha})$. This is a polynomial scaling that is quadratic in the best case. This effect is also responsible for the $\tau = \mathcal{O}(L^2)$ scaling of coherence time for the logarithmic potential we met above.

The power law potential can be mediated by interaction with cavity modes. This is a non-local interaction, but is nevertheless reasonable up to a cut-off system size. The self-correcting behavior is therefore not truly scalable, as we require. However, it may still be possible to achieve system sizes that are useful in practice.

C. Anyon-Vacuum Interactions

More recently, interacting anyon model proposals have focussed on engineering couplings between anyons and vacuum rather than anyons with other anyons. It is found that this approach allows significantly more powerful self-correction. The first studies of such models are found in Refs. (Hutter *et al.*, 2012b; Pedrocchi *et al.*, 2011).

These proposals consider Hamiltonians of the form

$$H_{\text{AV}} = \Delta H_{\text{toric}} - V \sum_k \sum_{k' \neq k} S_k S_{k'} \, r_{kk'}^{-\alpha}. \qquad (51)$$

Here S_k are the stabilizer operators, either A_v or B_p depending on whether each k is a vertex or a plaquette. The only difference between this Hamiltonian and that of the power law potential above is the substitution of anyon number projectors n_k with stabilizer operators S_k.

To compare H_{AV} with that for the anyon-anyon case, H_{AA}, we can rewrite it in terms of anyon number operators. This yields

$$H_{\text{AV}} = \mu(L) \sum_k n_k - 4V \sum_k \sum_{k' \neq k} n_k n_{k'} \, r_{kk'}^{-\alpha} + \text{const.} \qquad (52)$$

The first term here is the effective anyon gap, the energy that an anyon must overcome in order to be created

$$\mu_k(L) = \Delta + 4 \sum_{k'} (1 - \delta_{k,k'}) r_{kk'}^{-\alpha}. \qquad (53)$$

The large energy penalty for creation is due to the anyons being repelled by the majority of plaquettes and vertices, which are in the vacuum state. The second term in Hamiltonian (52) is an attractive and non-divergent anyon-anyon attraction.

The effects of thermal errors are suppressed first by the anyon gap, which significantly slows the creation of anyons. Once anyons have been created, errors are further suppressed by the attractive potential that favors reannihilation. Let us focus on the effects of the anyon gap.

To suffer a logical error, an error must first occur on a single qubit. This will create at least n anyons, where $n = 1$ for the planar code, for the case where a qubit is created on the boundary, and $n = 2$ for the toric code. These n anyons will feel a repulsion from all the $\mathcal{O}(L^2)$ plaquettes and vertices on which there is vacuum. This results in the energy gap $\mu(L) = \mathcal{O}(L^{2-\alpha})$ for each anyon when $\alpha < 2$. The typical time before the first error occurs on is then $e^{\beta n \mu(L)}$.

It is this timescale that dominates the lifetime of the code. Other factors must be taken into account to fully deduce the lifetime: the number of qubits on which it is possible for an error to occur; the probability that a pair, once created, will cause a logical error; and the time required for an anyon to diffuse across the code. However, these will contribute factors that are polynomial in L at most. They are insignificant in comparison to the exponential timescale to overcome the anyon gap. As such,
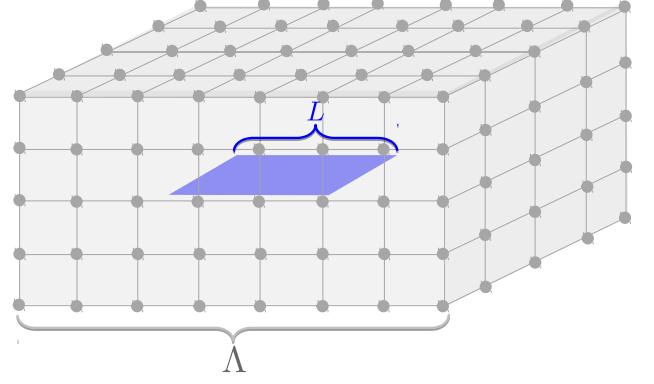

FIG. 11 Anyon-Vacuum interactions in a $L \times L$ code can be induced by embedding it in a Λ^3 lattice of hopping bosons for $\Lambda > L$. The stabilizers of the code locally couple to the bosonic lattice. The interactions are mediated by the low-energy collective excitations of the bosons.

we can simply say that $\tau = e^{\beta n \mu(L)} = e^{\beta \mathcal{O}(L^{2-\alpha})}$. Note that the higher n for the toric code will result in asymptotically longer lifetimes than the planar code, assuming all else is equal.

The main difference between proposals with this interaction is the physical system used to mediate it and the value of α that is achieved. Refs. (Hutter *et al.*, 2012b; Pedrocchi *et al.*, 2011) achieve the optimal case of $\alpha = 0$ by coupling to cavity modes. However, as above, this prevents the model from achieving the scalability that we require. A Hamiltonian simulation of this case was considered in (Becker *et al.*, 2013).

In Ref. (Pedrocchi *et al.*, 2013) the interaction is mediated by coupling to a three-dimensional lattice of hopping bosons, as shown in Fig. 11. The resulting interacting model corresponds to that of $\alpha = 1$. This gives rise to an energy barrier of $\mu(L) = \mathcal{O}(L)$ and coherence time $\tau = e^{\beta \mathcal{O}(L)}$. This model uses only local, bounded strength and constant weight interactions, and yet is able to preserve the quantum information for an exponentially long time. This provides the strongest proof-of-principle model currently known, satisfying all the *required* conditions we have set for self-correcting quantum memories. The model has bosonic operators that are unbounded and are not embeddable in two dimensions. For these reasons, the proposed model does not satisfy all *desirable* conditions for laboratory realization. However, we remark that it is possible to place the toric or planar code on one of the external sides of bosonic lattice. This would still allow much of the experimental accessibility that makes two-dimensional models desirable.

A related model was also proposed in Ref. (Hutter *et al.*, 2012a) by the same authors. Here the role of the bosons is played by magnons in a three-dimensional ferromagnet. The code is simply coupled to the spins of the ferromagnet, avoiding the need for unbounded operators. Perturbative gadgets (Bravyi *et al.*, 2011a, 2008) are used in order to realize the entire Hamiltonian using

only local two-body interactions on a three-dimensional system of spin-half particles.

The effective interacting anyon model in the case of the ferromagnet is the same as for the three-dimensional boson lattice. However, it is only expected to be valid in the low energy and low wavelength limit, where the coupling of the code to a thermal bath is much weaker than the coupling to the ferromagnet. The Monte-Carlo simulation of thermal noise described in Subsec. III.D therefore cannot be used. This approximates the true dynamics by allowing the thermal bath to instantaneously transfer large energies to the system, and so is unable to capture the subtle effects arising from the full time evolution of the system-bath interaction. It is in these effects that we would expect to observe self-correcting behavior. Since a study of this time evolution seems intractable, the full extent of the self-correcting behavior in this model is not known. This model can also be adapted to protect systems for which errors correspond to infinitely weak coupling to an infinite temperature bath (Kapit *et al.*, 2014).

D. Finite-Temperature Topological Order

Given a model with topological order at zero temperature, it is important to determine how high the temperature can be raised while topological order is retained. For many, the order disappears for any non-zero temperature (Chesi *et al.*, 2010a; Nussinov and Ortiz, 2008, 2009a,b). Indeed, it has been shown by Hastings that local commuting Hamiltonians in two dimensions are incompatible with a condition for topological order at finite temperature (Hastings, 2011). Some models however have a finite temperature phase transition.

The relationship between this behavior and self-correction is not completely known (Yoshida, 2011). It is often assumed that finite temperature topological order is required for self-correction. However, it is not entirely clear that this is the case. Self-correction is very much a feature of the dynamics of a model, whereas topological order is evaluated at thermal equilibrium. Despite that lack of concrete general results, we can gain an insight by considering specific models. See for instance Ref. (Mazáč and Hamma, 2012) where the topological entanglement entropy and coherence times of the toric code are studied on lattices of varying dimensionality. The interacting anyon models are also shown in Ref. (Wootton, 2013) to provide an interesting perspective on this problem. We review these results here.

The signature of topological correlations in systems such as the toric code are loop correlations. For finite temperature systems these can be found using the topological entropy (Hamma *et al.*, 2005a; Kitaev and Preskill, 2006; Levin and Wen, 2006), topological mutual information (Iblisdir *et al.*, 2009) or anyonic topological entropy (Wootton, 2013). In all cases one must consider a region of the system whose size is on the order of the (arbitrarily large) system size. If topological correlations

are detected for these arbitrarily large regions, the state is said to be topological ordered.

For power law anyon-anyon interactions, any finite temperature thermal state contains a diverging number of anyons (Chesi *et al.*, 2010b). These anyons will also be deconfined due to the repsulsive nature of the interactions. Such a diverging number of delocalized anyons ensures that topological order according to the above definition is not present for any finite temperature. However, the interactions are still known to support self-correction with a polynomial lifetime. This fact, along with the $\mathcal{O}(1)$ energy barrier, makes these models an interesting exception to widely held opinions about what is required for self-correction.

For the case of the logarithmic anyon-anyon interaction, it is found that the topological order persists up to a finite temperature of $T_c = v/2$. It therefore corresponds exactly to the confined anyon phase for which the lifetime is $\tau = \mathcal{O}(L^{V\beta})$. Beyond this temperature the topological order is no longer present, though the system is still self-correcting with a lifetime of $\tau = \mathcal{O}(L^2)$. The phase transition does not have the effect of destroying the self-correction, as we might expect, but it does alter the scaling of the lifetime.

To regain some semblance of our intuition that topological order is required at finite temperature for self-correction, we can redefine what we mean by topological order. Instead of simply considering whether topological correlations can be detected for regions on the order of the arbitrarily large system size, we can determine exactly what the range of these correlations is. This means considering regions of different sizes, seeing how the topological correlations decay as the size is increased, and then determining a correlation length to quantify this. This correlation length is denoted λ.

Even when a system is not topologically ordered, it is possible for topological correlations to be present on an $\mathcal{O}(1)$ length scale. The case of $\lambda = \mathcal{O}(1)$ therefore corresponds to topologically trivial states. Standard topological order requires that the correlations do not decay at all even up to the linear system size, L. This corresponds to a super-extensive $\lambda > \mathcal{O}(L)$. In between these extremes there exists the possibility for the range λ to increase with system size, but just not as quickly as is required for standard topological order. We refer to such states as *weakly topologically ordered.*

Studying the interacting anyon models from this perspective, it has been shown that all models at all temperatures are either in a standard or weakly topologically ordered phase (Wootton, 2013). All transitions between these two types of topological order correspond to a change in the way that the lifetime scales with system size. All known self-correcting memories correspond to phases that are either topologically ordered or weakly topologically ordered. As such, some relationship between finite temperature topological order and self-correction does persist. However, it would be interesting to determine whether counter examples exist even

for this weaker relationship.

VII. COMMUTING THREE-DIMENSIONAL MODELS

With limitations challenging the construction of finite-temperature quantum memories with commuting two-dimensional Hamiltonians, it is exciting to consider three-dimensional models. Indeed, as discussed in Sec. IV there are still no-go results towards the feasibility of a finite-temperature quantum memory in three dimensions. However, these results are considerably less restrictive. Recently proposed models have shown positive progress, which, together with supporting numerical data offer promise for the discovery of good quantum memories at finite temperature. In this Section we provide an overview of the positive results found in three-dimensional models. We first review the concept of partial self correction; a new paradigm for macroscopic coherence time scaling that has emerged from the study of three-dimensional models. In Subsection VII.B we study the cubic code model, a quantum system demonstrating partial self correction. In Subsections VII.C and VII.D we review other three-dimensional proposals that break translational invariance to achieve phenomena potentially important for self correction in quantum systems.

A. Partial Self-Correction

A new phenomenon to develop from studying three-dimensional systems is that known as *partial self correction*. Partially self correcting models are notable for polynomial coherence-time scaling with system size up to some cut-off size that depends on temperature. Moreover, they exhibit super-exponential inverse-temperature scaling. These features of known partially self-correcting models are attributed to its energy barrier, which grows logarithmically with the size of an error incident to a memory.

Partially self-correcting models have been discovered independently by both Haah (Haah, 2011), and by Castelnovo and Chamon (Castelnovo and Chamon, 2011). The known models were found by following remarkably different methods. In Ref. (Haah, 2011), the author exhaustively searches over all translationally invariant stabilizer models on a cubic lattice with one or two spins on each vertex of the lattice to find models that satisfy the 'no-strings' condition. Such models are expected to provide good protection against decoherence caused by environmental interactions. Indeed, it was later proved that models satisfying the no-strings condition have at least a logarithmic energy barrier (Bravyi and Haah, 2011b). Independent of the work of Haah, Castelnovo and Chamon (Castelnovo and Chamon, 2011) looked to find a quantum generalization of known classical models that have non-trivial energy barriers between

ground states which are well known in the context of glassy systems (Garrahan and Newman, 2000). The derived generalization is described locally in three dimensions. Similar models are studied in further generality in Ref. (Kim, 2012).

We now give a heuristic analysis explaining partial self correction. Known partial self-correcting memories are characterized by an energy barrier that grows logarithmically with the size of an error, ξ. The energy cost ϵ of an error that fits inside a region of size ξ is thus at least

$$\epsilon \sim \kappa \Delta \log \xi, \tag{54}$$

where κ is a positive constant and Δ is the gap of the model. Given the typical finite-temperature noise analysis we described in Sec. III, we assume that errors are created with an average separation that scales with β like $\Lambda \sim e^{\beta \Delta / 3}$, where the factor of $1/3$ arises due to the dimensionality of the system. Given then that we require $\xi \sim \Lambda$ for the memory to decohere, we arrive at the typical excitation energy of the model as a function of β. Namely, we obtain $\epsilon \sim \kappa \Delta^2 \beta / 3$ at the point of decoherence. Applying this to Arrhenius' law, Eqn. (21), we obtain

$$\tau \sim e^{\kappa \Delta^2 \beta^2 / 3}. \tag{55}$$

We can follow a similar analysis to study small system sizes such that $L \lesssim \Lambda$. In this case a diffusing error must attain energy $\epsilon \sim \kappa \Delta \log L$. Once again, applying this expression to Arrhenius' law it follows that partially self-correcting quantum memories have a coherence time that grows polynomially in system size

$$\tau \sim L^{\kappa \Delta \beta}, \tag{56}$$

whose exponent is linear in β. This scaling is effective up to some cutoff $L_{\text{opt.}} \sim \Lambda$. We thus obtain a cutoff, $L_{\text{opt.}} \sim e^{c\beta}$, that grows exponentially in β for positive constant, c (Haah, 2013).

An interesting feature of the known partially self-correcting models is that they do not have a constant ground-state degeneracy, which is outside the assumptions of the no-go theorem of Yoshida (Yoshida, 2011). As an aside, it is interesting to consider that the known partially self-correcting models are not *purely* topological models. While the ground space of these systems are topologically ordered in the sense that the degenerate ground states of the model cannot be locally distinguished, their ground-state degeneracy still depends on the local physics of the model. A similar model whose ground-state degeneracy depends on microscopic details (Bravyi *et al.*, 2011b) is introduced by Chamon in Ref. (Chamon, 2005). We remark however that unlike the cubic code, the model due to Chamon is known not to give rise to self-correcting properties (Castelnovo and Chamon, 2011; Chamon, 2005; Nussinov *et al.*, 2012). From this example it follows that system-size dependent ground state degeneracy is not a sufficient condition for partial self correction. we finally remark that the study
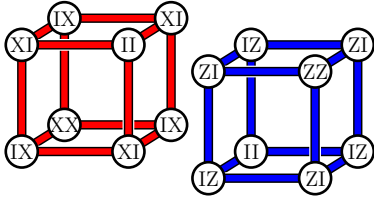
FIG. 12 The S_j^X and S_j^Z stabilizers for the three-dimensional cubic code model. The model is defined on a cubic lattice with two qubits on each vertex where Pauli operators X, Y, Z and the identity I can act.

of exotic partially self-correcting systems has led to new classifications of systems under the context of *fractal topological quantum field theories* (Haah, 2014; Yoshida, 2013).

In the following Section we will review and reproduce previously obtained numerics of the rigorously studied cubic code model. We remark that the fragile glassy model introduced by Castelnovo and Chamon is expected to behave in a phenomenologically equivalent way to the cubic code model (Castelnovo and Chamon, 2011).

B. The Cubic Code

The cubic code model (Haah, 2011) is defined on a three-dimensional lattice of $L \times L \times L$ vertices, where two qubits lie on each vertex of the lattice. Associated to each of the fundamental cubes of the lattice, indexed j, we have two stabilizers S_j^X and S_j^Z shown in red and blue in Fig. 12, respectively. We then write the Hamiltonian

$$H_{\text{cubic}} = -\frac{1}{2} \sum_j \left(S_j^X + S_j^Z \right). \qquad (57)$$

We take constant interaction strength $1/2$ such that excitations have unit energy cost. The model has a non-trivial ground state degeneracy that varies with L. The ground state degeneracy is studied in detail in Ref. (Haah, 2013) using the language of commuting free modules. For simplicity, we consider only lattices of size $L < 200$ that do not have factors 2, 15 or 63. All of these system sizes have a four-fold ground state degeneracy (Bravyi and Haah, 2011a). We do not discuss the complex fractal structure of the logical operators of the model here, but we refer the interested reader to Ref. (Haah, 2013). We point out however that for lattices of odd L, we find two logical operators by taking $\overline{X}_1 = \prod_{k \in \mathcal{L}} X_k$, $\overline{Z}_1 = \prod_{k \in \mathcal{L}} Z_k$, $\overline{X}_2 = \prod_{k \in \mathcal{R}} X_k$ and $\overline{Z}_2 = \prod_{k \in \mathcal{R}} Z_k$, where $\mathcal{L}$ and $\mathcal{R}$ denote the subset of all the left and right qubits of each vertex, respectively. It is easily checked that these operators satisfy a suitable algebra for the logical qubits of the model. These of course are not the minimum-weight logical operators (Bravyi and Terhal, 2009). However, we find these logical operators particularly convenient for numerical simulations.
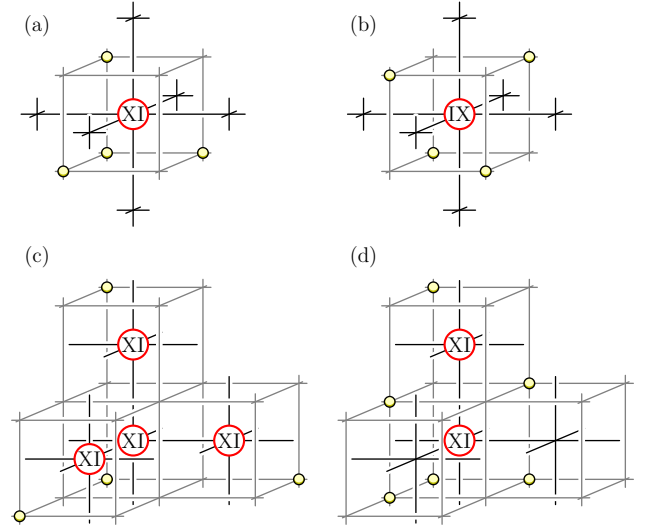

FIG. 13 The cubic lattice shown in black where two spins lie on the vertices of the lattice. The dual lattice that supports excitations is shown in grey. (a) and (b) show the excitations generated by an XI and an IX error to a single two-spin vertex, respectively. Both errors generate four point-like excitations, marked on vertices of the dual lattice in yellow. (c) The error configuration that creates four excitations delocalized over two lattice spacings. (d) A high-energy intermediate error configuration that is likely to be achieved to delocalize four excitations over a long distance.

1. Excitations of the Cubic Code

The excitations of the cubic code have a more complicated structure to those of the two-dimensional models considered in earlier Sections. Indeed, the model was designed such that its excitations are created by operators that satisfy the no-strings rule (Haah, 2011), and instead have a fractal-like structure. In Fig. 12 we can observe a symmetry over the S_j^X and S_j^Z stabilizers, such that both Pauli-X and Pauli-Z type errors act with equal effect on the S_j^Z and S_j^X stabilizers of the model. A study of only Pauli-X type errors therefore serves for a sufficient study of the excitations of the cubic code.

Pauli operators acting on single qubits of the lattice in the ground state create four localized excitations to the dual lattice of the model, shown in Figs. 13(a) and (b). We mark the stabilizers violated by the error by yellow points on the vertices of the dual lattice, where vertices of the dual lattice correspond to fundamental cubes of the primal lattice. Similar to the excitations of the string-like models we have already discussed, these particles are delocalized. Also, the excitations are their own anti-particles, which are transported by applying additional error operators that annihilate excitations, and create additional excitations at other locations on the lattice. In this way, it is possible to delocalize these excitations over arbitrary distances. We show an error configuration in Fig. 13(c) where four fundamental excitations have delocalized over two lattice spacings.
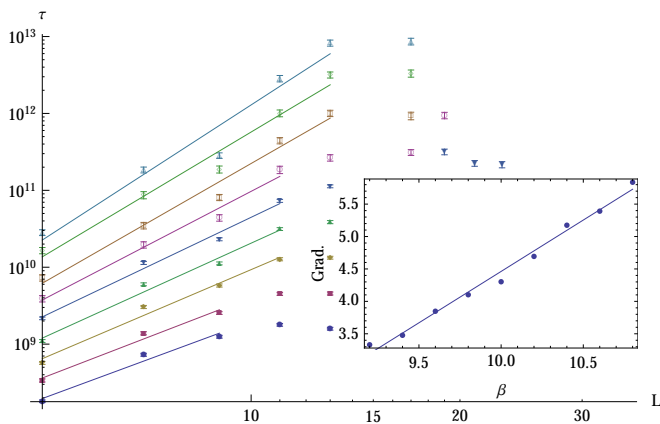
FIG. 14 Coherence times as a function of system size for $\beta = 9.2, 9.4, \ldots, 10.8$. . (Inset) The gradients in this regime grow like $\tau \sim L^{1.58\beta - 11.38}$.

An important distinction between the excitations of the cubic code model and excitations in two-dimensional models is that the delocalization of these particles cannot be achieved using string-like operators. Instead, if we wish to delocalize the excitations of the cubic code model over arbitrary distances, we have to use transport operators that have a fractal-like support. As a finite temperature noise model will only apply transport operators to the lattice via local single qubit operations, such operators are only achieved by temporarily increasing the energy of the error configuration, which reduces the propagation of excitations. In Fig. 13(d), we show an intermediate error configuration necessary to delocalize excitations over two lattice sites.

The error configuration creates six excitations, which increases the energy of the system. Models where excitations are not propagated by string-like operators satisfy the 'no-strings rule'. This is an important concept for partial self correction. An extensive program of analytical study from Bravyi and Haah has proved that models satisfying the no-strings rule necessarily has at least a logarithmic energy barrier (Bravyi and Haah, 2011b). Further work in this program of research showed numerically that the cubic code model behaves as a partially self correcting memory with a logarithmic energy barrier (Bravyi and Haah, 2013).

In the remainder of this Subsection we numerically simulate the cubic code at finite temperature to demonstrate its partial-self correcting behavior.

2. Numerical Simulations

In this Subsection we simulate the cubic code coupled to a finite temperature environment using the numerical Monte Carlo methods described in Subsec. III.D. We reproduce the phenomenological behavior demonstrated by Bravyi and Haah in Ref. (Bravyi and Haah, 2013). We remark that the results we present differ due to the

choice of rate equation used in the simulation. While we use Eqn. (19) discussed in Subsec. III.A, Bravyi and Haah use the rate equation of Ref. (Bortz *et al.*, 1975). Both rate equations are valid as they satisfy the detailed balance given in Eqn. (20), and ultimately will reproduce the same physics, up to some variation in the constant factors we obtain.

We simulate Hamiltonian (57) under rate Eqn. (19). We periodically attempt to decode an eigenstate of the Hamiltonian over time intervals $10^{-10} \cdot e^{4\beta}$ using a variant of the clustering decoder described in App. A. The first time where the decoder fails is the coherence time of the sample. We find the coherence time by averaging over N samples. Errors are determined by the standard deviation of the samples, divided by $\sqrt{N}$. We attempt to decode with very high frequency as this reduces computation time. This is due to the simulation of the thermal noise acting on the cubic code typically becoming very slow as we approach the point of decoherence. Increasing the frequency of decoding reduces the number of error events incident to the lattice before the simulation is over. We identify an error threshold $p_{\text{th.}} \sim 0.0117$ for the decoder we use when tested against an identically and independently distributed noise model where each qubit suffers an error with probability p. These results are shown in Fig. 26 of App. A.

To identify partial self correction in the cubic code we plot the coherence times as a function of L in Fig. 14. Here, we consider many different temperatures to identify polynomial coherence time scaling with system size whose exponent depends on β. We plot the gradients of the linear fittings, shown in the inset of Fig. 14. The gradients we obtain show good agreement with polynomial coherence time scaling whose exponent grows linearly with β, as we expect for partial self correction, derived in Eqn. (56). We also plot the optimal coherence time as a function of system size for a given β, as shown in Fig. 15. We identify super-exponential inverse-temperature scaling, as we expect for a partially self correcting model due to Eqn. (55).

We use the fittings we obtain from the presented numerical data to obtain Δ and κ of Eqns. (55) and (56) for the cubic code model

$$\Delta_{\text{CC}} = 2.0, \quad \kappa_{\text{CC}} = 0.79, \tag{58}$$

thus identifying the partial self correcting behavior described in the previous Subsection. It is shown in Ref. (Haah, 2013) that by imposing translational invariance on three-dimensional commuting Pauli Hamiltonians we cannot expect to find a system where the energy barrier scales better than logarithmically with system size. In the remainder of this Section we consider commuting Pauli-Hamiltonian models that surpass the result of Haah (Haah, 2013) by breaking translational invariance. The models of interest are the welded three-dimensional toric code (Michnicki, 2014), and embeddable fractal product codes (Brell, 2014).
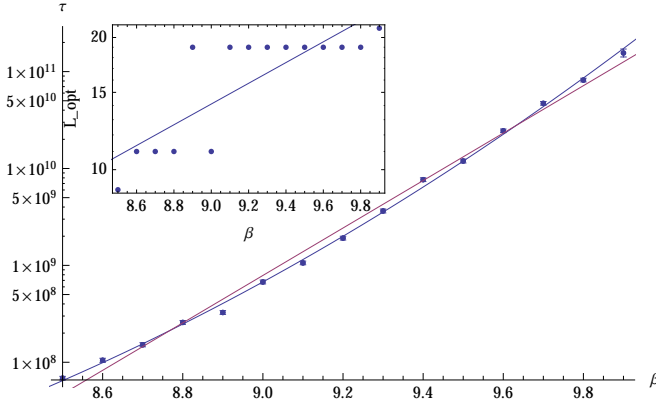
FIG. 15 Coherence times as a function of inverse temperature, where we choose system size, $L_{\text{opt.}}$, to find the best available coherence time, shown in the inset. We find a fitting $\tau \sim e^{1.05\beta^2 - 13.7\beta + 58.5}$. The linear fit is $\tau \sim e^{5.6\beta - 30.3}$. The inset shows $L_{\text{opt.}} \sim e^{0.54\beta - 2.2}$.

C. The Welded Toric Code

The welded-toric code (Michnicki, 2012, 2014), due to Michnicki, is the first explicit example of a three-dimensional commuting Pauli Hamiltonian with a power-law energy barrier. Remarkably, the model surpasses the no-go result of Haah (Haah, 2013) by breaking the translational invariance assumption that is required to complete the theorem.

The model is found using an idea called *welding*, described in (Michnicki, 2012). Welding gives a procedure to combine stabilizer codes. The advantage of welding codes is that logical operators are also combined nontrivially over a weld. We follow the exposition of Michnicki showing how he arrived at the welded toric code.

The welded toric code is achieved by welding a macroscopic number of copies of the three-dimensional toric code (Hamma *et al.*, 2005c). The three-dimensional toric code is defined on a cubic lattice with spins on the lattice edges. The model has two types of stabilizer, vertex operators, and face operators, as shown in Fig. 16(a). Vertex operators are six-body operators of Pauli-X operators supported on the edges incident to a vertex. Face operators are four-body Pauli-Z operators supported on edges that bound faces of the cubic lattice.

With a suitable choice of boundary conditions the three-dimensional toric code will support one logical qubit. The model has two types of boundaries; rough boundaries and smooth boundaries. We show a macroscopic picture of the code in Fig. 16(b), where we have a rough boundary on the top and bottom face of the lattice. Later, we will refer to one copy of the three-dimensional toric code that encodes a single logical qubit as a *block*.

There are two types of logical operators, membrane logical operators, and string logical operators, shown in red and blue respectively in Fig. 16(b). The membrane logical operators have dynamics akin to those of the two-
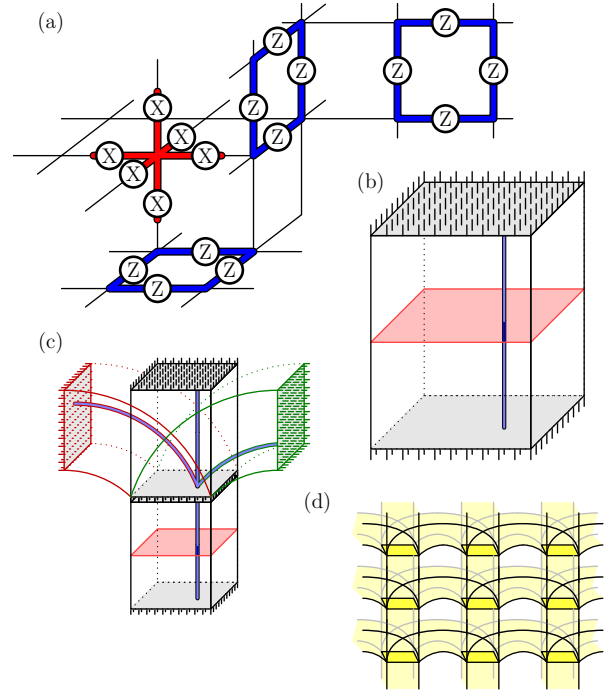

FIG. 16 (a) The vertex and face operators of the three-dimensional toric code are shown in red and blue, respectively. Vertex operators are the tensor product of Pauli-X operators supported on all the edges adjacent to a vertex and face operators are the tensor product of Pauli-Z operators supported on the edges that bound a face of the lattice. (b) The three-dimensional toric code with two disjoint rough faces. The model supports one encoded qubit described by a membrane logical operator, shown in red, and a string-like operator, shown in blue, that runs between the two disjoint rough edges. (c) A single weld between the rough faces of four blocks of three-dimensional toric code. We outline one block in red and one block in green where the blocks are overlapping. The string-like logical operators of the original code blocks now must overcome the a high energy barrier at the interface between the welds. (d) Many blocks of three-dimensional toric code are welded into a lattice. In this welded configuration, the string-like logical operators are combined into a two-dimensional operator that spans the lattice.

dimensional Ising model, and as such are stable below a critical temperature, (Alicki *et al.*, 2010; Castelnovo and Chamon, 2007). However, string-like logical errors introduce point-like anyonic excitations whose creation and transport need only overcome a finite energy barrier. It is for this reason that a thermal noise model is able to introduce string-like logical errors in constant time. The three-dimensional toric code therefore does not behave as a self-correcting quantum memory.

Michnicki surpasses the problem of string-like logical operators using welding. He shows that it is possible to weld blocks of three-dimensional toric code along rough faces to generate a large energy barrier. We show an example of a weld in Fig. 16(c), where four copies of the three-dimensional toric code are welded along a common rough boundary. The diagram shows that the string-

like logical operator divides at the weld. A single anyon therefore cannot pass through a weld from one code block to another, but must instead split into $v - 1$ where v is the valency of the weld, i.e. the number of code blocks that meet at the weld. Since these excitations must overcome an energy barrier to propagate across the weld, the diffusion of errors is suppressed.

Michnicki combines many three-dimensional toric code blocks in a lattice-like structure with dimensions greater than one to generate a macroscopic energy barrier over the string-like logical operators of the model. We show such a lattice of two dimensions in Fig. 16(d). Now, the string-like logical operators of the composite parts of the code are combined into a coarse lattice whose vertices are welded faces and whose edges are code blocks. Interestingly, the model has interactions resembling high-dimensional Ising-like interactions across the welded boundaries, separated by three-dimensional blocks of toric code lattice. With this lattice configuration, thermal fluctuations must overcome a polynomial energy barrier in the number of welds of the macroscopic welded lattice to introduce a logical error to the model.

The membrane logical operator of a code block is not extensive with the number of welded interfaces of the lattice. In fact, the membrane logical operator can be supported on a single block used in the weld. To scale the power-law energy barrier correctly, the volume of the blocks must grow with the size of the welded lattice. Michnicki (Michnicki, 2014) suggests scaling the volume of the block size like polynomially with the number of welds in the lattice. It is with this point that we see the model breaks translational invariance; we can vary the size of the model over two different length scales, the block size, and the volume of the lattice of welds.

1. Limitations of the Welded Toric Code

The welded toric code model shares many similarities to the Ising model, with the code blocks in the former serving a similar function as the nearest neighbor ferromagnetic couplings, or 'bonds', in the latter. We now discuss this analogy to find a better understanding of the finite temperature behavior of the welded toric code.

We consider the simple case in which we do not know the full details of the anyon configuration within each code block. Instead we know only the total parity of the number of point-like anyons that each block contains. Each code block then has two possible states: even or odd parity. These correspond to the two possible states of a bond of the Ising model: aligned and anti-aligned. In general we are able to determine the locations of all the anyons in a code block. However, since the anyons of the code blocks become disordered after a constant time, information regarding their locations becomes irrelevant. For this reason the total parity of each code block will be the only useful syndrome information after thermalization occurs. The error correction procedure of the welded toric code is then equivalent to that of the corresponding Ising model.

The parity of a code block is changed only if a point-like excitation moves through one of its welds, which occurs only if an error occurs on one of the qubits involved in a weld. We refer to a weld that has suffered an odd number of errors as 'broken'. Breaking a weld is equivalent to flipping the spin on a vertex of its corresponding Ising model. A region of broken welds (flipped spins) will be surrounded by a surface of odd parity codes (anti-aligned bonds). To perform a logical error, these surfaces must be removed by breaking all welds or flipping all spins, respectively.

Given this correspondence between the welded toric code and the Ising model, we may expect the former to inherit the exponential lifetime and finite temperature phase transition of the latter. However, this is not the case, since the welds of the welded toric code experience temperature differently from the spins of its corresponding Ising model. We observe that due to the $\mathcal{O}(L^2)$ area of each weld, for code blocks of size $L \times L \times L$, the probability that any given weld is broken after the constant thermalization time converges exponentially to $1/2$ as $L \to \infty$. It follows from this that the probability of finding any code block in odd parity also quickly converges to $1/2$ as the model approaches the thermodynamic limit. For the Ising model at effective inverse temperature $\tilde{\beta}$, the probability of finding a bond in anti-alignment approaches $1/2$ only as $\tilde{\beta} \to 0$. Equating these probabilities it is clear that $\tilde{\beta}$ vanishes as $L \to \infty$. Hence, the welded toric code at finite temperature corresponds to an Ising model with an effective temperature that diverges with system size, and so it does not fare well as a memory in the thermodynamic limit.

We next consider the low-temperature behavior of the welded code. To decay encoded information, the thermal environment must overcome a macroscopic number of welds. The most energetically challenged process for a weld to break is for an error to occur on a qubit involved in a weld. This event happens at a constant rate $\sim e^{-\beta v}$ where v is the valency of the welded lattice and excitations have unit mass. A weld breaks then at a rate $r_1 \sim L^2 e^{-\beta v}$ where we include an L^2 term to account for the size of the welded surface. High-energy processes such as creation on a weld are exponentially suppressed with inverse temperature compared with processes that reduce the energy of the system and we might thus expect the Hamiltonian to reverse the effects of thermal errors. Indeed, this is ultimately why the two-dimensional Ising model performs as an effective memory in its ordered phase.

In spite of having favorable energetics that are analogous to those of the Ising model, at low temperatures we expect to observe processes that break the weld at a rate much quicker than r_1, which are due to the large volume of qubits within each code block involved in a weld. These processes are summarized in Fig. 17. To analyze the low-energy processes we examine the sur-
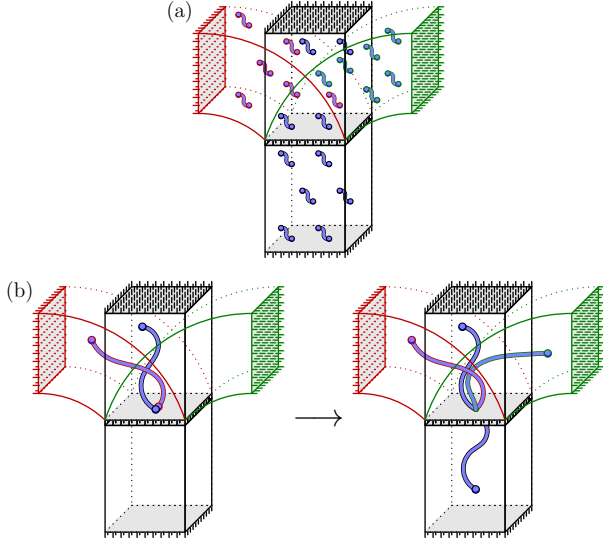
FIG. 17 (a) The blocks that make up the welded code contain an excitation gas of density $\rho \sim e^{-\beta}$ at thermalization. (b) A zero-energy process. If $v/2$ excitations of different blocks meet at a common point on a v-valent weld, a weld can be broken at no energy cost.

face of a weld. A single excitation created within a code block cannot pass the weld without incurring a high energy cost. However, if multiple excitations from different blocks meet at the same point along the weld, the excitations can pass through at a low energy cost. We make use of the ideal gas equation, $PV = nRT$, to show that we can expect these low energy processes to occur most commonly in the low-temperature limit.

We model the excitations that have occurred in a single block of volume $V = L^3$ as an ideal gas of anyons of density $e^{-\beta}$, as shown in Fig. 17(a), which is achieved quickly as the model approaches equilibrium. Using that the number of point excitations in a given block is $n = Ve^{-\beta}$ and that $T = 1/\beta$, the excitation pressure on the boundaries of a given block follows from the ideal gas equation

$$P \sim e^{-\beta}/\beta, \qquad (59)$$

where we take the gas constant, R, as unity. Using that the pressure is the rate at which excitations fall on a particular point on the boundary, we find the rate at which multiple excitations from different blocks of the weld meet at a common point, as shown in Fig. 17(b). If $v/2$ point particles from $v/2$ different blocks that are welded at a face meet at a common point, a weld can be overcome at no energy cost. This event occurs at a rate $r_2 \sim L^2 P^{v/2}$ where the L^2 term comes from the size of the welded face. We compare this rate with r_1, the rate at which errors occur on a membrane to find

$$\frac{r_1}{r_2} \sim \beta^{v/2} e^{-\beta v/2}, \qquad (60)$$

which vanishes in the limit that $\beta \to \infty$. This shows that low energy processes are the dominant processes in the

low-temperature limit and we thus argue that the energy barrier will be ineffective in this regime. We obtain the same conclusion by modeling the free motion of excitations using other physically reasonable dynamics.

By consideration of low-energy processes and heuristic calculations we have argued that we cannot easily predict the thermal behavior of the welded model by simple understanding of its non-trivial energy barrier or by application of Arrhenius' law. Further analysis and numerical study will be necessary to interrogate its coherence time scaling. It will certainly be interesting to learn if the model supports self correction or partially self-correcting behavior at any intermediate size or temperature regime. Careful study of the model may allow us to derive new no-go theorems for finite-temperature stability that rely on a clearer understanding of entropic mechanisms that decohere encoded quantum information.

D. Embeddable Fractal Product Codes

We finally remark on the forthcoming result of Brell (Brell, 2014), where he introduces embeddable fractal product codes. In this Reference, the proposed family of models are mapped onto a classical model known to have a finite-temperature phase transition to argue that the model will be stable below a finite critical temperature.

The model is found using the formalism of homological product codes (Bravyi and Hastings, 2013; Freedman and Hastings, 2014). Homological product codes offers a mechanism of combining pairs of codes that in general live in higher-dimensional spaces. For instance, the middle homological product of two two-dimensional toric codes return the four-dimensional toric code.

In Ref. (Brell, 2014), the Author takes the homological product of two two-dimensional toric codes defined on the graph of a *Sierpiński carpet graph*. This gives a code that resembles the four-dimensional toric code defined on a fractal-like sublattice of the four-dimensional hyper-cubic lattice. The choice of graph enables a local embedding of the product code in three dimensions. To demonstrate the stability of the model, the Author goes on to map the partition function of the product code onto an Ising model defined on a Sierpiński carpet; a model which has been rigorously proved to have a finite temperature phase transition (Campari and Cassi, 2010; Shinoda, 2002; Vezzani, 2003).

The study of the embeddable fractal product codes is in its infancy, and as such has many open questions. For instance, it is yet to be shown that the model can be efficiently decoded. Moreover, the model has an extensive ground state degeneracy. This means we cannot easily apply known perturbative stability results to prove that it is perturbatively stable. Further study of this model may lead to exciting insights towards stable quantum memories.

VIII. OTHER PROTECTION MECHANISMS

Following the restrictive no-go theorems described in Sec. IV for large classes of two-dimensional commuting systems it is interesting to consider other mechanisms that inhibit the long-range propagation of errors. Such study is well motivated as protection mechanisms that do not require a macroscopic energy barrier may be compatible with experimentally amenable two-dimensional models. The purpose of this Section is to discuss other proposed mechanisms for the preservation of quantum information that do not rely on macroscopic energy barriers.

One mechanism studied for zero-temperature coherent noise is that of disorder-assisted protection. In Refs. (Bravyi and König, 2012; Röthlisberger *et al.*, 2012; Stark *et al.*, 2011; Wootton and Pachos, 2011a) it is shown that randomizing the Hamiltonian interaction strengths inhibit the coherent propagation of excitations across the lattice. This is attributed to the Anderson localization effect (Anderson, 1958), where it is understood that randomized Hamiltonian interactions lead to 'friction' in the motion of excitation dynamics due to quasi-particles becoming trapped in small potential minima of the random energy landscape. It is tempting then to believe that randomness might then be useful as a resource for error suppression. However, Anderson localization is not a well understood principle. Remarkably, in Ref. (Bravyi and König, 2012) it is shown that pseudo-random potentials outperform truly randomly chosen potentials. Little study has been conducted with respect to introducing friction to the propagation of excitations in the presence of incoherent thermal noise. Indeed, Anderson localization is a quantum effect, and it is not even clear how one might introduce randomness to a system protect against thermal errors. Nevertheless, it is interesting to consider randomization as a resource to protect quantum information over energetics.

We point out also Ref. (Al-Shimary *et al.*, 2013). Here, the authors consider geometric modifications for the two-dimensional toric-code model on different graphs to find improvements for coherence times with respect to the different types of noise introduced by a thermal environment; both bit-flip and dephasing noise. It is identified that reducing the connectivity of the lattice geometry which embeds the toric code will reduce the rate of one type of noise from decohering the lattice. However, due to the dual structure of the toric code lattice, changing the lattice geometry to protect against one type of noise will detrimentally affect the performance of the lattice against the other type of noise. This approach therefore presents a tradeoff between protection against bit-flip and dephasing noise introduced by a general thermal noise model. Therefore these effects provide a constant improvement in coherence in the presence of an asymmetric noise model that may be present in a realistic experimental setting (Douçot *et al.*, 2003).

In the remainder of this Section we discuss a model recently introduced by some of the present authors (Brown *et al.*, 2014). The model generalizes Kitaev's quantum double models to encourage errors incident to the system to achieve high-energy configurations with high probability in a low temperature regime.

A. Entropically Suppressed Thermal Errors

In this Subsection we describe a two-dimensional model (Brown *et al.*, 2014) that relies exclusively on entropic effects to protect encoded quantum information at finite temperature. The local commuting Hamiltonian has topologically ordered ground states, and as such necessarily has a constant energy barrier between ground states (Landon-Cardinal and Poulin, 2013). Nevertheless under suitable conditions the typical excitations of the model achieve high-energy states with high probability. We see this by consideration of the expected dynamics of commonly occurring excitations. Here we give a heuristic picture of the mechanism that gives rise to entropic behavior by consideration of the anyonic excitation spectrum of the model. For a technical description of the underlying Hamiltonian, we refer the reader to the original Reference.

The entropically protected model makes use of the fusion space of a generalized toric code model defined on a lattice of $L \times L$ vertices with N-level spins on the edges of the lattice. For the reader familiar with quantum double models (Kitaev, 2003), we are considering the quantum double of the group $\mathbb{Z}_N$.

The relevant feature of the generalized toric code model that we discuss here is its anyonic excitation structure. Like the toric code, the generalized model has two types of anyons, electric charges and magnetic fluxes. However, in the generalized model they carry integer charges $1 \leq k \leq N - 1$. We label excitations e_k and m_k. The relevant fusion rules for the model are

$$e_k \times e_l = e_{k \oplus l (\mathrm{mod}\ N)}, \text{ and } m_k \times m_l = m_{k \oplus l (\mathrm{mod}\ N)}. \tag{61}$$

It follows from these fusion rules that the anti-particles of e_k and m_k excitations are $\overline{e_k} = e_{N-k}$ and $\overline{m_k} = m_{N-k}$. Henceforth, we will restrict the discussion to only e_k particles. Due to the symmetries of the model an equivalent discussion holds for m_k particles.

1. Thermal Dynamics

As with the case of the toric code, excitations of the generalized model are free to propagate long distances across the lattice at no energy cost. This introduces large errors to the underlying physical lattice and thus rapidly decoheres information encoded in the ground state. Unlike the toric code, the excitations of the generalized model have a splitting structure where excitations of charge k can divide into two spatially separated excitations of charge j and l provided the charge is conserved, i.e. $j \oplus l = k\,(\mathrm{mod}\ N)$. We write this splitting process
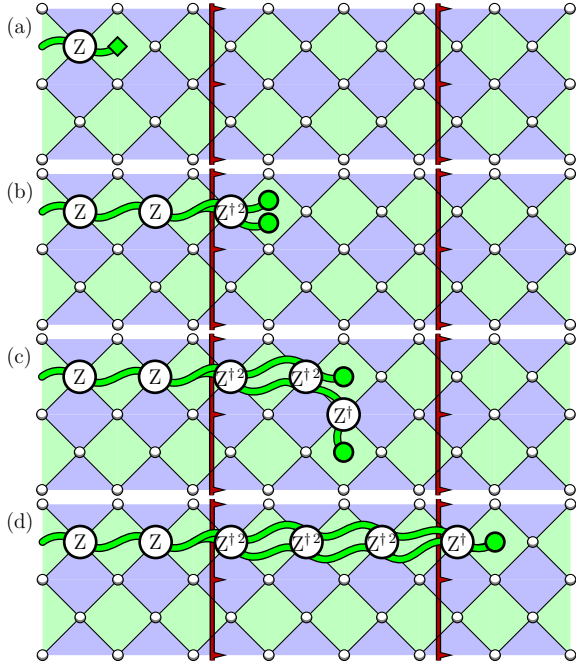
FIG. 18 (a) A single e_4 excitation marked by a diamond. Red defect lines are drawn vertically along the lattice. The positive direction is indicated by small red arrows. (b) The e_4 particle propagates in the positive direction across the defect line to become an e_2 charge. This process is energetically suppressed by the choice of Hamiltonian. (c) A common process for the entropically protected model is for high mass excitations to decay into pairs of low mass excitations. The low mass excitations are confined between the defect lines. (d) In the limit of very low temperatures, the lowest energy process for pairs of low mass excitations to pass a defect line is by recombination. This limits the entropic effects we describe at low temperatures.

$e_k \to e_j \times e_l$. This additional structure follows immediately from the fusion rules (61). Errors incident to the lattice can achieve high energy configurations of many excitations due to the splitting structure of the model. We adapt the generalized toric code to exploit this splitting structure.

To encourage splitting processes to occur when coupled to the thermal environment, we write a Hamiltonian that assigns different masses to excitations of different charges. We choose the masses of the model such that it is energetically favorable for a subset of excitations to split. At this point we consider the explicit case for $N = 5$. We set the Hamiltonian such that masses M_k of particles e_k are such that

$$2M_1 = 2M_4 \leq M_2 = M_3. \tag{62}$$

With this setup, it is energetically favorable for the decay processes $e_2 \to e_1 \times e_1$ and $e_3 \to e_4 \times e_4$ to occur.

With the described setup at moderately low temperatures, and given that the model is initialized in the ground state, the most common process that we expect will decohere the information encoded in the ground

space is the creation of an $e_1 \times e_4$ pair, that will subsequently propagate rapidly across the lattice. The innovation of Ref. (Brown *et al.*, 2014) is the introduction of defect lines that entropically inhibit the long-range low-energy propagation of excitations by encouraging high-energy splitting processes. Defect lines are studied in generality in Ref. (Barkeshli *et al.*, 2014; Kitaev and Kong, 2012). Loosely speaking, in the general theory of defect lines, Hamiltonian terms are modified along a defect line such that when anyonic excitations cross they defect line, they modify their particle type according to some mapping.

The entropically protected model uses oriented defect lines that modify the charge of crossing excitations. We show two vertical defect lines lying on the spin lattice in red in Fig. 18(a) with the positive orientation marked by small red arrows. Importantly, a defect line maps e_k excitations crossing the line in the negative direction onto $e_{k \oplus k}$ excitations, where addition is carried out modulo N. Conversely m_k excitations multiply their charge to become $m_{k \oplus k}$ excitations if they cross the defect lines in the negative direction. The inverse operation occurs if excitations move over the defect line in the opposite direction. Importantly, the defect lines are designed such that if the commonly occurring low-mass e_1 and e_4 excitations cross defect lines in either direction their charge will always be modified to those of high-mass excitations.

We consider the long-range propagation of excitations in a moderately low temperature regime, where low-mass excitations are generated sparsely across the lattice. In Fig. 18(a) an e_4 excitation is shown to the left of the lattice. Due to the choice of masses (62), commonly occurring low-mass excitations are energetically suppressed from moving right across a defect line. The energy penalty reduces the rate of decoherence. The energetically suppressed process is shown in Fig. 18(b).

Once the excitation crosses the defect line, it can continue to propagate right across the lattice and over the next defect line as an e_2 particle with no energy penalty. However, we can configure the model such that this process is highly improbable. Due to the energetics of the model, it is favorable for the decay process $e_2 \to e_1 \times e_1$ to occur. This process is shown in Fig. 18(c). Following the decay process, the two e_1 excitations are confined between its enclosing defect lines, as they are subject to an energy penalty to propagate beyond a defect. Given the freedom to choose the defect line separation, we can optimize the system to make this process highly probable, thus commonly suppressing low-energy diffusion of errors. In what follows we present numerics demonstrating the entropically favorable process describe thus far.

2. Numerical Simulations

We simulate the described model in a thermal environment using the methods we introduce in Subsec. III.D. The data provided here was originally presented in
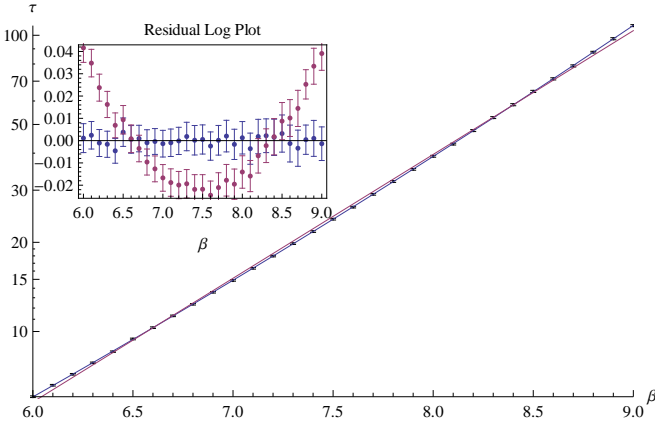
FIG. 19 The coherence time of the entropically protected model as a function of β for a large system size, where $L = 72$ and the separation between defect lines arranged in a square grid alternates between one and two lattice spacings. We identify super-exponential inverse temperature scaling in the considered temperature regime. We show this clearly in the residual log plot shown in the inset of the Figure.

Ref. (Brown *et al.*, 2014). The model is set up with a square grid of defect lines with separations alternating between one and two lattice units. This inhibits the propagation in all directions around the lattice. We choose $M_1 = M_4 = 0.38$ and $M_2 = M_3 = 1$. The system is chosen to embellish the entropic effects using numerically tractable system sizes.

We wish to identify that the common errors incident to the model increase in energy as they diffuse. To demonstrate this behavior we take the partial self correction hypothesis we have introduced in Subsec. VII.A. We use numerical simulations to evaluate the coherence time for varying system sizes L and inverse temperatures β. Coherence time τ is defined as the time at which the probability of successfully decoding the lattice model coupled to the thermal bath that is described by rate Eqn. (19) falls to 99%. We plot τ as a function of β for a large system size $L = 72$. This data is shown in Fig. 19 for $6 \leq \beta \leq 9$. We identify super-exponential coherence time scaling, such that

$$\tau \sim e^{0.028\beta^2 + \mathcal{O}(\beta)}. \tag{63}$$

We find additional evidence for partial self correction by plotting coherence time as a function of system size for small system sizes in Fig. 20. We plot this for many values of β. We find polynomial system size scaling for system sizes smaller than $L = 24$ that scales like

$$\tau \sim L^{0.11\beta - 0.15}, \tag{64}$$

that is evaluated using the fitting of the inset of Fig. 20.

We compare Eqns. (63) and (64) with respect to the partial self-correcting analysis given in Subsec. VII.A to obtain values

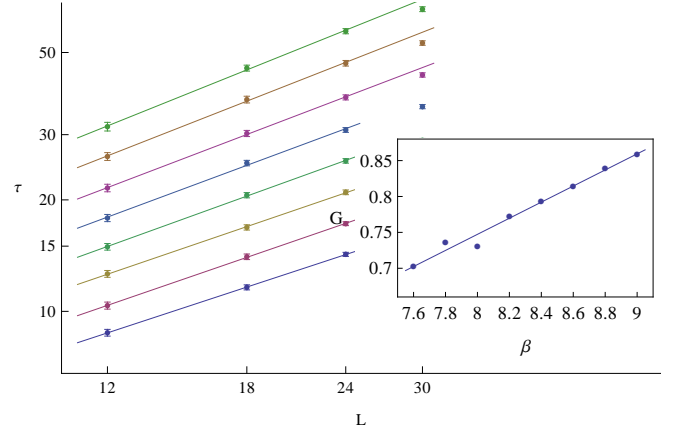$$\Delta_{\mathrm{EP}} \sim 0.5 \text{ and } \kappa_{\mathrm{EP}} \sim 0.2, \tag{65}$$

FIG. 20 Coherence time against system size for small system sizes, for $\beta = 7.6, 7.8, \ldots, 9.0$ The gradient increases linearly with β in the log log plot. We plot the gradients, G, in the inset. We use the fit of the inset to identify $\tau = L^{0.11\beta - 0.15}$.

for the entropically protected model. The positive κ_{EP} value is indicative of error dynamics with excitation masses that grow with the total size of the error. We remark however that unlike the cubic code model, for the choice of defect line separation, these effects are limited to the regime below $\beta \leq 9$, and as such, does not satisfy all the conditions we require of a quantum memory. This is because at very low temperatures, the thermal environment will find lower energy path to propagate excitations, such as that shown in Fig. 18(d). We further remark that these effects are significantly weaker than the data obtained in (58). We give some insights into this in the following Subsection.

B. On Entropic Protection

Entropic protection is an idea very much in its infancy. The model presented in the previous Subsection exclusively makes use of entropic effects for protection against thermal noise. In this Subsection we use the entropically protected model as a basis to discuss the nature of entropic protection compared with energetically protected models, the drawbacks of entropic protection and proposals to overcome these problems.

The numerical results have shown that the entropically protected model imposes very weak error suppression compared with three-dimensional models that rely on macroscopic energy barriers, such as the cubic code model. Indeed, this can be partially explained by relying on probabilistic effects for energetic suppression, instead of using a Hamiltonian with a hard-wired energy barrier, where error suppression occurs deterministically. One could expect to enhance the probabilistic splitting of excitations by careful optimization of parameters, such as defect line separation and bounded Hamiltonian interaction strengths. It will be interesting to understand how the model must be varied as a function of temperature,

and the limits at which entropic protection works reliably. This may help to design new models with a better performance compared with energetically protected models. More importantly still, such a study may help us to learn if it is possible to find an entropically protected model that is robust in the limit of zero temperature.

Further, in the entropically protected model we identify that the entropic protection is only effective above a certain moderately-high temperature. As such, we cannot expect entropic protection in the zero-temperature limit. This is a remarkable feature we have observed in the proposed model. We suggest that this may be because the model relies on the thermal bath as a *source of entropy*; the environment mediates the decay mechanism which suppresses the rate of decoherence. Without sufficient heat, we do not identify the splitting mechanism we describe, and diffusing errors find low energy paths to propagate. Following this thought, it is interesting to consider other mechanisms or sources of randomness that mediate excitation decay for anyonic models with a splitting structure that work independently of bath temperature.

IX. BEYOND COMMUTING HAMILTONIANS - SUBSYSTEM CODES

In this Section we discuss progress towards the study of a class of non-commuting models that has developed over the last decade, namely, the *subsystem codes*. This framework provides a natural extension to the stabilizer formalism that we have relied upon throughout this Review. Amongst the subsystem code literature are three-dimensional models that are conjectured to be self-correcting quantum memories.

Subsystem codes were introduced in Refs. (Kribs *et al.*, 2005, 2006). The language of subsystems was introduced to find a unifying language for decoherence free subspaces (Beige *et al.*, 2000; Duan and Guo, 1997; Lidar *et al.*, 1998; Pachos and Beige, 2004; Palma *et al.*, 1996; Zanardi and Rasetti, 1997) and noiseless subsystems (Kempe *et al.*, 2001; Knill *et al.*, 2000; Zanardi, 2000). Initially coined operator quantum error correction, subsystem codes principally encode logical information in a quantum error correcting code that is embedded in a *subsystem* of a larger Hilbert space. In a subsystem code the remainder of the Hilbert space of the total system is referred to as the *gauge subsystem*.

A general language for subsystem codes is provided in Ref. (Poulin, 2005). A subsystem code is uniquely defined by its gauge group, $\mathcal{G}_n$, a subgroup of the Pauli group of n qubits. Given a gauge group, a stabilizer code is defined on the subsystem acted upon by the normalizer of the gauge group $\mathcal{N}(\mathcal{G}_n)$, i.e. operators that commute with elements of $\mathcal{G}_n$. The stabilizers of the code are also members of the gauge group, $\mathcal{S} = \mathcal{N}(\mathcal{G}_n) \cap \mathcal{G}_n$, whereas logical operators, $\mathcal{L} = \mathcal{N}(\mathcal{G}_n) \backslash \mathcal{G}_n$, commute with, but are not themselves members of the gauge group. It is easily checked that for the special case that $\mathcal{G}_n$ is Abelian, we recover the stabilizer formalism where $\mathcal{G}_n = \mathcal{S}$ up to phases.

Throughout this Section we give examples showing that this innocuous subsystem abstraction of the stabilizer formalism behaves qualitatively differently from the stabilizer error correcting models. For instance, the gauge subsystem can be arbitrarily mixed, due to incident noise or otherwise, and encoded quantum information will remain robust. One can also consider using the gauge subsystem for other practical purposes. The Authors of Ref. (Herrera-Martí *et al.*, 2014) make frequent measurements on the subsystem surface code presented in Ref. (Bravyi *et al.*, 2013) to suppress the coherent diffusion of excitations at zero-temperature. We remark that subsystem code protocols have some differences in their practical realization than their stabilizer counterparts. This is beyond the scope of this Review, but we urge the reader to find a comprehensive review of this topic in Ref. (Terhal, 2013) and references therein.

Little is known about the fundamental features or thermal characteristics of subsystem codes, though progress has been made in this area in Ref. (Chesi *et al.*, 2010a). Much of the work in this area has been a constructive search for models that we might expect to give rise to favorable properties for self correction. Of particular interest is the three-dimensional Bacon-Shor code (Bacon, 2006). This model has drawn significant attention to subsystem codes as it was conjectured to behave as a self-correcting memory. This argument is made as its Hamiltonian has common features of thermally stable classical models, namely, the Ising model, discussed in Subsec. V.A. We introduce the three-dimensional Bacon-Shor code by first reviewing the two-dimensional Bacon-Shor code; a simple example of a subsystem code that has some qualitatively different features from a local stabilizer code.

Subsystem codes are of further interest when considered in the context of topological order. For the reader familiar with topologically ordered lattice models, we remark that Kitaev's honeycomb model (Kitaev, 2006) provides an illustrative example of a subsystem code (Suchara *et al.*, 2011); the model is studied by considering loop degrees of freedom that commute with its non-commuting parent Hamiltonian. The honeycomb model falls into a broader subclass of subsystem codes, known as *topological subsystem codes* (Bombin, 2010b; Suchara *et al.*, 2011). Recent three-dimensional generalizations of topological subsystem codes, namely the gauge color code model, has recently been conjectured to be self-correcting. We conclude this Section with an overview of this model, and its features that have led to this conjecture.
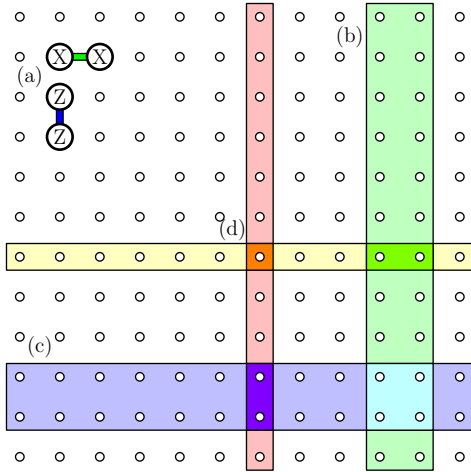
FIG. 21 The Bacon-Shor code in two dimensions. Qubits are represented by white circles. (a) Example of gauge generators. The gauge group $\mathcal{G}_n$ is generated by nearest-neighbor two-body A_j or B_j operators in the horizontal or vertical direction, respectively, as shown in green and blue. (b) and (c) show the support of stabilizers of the Bacon-Shor code. (d) The support of $\overline{X}$ and $\overline{Z}$ is supported on the red vertical and yellow horizontal strip, respectively. The operators intersect at a single point, colored orange, near to label (d).

A. The Bacon-Shor Code

The Bacon-Shor code (Bacon, 2006), otherwise known as the quantum compass model (Dorier *et al.*, 2005; Kugel and Khomskii, 1973), provides a non-trivial example of a subsystem codes that demonstrates physical features not accessible with local stabilizer codes. For an extensive review of compass models we direct the reader to Ref. (Nussinov, 2013). In the two-dimensional model we observe its local gauge generators that give rise to non-local stabilizer generators. Moreover, we see how the non-trivial gauge group affects the error correction procedure. We conclude this Subsection by reviewing results that show the fundamental differences between subsystem codes and commuting models.

The two-dimensional Bacon-Shor code is defined on an $L \times L$ square lattice with qubits on its vertices, as shown in Fig. 21. The gauge group $\mathcal{G}_n$ where $n = L^2$ is generated by two types of operator. It has two-body nearest-neighbor interactions A_x and B_x associated to lattice sites $x = (j,k)$, where $A_{j,k} = X_{j,k} X_{j+1,k}$ are aligned along the horizontal direction and $B_{j,k} = Z_{j,k} Z_{j,k+1}$ operators are aligned in the vertical direction, as shown in Fig. 21(a) in green and blue, respectively. We write the corresponding Hamiltonian of this model

$$H_{\text{2DBS}} = -\sum_x \left(A_x + B_x \right). \qquad (66)$$

In general, A_x and B_x operators do not commute. The stabilizers of this code, $\mathcal{S} = \mathcal{N}(\mathcal{G}_n) \cap \mathcal{G}_n$, are non-local operators of the gauge group generated by products of A_x and B_x operators. They are $S_j^X = \prod_k A_{j,k}$ and $S_k^Z =$

$\prod_j B_{j,k}$. Stabilizers S_j^X and S_k^Z are supported on bands, two vertices wide, such as those shown in green and blue in Fig. 21(b) and (c). The horizontal bands that support S_k^Z stabilizers have four common qubits with the support of the vertical bands supporting S_j^X stabilizers. As such, it is easily checked that all stabilizers commute. The model encodes a single logical qubit. Its logical operators, $\mathcal{L} = \mathcal{N}(\mathcal{G}_n) \backslash \mathcal{G}_n$, are $\overline{X} = \prod_k X_{j,k}$ for fixed j and $\overline{Z} = \prod_j X_{j,k}$ for fixed k. The support of $\overline{X}$ and $\overline{Z}$ are shown in red and yellow on Fig. 21. They cross at a single point by Fig. 21(d).

The two-dimensional Bacon-Shor code shows how subsystem codes respond differently to noise. We consider a noise model that introduces Pauli-X errors. An equivalent discussion holds for Pauli-Z errors where the lattice is rotated by $\pi/2$. Remarkably, for any given row of the lattice, we only need to correct the *parity* of errors. A pair of Pauli-X errors along a horizontal strip are elements of $\mathcal{G}_n$, and therefore commute with all $\mathcal{S}$ and $\mathcal{L}$. Errors of this type therefore do not affect information encoded in the subsystem code. As in the case for stabilizer codes, we make stabilizer measurements to identify the parity of errors between pairs of strips, and we correct the row parity using a low-weight Pauli-X correction operator.

The model presented here is not of practical interest for finite temperature stability. As pointed out in the original paper (Bacon, 2006), it is argued persuasively that the gap for the Hamiltonian (66) vanishes in the thermodynamic limit, making it impractical for a memory. This is shown in Ref. (Dorier *et al.*, 2005) using extensive numerical methods in an extended region of phase space. Nevertheless, the example shows that a clever choice of gauge enables us to ignore large classes of errors that affect only the gauge subsystem. Further to this, the Bacon-Shor code provides the first example of a local subsystem model that gives rise to a non-local stabilizer code, thus indicating a fundamental difference between local stabilizer and subsystem codes.

Indeed, the study of local subsystem codes that give rise to non-local stabilzer codes has been significantly extended due to the recent work by Bacon *et al.* (Bacon *et al.*, 2014). In this work they show a very general scheme where one can find a local subsystem code that gives rise to any given stabilizer code, that is not necessarily local, given the quantum circuit that measures the stabilizer generators of the stabilizer code. The Authors use their formalism to find codes with favorable code distance scaling that saturate known bounds for commuting projector codes. As remarked in Ref. (Bacon *et al.*, 2014), perhaps one could consider using their formalism to construct local subsystem codes that correspond to non-local stabilizer models with favorable properties at finite temperature to find stable quantum memories. Indeed, the presented class of models provably have no string-like logical operators, even if one considers the more general class of *dressed* logical operators, i.e. logical operators with non-trivial action on the gauge subsystem of the model.

We finally remark on an extension of the Bacon-Shor code due to Bravyi (Bravyi *et al.*, 2013), where he shows that the fundamental storage capacity of a two-dimensional subsystem code can surpass the storage capacity of commuting models (Bravyi *et al.*, 2010b). In the commuting case, it is known that $kd^2 \leq \mathcal{O}(n)$, where k is the number of qubits of the code, and d is the minimum weight of the lowest weight logical operator of the code. Bravyi shows that in the case of subsystem codes we can obtain scaling like $kd \leq \mathcal{O}(n)$ with a local gauge group, and that randomly chosen codes saturate this bound asymptotically in the limit of large n. Unfortunately, this bound cannot be saturated for codes with constant k. Indeed it is also known from Ref. (Bravyi and Terhal, 2009; Haah and Preskill, 2012) that distance of subsystem codes must satisfy $d^2 \leq \mathcal{O}(n)$. Results such as these provide further intrigue and motivation towards the study of subsystem codes, as we clearly see that these non-commuting codes are capable of supporting encoding properties provably unattainable by commuting models.

B. The Three-Dimensional Bacon-Shor Code

Subsystem codes have attracted a lot of interest from the point of view of thermal stability due to the three-dimensional Bacon-Shor code. In Ref. (Bacon, 2006), Bacon conjectures that the model gives rise to self-correcting behavior in a thermal setting.

The model is defined on an $L \times L \times L$ lattice for odd L with sites labeled by $x = (j, k, l)$. The corresponding Hamiltonian is given by

$$H_{\text{3DBS}} = -\sum_x \left(A_x + B_x + C_x + D_x \right), \qquad (67)$$

where the interaction terms are two-body nearest neighbor Pauli operators $A_{j,k,l} = X_{j,k,l}X_{j+1,k,l}$, $B_{j,k,l} = X_{j,k,l}X_{j,k+1,l}$, $C_{j,k,l} = Z_{j,k,l}Z_{j,k+1,l}$ and $D_{j,k,l} = Z_{j,k,l}Z_{j,k,l+1}$ which generate the gauge group. The logical operators of the code are two-dimensional plane like operators $\overline{X} = \prod_{k,l} X_{1,k,l}$ and $\overline{Z} = \prod_{j,k} Z_{j,k,1}$ that anti-commute due to the condition that L is odd. The stabilizer generators are two-dimensional plane-like operators that are two vertices wide, such that $S_j^X = \prod_{k,l} X_{j,k,l}X_{j+1,k,l}$ and $S_l^Z = \prod_{j,k} Z_{j,k,l}X_{j,k,l+1}$.

The Hamiltonian of the three-dimensional Bacon-Shor code contains gauge group elements of intersecting two-dimensional Ising model. It has two-body Pauli-X type interactions along one two-dimensional plane, and Pauli-Z type interactions along an orthogonal plane. We show the construction in Fig. 22. It is shown in Ref. (Bacon and Casaccino, 2006) that in general one can design generalized Bacon-Shor codes where one takes an arbitrary classical code input to find its gauge group. Its overlying stabilizer code then inherits the properties of the input classical code. The intuition of the three-dimensional Bacon-Shor code is that it inherits the stability properties of its input code, the two-dimensional Ising model,
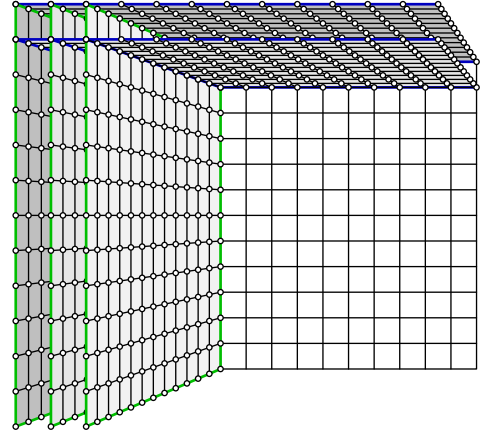

FIG. 22 The three-dimensional Bacon-Shor Hamiltonian can be regarded as two overlapping two-dimensional classical Ising model Hamiltonians. The figure shows some of the qubits of the cubic lattice, where the blue planes show two-dimensional square lattices with nearest-neighbor Pauli-X interactions between qubits, and similarly, the green planes are subject to nearest-neighbor Pauli-Z interactions. The full model has a complete array of L planes along both the horizontal and vertical directions that are marked on the white square array at the back of the image.

as discussed in Subsec. V.A. In Ref. (Bacon, 2006), the Author considers a simple Pauli noise model and mean-field arguments to show that the model may demonstrate a macroscopic power-law energy barrier. The question of stability of the three-dimensional Bacon-Shor code remains an open problem.

The challenge of interrogating this conjecture, as pointed out in Ref. (Bacon, 2006), is that the noise model the Author considers is not representative of all possible channels under which encoded information can decohere. It may be possible that a finite temperature environment may find a low energy path to introduce errors to the encoded logical information. Indeed, no exact diagonalization of Hamiltonian (67) has yet been found and without one it is difficult to make strong statements about the model.

Certainly, flaws have been identified with the model that must be overcome to realize a memory that satisfies all the required conditions for a stable memory. First of all, the model provably has no error-correction procedure (Pastawski *et al.*, 2010). Two-dimensional planes of the model aligned parallel with the stabilizer operators can be regarded as bits of a one-dimensional repetition code, where stabilizers measure the parity of errors between pairs of planes. In the limit of large system size, the probability that a given plane has an odd number of errors tends to half. In this limit, we approach the threshold noise rate of this coarse-grained one-dimensional repetition code. This is problematic as any candidate model that potentially supports thermal stability will require a suitable error correction procedure, lest we cannot expect to read information from the code. Further, given

that we are relying the model to inherit the stability properties of the two-dimensional Ising model, we may also expect it to inherit its perturbative instability, described in Refs. (Cirillo and Lebowitz, 1998; Grinstein, 2004; Pastawski *et al.*, 2010; Richards *et al.*, 1995). One might support this assertion by extrapolating results regarding the gap from the well studied two-dimensional case (Dorier *et al.*, 2005).

C. The Gauge Color Code

We conclude this Section with a discussion of the *gauge color code* (Bombin, 2013). The model represents a three-dimensional topological subsystem code. Topological subsystem codes are discussed in two dimensions in Refs. (Bombin, 2010b; Bravyi *et al.*, 2013; Brell *et al.*, 2011; Kubica and Beverland, 2014; Sarvepalli and Brown, 2012; Suchara *et al.*, 2011). The model is of particular interest as it is conjectured to give rise to finite-temperature stability (Bombin, 2013). For a comprehensible overview of the gauge color code see Ref. (Kubica and Beverland, 2014).

We briefly elaborate on the fault-tolerant computational properties of the color codes. Notably, the stabilizers of color code models are favorable for the implementation of transversal gates. The two-dimensional color code has a transversal implementation of the Clifford gate set (Bombin and Martin-Delagado, 2006) which, importantly here, includes the Hadamard gate. In the two-dimensional model, the feature that enables its implementation is the *self-duality* of its stabilizers. Explicitly, a self-dual stabilizer group is such that for every stabilizer $S^X = \prod_{j \in \mathcal{T}} X_j$ supported on subset of qubits $\mathcal{T}$, there exists also the stabilizer $S^Z = \prod_{j \in \mathcal{T}} Z_j$.

The three-dimensional stabilizer color code (Bombin and Martin-Delagado, 2007b) gives rise to a transversal implementation of the controlled-not gate and the $\pi/8$-gate. Supplemented by the Hadamard gate, the gate set of the three-dimensional color code is capable of universal fault-tolerant quantum computation. However, the three-dimensional stabilizer color code is not self dual, and as such, does not have a universal gate set.

In Ref. (Bombin, 2013) Bombin shows that a universal gate set can be realized using a subsystem generalization of the three-dimensional color code. Importantly, the stabilizer group of the three-dimensional color code contains a self-dual subset of stabilizers that are capable of successfully identifying an arbitrary set of errors below a certain weight. Given a suitable choice of gauge generators, we can restrict the gauge color code stabilizers to its self-dual subset, thus enabling the transversal implementation of the Hadamard gate. We refer to the gauge generators that gives rise to the self-dual stabilizer group as the *self-dual gauge*.

The proposal of Bombin represents an explicit lattice realization of *gauge fixing*, introduced in Ref. (Paetznick and Reichardt, 2013). Gauge fixing avoids resource
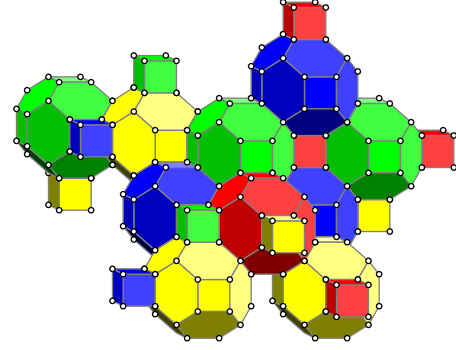

FIG. 23 A piece of color code lattice. Qubits reside on the vertices of a four valent lattice. Individual cells of the lattice are colored red, blue green and yellow. No two cells of the same color touch, showing four colorability.

costly methods of achieving a universal gate set using, for instance, magic state distillation (Bravyi and Kitaev, 2005). This is achieved by switching between different codes by choice of suitable subsystem gauge operators. Gauge fixing is shown explicitly for Reed-Muller codes in Ref. (Anderson *et al.*, 2014). The idea of gauge fixing extends ideas presented in Ref. (Knill *et al.*, 1996) where transversal gates that do not preserve the code space are suggested.

We consider the self-dual gauge color code for self correction. A lattice suitable to describe the code is shown in Fig. 23. Importantly, the lattice is four valent and four colorable, i.e. the lattice is such that we can assign to each cell one of four colors in such a way that no two neighbouring cells are of the same color. The generators of the gauge group are associated to the faces, f, of cells of the lattice. Specifically, for every face of a cell, we have gauge generator $A_f = \prod_{v \in f} X_v$ and $B_f = \prod_{v \in f} Z_v$, where we use shorthand $v \in f$ to mean the vertices adjacent to face f. On the lattice shown, gauge generators are either four- or six-body terms. We therefore write the Hamiltonian

$$H_{\mathrm{GCC}} = -\sum_f \left(A_f + B_f \right). \tag{68}$$

The self-dual stabilizers are then associated to the cells, c, of the lattice, such that $A_c = \prod_{v \in c} X_v$ and $B_c = \prod_{v \in c} Z_v$, where $v \in c$ are qubits associated to vertices adjacent to cell c.

The conjecture due to Bombin is based on the structure of the A_f and B_f Hamiltonian terms. Specifically, if one considered the simpler Hamiltonian $H^X = -\sum_f B_f$ subject only to Pauli-X errors, then the excitations of the model are exclusively akin to Peierls contours, as discussed in Sec. V. An equivalent argument holds for Pauli-Z noise for Hamiltonian $H^Z = -\sum_f A_f$, and as such one can argue that there may be a macroscopic energy barrier for arbitrary local quantum noise channels. Of course, given the difficulty in diagonalizing Hamiltonian (68) this argument is not rigorous.
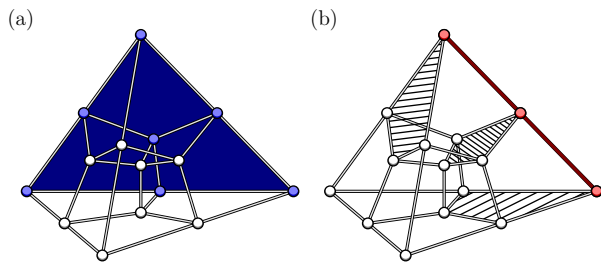
FIG. 24 A fifteen-qubit tetrahedral lattice that supports the gauge color code. (a) The two-dimensional logical operator of the gauge color code, marked in blue. (b) The support of the dressed logical operator is shown in red. Faces that support Hamiltonian terms that anti-commute with the dressed logical operator are shaded.

When defined on a tetrahedron, the logical operators that commute with the gauge generators are two dimensional. We show the smallest tetrahedron that embeds a gauge color code in Fig. 24. Both $\overline{X}$ and $\overline{Z}$ are supported on one face of the tetrahedral lattice. Their support is shown in blue on the example lattice in Fig. 24(a). The geometry of the color code ensures that the support of a face of the tetrahedron remains odd for any size of lattice.

While it is promising feature for discovering self correction that the logical operators are two dimensional, it is not clear that such logical operators are sufficient for self correction in subsystem codes. Indeed, the support of logical operators of subsystem codes can be reduced by multiplication by gauge generators. Such a logical operator will not necessarily commute with the gauge group, while still commuting with the stabilizer group, as is required. A logical operator of this type is known as a *dressed logical operator*.

In contrast to the models proposed by Bacon *et al.* (Bacon *et al.*, 2014), the gauge color code has one-dimensional dressed logical operators. We show the support of a dressed logical operator in Fig. 24(b). We can conclude little from discovering this operator, but we make this point only to illustrate some of the additional complexity involved in studying subsystem codes. Indeed, due to the non-trivial commutation relations of the dressed operator with respect to the interaction terms of Hamiltonian (68), it is not clear that such an operator can be achieved at constant energy cost. As such, the discovery of a dressed logical operator does not rule out the possibility of self correction in the gauge color code model. We additionally remark that, like the three-dimensional Bacon-Shor code, it is not even obvious that the gauge color code is gapped.

We finally mention further progress in the study of the gauge color code in Ref. (Bombin, 2014) with respect to its error correcting capabilities. Indeed, as identified in Ref. (Dennis *et al.*, 2002), there are advantages to be gleaned from choosing an error correcting code whose corresponding Hamiltonian has stable properties at finite temperature. In (Bombin, 2014), Bombin shows that the gauge color code model has favorable proper-

ties for decoding when measured using unreliable laboratory equipment. Specifically, he shows that given gauge measurements that may return the wrong measurement outcomes with some small but finite probability, we can successfully decode the gauge color code with a constant number of syndrome measurements in the limit of large system sizes. This differs from the well studied case of two-dimensional stabilizer models that are read out using unreliable measurement apparatus. There it is required that the number of measurements of each stabilizer must scale with the size of the system (Wang *et al.*, 2003). He goes on to argue that the error correcting properties he demonstrates are analogous to self-correcting behavior at finite temperatures. In spite of this progress, it remains an open problem to determine the self-correcting behavior of the gauge color code.

X. DISCUSSIONS AND OUTLOOK

Among the major discoveries that led to scalable classical information processing was the discovery of a transistor (Bacon, 2006). The physics of these little solid-state devices ensure the reliable storage *and* robust processing of classical information that is easily scaled. The discovery of an experimentally amenable stable quantum memory presents a monumental hurdle, which, if overcome, will be invaluable for the discovery of fault-tolerant quantum information processing. In the present Review we have given an overview of the analytical and numerical tools we use to approach the study of many-body quantum systems at finite temperature. We have examined the no-go theorems that have been discovered in this field, and we have presented many new physical models with certain properties suitable for the passive protection of quantum information. We conclude by highlighting some of the forthcoming challenges we face towards discovering and developing a quantum memory.

This Review has highlighted many open problems in this field. We have discussed models that arguably present favorable properties to make them resilient in a thermal environment. Such models include the ferromagnet-coupled toric code, the welded toric code, embeddable-fractal product codes, the three-dimensional Bacon-Shor code and the gauge color code. These conjectures need to be interrogated by numerical experiments or by rigorous proofs. To study these models we need to develop both analytical and numerical techniques in both condensed-matter physics and fundamental statistical mechanics. In addition to this, it needs to be checked that these models have other features that are required of a passive quantum memory, such as efficient decoding algorithms and perturbative stability.

A noteworthy theme that has occurred frequently throughout this Review is that many of the candidate models for finite temperature stability are composed of simpler macroscopic systems. For instance, the work in Sec. VI shows that we can introduce anyonic interactions

with a local model by coupling the toric code to either a system of bosons or a Heisenberg ferromagnet. Similarly, the non-translationally invariant models in Subsecs. VII.C and VII.D are constructed by combining simpler topologically ordered models using either welding or by taking the homological product of many codes. Indeed, the entropically protected model presented in Subsec. VIII.A can be regarded as a patchwork lattice of many different, albeit equivalent, topological phases. Moreover, the Bacon-Shor codes enable the combination of favorable classical models using the underlying gauge structure. To develop new models one might consider adapting these composition tools further to construct new hybrid Hamiltonians with features we require of a quantum memory.

Finally, we conclude by emphasizing that all the promising theoretical models that are proposed must be developed until they are sympathetic to the engineering constraints of the laboratory. Certain proposals for a finite-temperature quantum memory are more amenable to experimentalists than others, for instance, the ferromagnetic coupled toric code was designed with physical media in mind in its development. Moreover, subsystem codes offer an avenue to simplify the architectural challenges of building high-weight stabilizer models. However, in spite of a few examples, the study of experimentally amenable quantum memories that can be built in the laboratory is very much in its infancy. We consider the example of the celebrated cubic code model; a well studied model whose favorable partial self-correcting properties have been analyzed and numerically verified. We must work now to develop models such as these into a form that an experimentalist can build in the laboratory. Undoubtedly, such an achievement will be directly incorporated in the design of fault-tolerant quantum technologies of the future.

Appendix A: Decoders

Throughout this Review we make use of decoding algorithms for numerical analysis. Given an encoded quantum state that has been subject to noise, a decoder takes classical syndrome information, i.e. all the outcomes of stabilizer measurements, and returns a correction operation that returns the state to the code space (Dennis *et al.*, 2002). Provided the errors occur at a suitably low density, the decoder will successfully find a correction op-
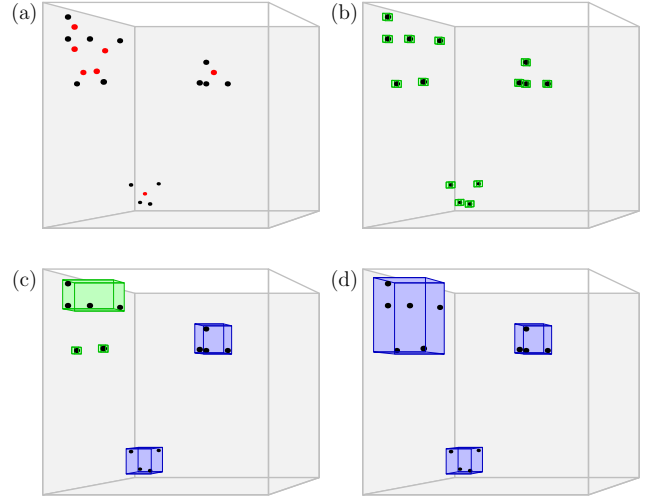

FIG. 25 (a) Unknown errors, marked in red in a three-dimensional lattice, are identified by syndrome measurements, marked in black. (b) Syndromes are initially contained in unit boxes. (c) Box sizes increase to contain other nearby syndromes within a small fixed radius of the existing boxes. Boxes that contain a correction operator are colored blue, they are otherwise colored green. (d) The search increases the box size to find boxes large enough to contain correction operators for all the syndromes on the lattice.

erator that will recover the initially encoded state with probability that grows with the size of the system. Here we briefly discuss decoding, and a particular decoding routine, namely the clustering decoder. This present discussion make use of the stabilizer formalism described in Sec. II.

Even in the case that we find a self-correcting quantum memory, a decoding step will still be required to correct for errors caused by small thermal fluctuations when information is read from the system. To illustrate this, we briefly consider the two-dimensional Ising model, as discussed in Subsec. V.A. We encode classical bits in the two-fold degenerate ground space, and we read out by measuring the magnetization; the average spin value of all the spins of the system. The ground states for the model have magnetization ± 1. At finite temperature in the limit of large system sizes we cannot expect all the spins to be aligned. Instead it is suitable to take the sign of the magnetization measurement to readout the memory. This measurement corresponds to taking a majority vote over all the encoded spins of the lattice. Measuring the encoded ferromagnet in this way accounts for small thermal fluctuations that take the spin configuration out of the ground space. For robust quantum information storage we require a decoding algorithm to deal with small errors incident to a code during readout.

As we cannot measure the state of individual physical qubits of a code, accounting for the errors during the readout of a quantum code is not as straight forward as the classical case we have described. Instead, for the quantum case, we perform stabilizer measurements

to learn the errors that are incident to a code. The stabilizer measurements perform the task of collapsing the incident noise onto an error E that is an element of the Pauli group, and provides syndrome information we can use to attempt to determine E. It is the task of the decoder to predict the error E of the Pauli group, and return a correction operator C such that CE acts trivially on the encoded state.

Many approaches to decoding have been studied with tradeoffs between speed, performance, and versatility. Decoders have been designed that make use minimum-weight perfect matching (Dennis *et al.*, 2002), renormalization group techniques (Duclos-Cianci and Poulin, 2010, 2013), and Monte-Carlo methods (Hutter *et al.*, 2014b; Wootton and Loss, 2012). Moreover, the study of decoding has foundations in the study of glassy statistical mechanical models (Andrist *et al.*, 2014; Bombin *et al.*, 2012; Dennis *et al.*, 2002; Wang *et al.*, 2003).

Here, we describe the clustering decoder which is commonly used throughout this Review. The clustering decoder is introduced in (Harrington, 2004) and developed by Bravyi and Haah specifically for the study of the cubic code at finite temperature in Refs. (Bravyi and Haah, 2011a, 2013), as we have discussed in Subsec. VII.B. The clustering decoder is further refined in Refs. (Anwar *et al.*, 2014; Hutter *et al.*, 2014a). This simple algorithm is particularly suitable for the present work as it can be adapted for any local stabilizer code (Bravyi and Haah, 2011a).

To find a correction operator for the most-likely error configuration, the clustering decoder will implicitly make use of the locality constraint commuting Pauli Hamiltonian models. In addition to this, we assume that a low-weight correction operator will approximate the inverse of the most probable error that has occurred in the limit of a low error rate.

Here we sketch the clustering algorithm routine. A rigorous explanation of the implementation of the decoder can be found in Refs. (Anwar *et al.*, 2014; Bravyi and Haah, 2011a; Hutter *et al.*, 2014a). In Fig. 25(a) we show a series errors, marked in red, and syndromes, marked in black that correspond to an error and syndrome configuration for some topological code. We consider this example syndrome to demonstrate the clustering decoder.

To find a low-weight correction we find a set of small box that enclose all of the error syndromes. We search for a set of boxes that contains a correction operator that is consistent with all the syndromes in the box. The algorithm begins by putting all the syndromes in individual boxes of unit size, as shown in Fig. 25(b). The algorithm then proceeds by incrementally increasing the size of the boxes. This is achieved by combining pairs of boxes that lie within a some small radius of one another. The routine continues until the boxes are large enough to contain a correction operator that corrects for all the syndromes contained within the box.

For the initially chosen boxes, where all of the boxes are of unit size, we cannot find a local correction operator
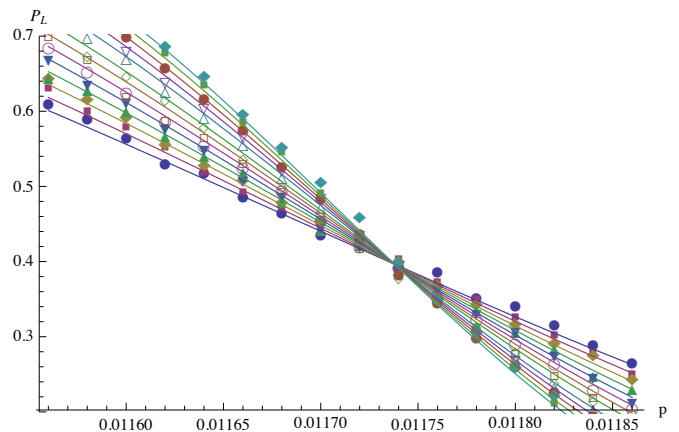

FIG. 26 The threshold calculation using the clustering decoder for an identically and independently distributed bit-flip noise model for the cubic code model using system sizes between $L = 101$ and $L = 201$. We find the crossing at $p_{\mathrm{th}} = 1.17\%$.

that is consistent with its single syndrome. We increase the size of the boxes by checking within a fixed radius r of each of the syndromes of each box. In the event that a new syndrome of a different box is found within a distance r of the searching syndrome, their two respective boxes are combined. Once it is confirmed that no pairs of disjoint boxes contain any syndromes that lie within distance r of one another, we check to find a correction operator that reverses the syndromes contained in the box.

If a box contains a correction operator that is consistent with all of its contained syndromes, the box is considered neutral, and its contained syndromes are no longer considered in the algorithm. In the case that all the boxes are neutral, the algorithm terminates and the correction operator contained in each of the boxes are returned. If not all the boxes are neutralized, r is increased and the algorithm is repeated for the syndromes of boxes that are not neutral.

We continue to follow the example syndrome in Fig. 25. In Fig. 25(c) we show the new boxes obtained after searching within a radius of $r = 1$ of each of the syndromes. After this search, not all the boxes contain a local correction operator. Two new boxes, colored blue, are neutralized. Syndromes in the blue boxes are no longer considered in the algorithm. Three boxes found at radius $r = 1$, marked in green, do not contain a correction operators consistent with their syndromes. To find correction operators for the syndromes in the green boxes, the algorithm increases its box search radius once again to $r = 2$ for all the remaining unneutralized syndromes. At $r = 2$, all boxes contain a correction operator that is consistent with all error syndromes. Fig. 25(d) shows the boxes that together contain a correction operator consistent with all the syndromes of the configuration. The decoder will return the correction operator contained within the blue boxes to return the encoded information to the ground
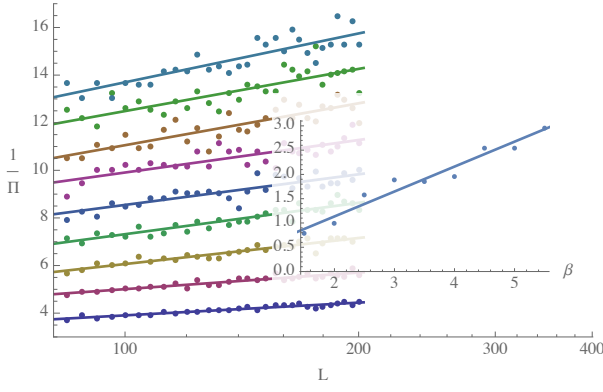
FIG. 27 Log-linear plot of the reciprocal of Π plotted against L, for a range of β values. We find $1/\Pi$ grows linearly with $\ln(L/2)$. The Inset shows the gradient of the fits in the main plot as a function of β.

state, enabling the readout of the encoded quantum information.

We remark that this algorithm is suitable for any local stabilizer code. The description of the algorithm we give makes no reference to the underlying code. We need only assume that the code is local, such that error syndromes occur within a fixed radius of an incident error. Moreover, it is shown in Ref. (Bravyi and Haah, 2011a) that we can determine efficiently if a box can contain a correction operator consistent with its enclosed syndromes.

We can evaluate decoder performance by obtaining a *threshold* with respect to an identically independently distributed noise model. This noise model is where each qubit suffers an error with probability p. The threshold value p_{th} is the value below which the logical error rate of a quantum error-correcting code decreases as we increase the size of the system to the thermodynamic limit. In this Review we use cluster decoding for the toric code model in Subsec. III.E, and the cubic code in Subsec. VII.B. The toric code threshold is already found to be $\sim 8.3\%$, shown in Ref. (Anwar *et al.*, 2014). Threshold for the for the cubic code using the clustering algorithm have not been published to the best of the Authors' knowledge, though good estimates are given in Ref. (Bravyi and Haah, 2011a). We find $p_{\mathrm{th}} \sim 1.17\%$ for a bit-flip noise model. We show the threshold data in Fig. 26.

Appendix B: Numerical Results for the Finite Temperature Toric Code

Here we present additional numerical results for the finite temperature behavior of the toric code, supporting the arguments we make in Sec. III.E.

For low temperatures the decoherence of a system of linear size L is the result of the dynamics of a single pair of anyons. In Sec. III.E we predicted scaling with L and inverse temperature $\beta = 1/T$ of three independent elements of the coherence time, which we called $\Pi(L, \beta)$,

τ_c and τ_m. We isolate each of these terms and estimate them numerically.

We first investigate $\Pi(L, \beta)$. This term quantifies the probability that after a pair of anyons is created they do not annihilate by mutually fusing together before reaching a logical distance. Put another way it is the probability that a pair, once created, will cause a logical error. To evaluate this function we alter the standard simulation scheme; rather than beginning in a ground state we initialize the system with a single pair of anyons present on the lattice, where the initialized anyons are separated by a single lattice spacing. We additionally set the rate of creation equal to zero such that no additional pairs of anyons are created. Indeed, we model only the random motion of a single pair of anyons walking across the lattice. We evolve the system until either the separation of the anyons reaches the Euclidean distance $L/2$, or the pair meet at a common point on the lattice and annihilate. Quantity Π is estimated as the fraction of samples that reach separation $L/2$ rather than annihilating, we estimate by sampling over 10^4 trials. The results we obtain are shown in Fig. 27. The fit we find to the data is

$$1/\Pi = (0.108 + 0.513\beta)\ln(L/2). \tag{B1}$$

This is in good agreement with the scaling form we hypothesised in Eqn. (29), where constant $A \approx 5$.

We next numerically study how τ_c and τ_m scale with L and β. Time τ_c is the typical wait time for the creation of the pair of anyons that will cause a logical error, τ_m is the average length of time from their creation until they reach a logical distance, $L/2$, from each other. To find these values we simulate the thermal evolution of the system prepared in a ground state. We attempt to decode the lattice after each event that occurs due to the noise simulation, and the simulation is stopped once the decoder fails. Every time a pair of anyons is created its creation time is recorded, this information is discarded if the pair annihilate. We verify that the environment never creates more than a single pair of anyons at a given time. Estimates of the creation timescale τ_c and diffusion time τ_m are obtained by averaging over 10^3 simulation runs. The data for each is plotted in Fig. 6, presented in Sec. III.E, and Fig. 28, respectively. The data we obtain correlates well with the forms we expect, Eqns. (28) and (30), where we find numerical fits $\tau_m \simeq 0.028\beta L^2$ and

$$\tau_c = 0.150\frac{e^{1.99\beta}}{L^{2.01}}\frac{1}{\Pi}, \tag{B2}$$

where we take for the function Π the one we evaluated numerically, Eqn. B1.

At high temperatures, decoherence results due to the interaction of many thermally created anyons. In Sec. III.E we describe a model of the high-temperature dynamics that gives an estimate, Eqn. (34), of the coherence time τ_{high}. We test some of the assumptions of this model and compare the predicted coherence time to numerical values.
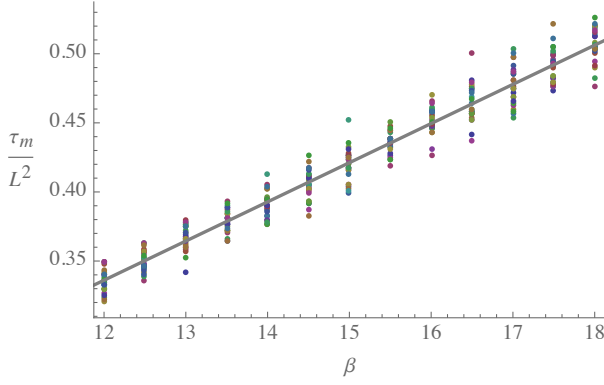
FIG. 28 Contribution to the coherence time from anyon motion τ_m plotted against β for a range of system sizes $L = 50$, 52, 54, ..., 100. By dividing τ_m by L^2 we see data collapse of different system sizes. The linear fit displayed uses the average values of the fit parameters obtained from the separate system sizes $\tau_m \simeq 0.028\beta L^2$.
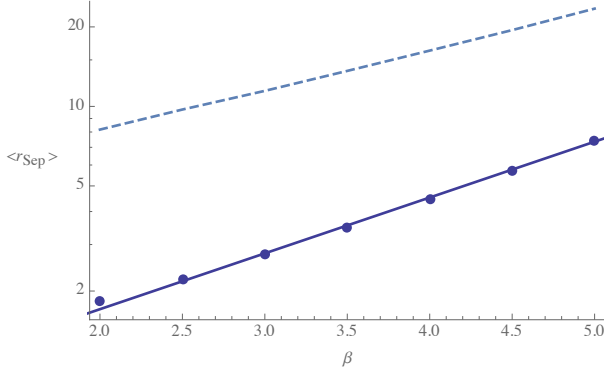

FIG. 29   Log plot of average separation between paired anyons at the time the decoder fails as a function of β, for system size $L = 200$. This is typical of our results for different system sizes. The solid line is a fit to the data with linear gradient approximately 0.49 in this Log plot, consistent with scaling $\langle r_{\text{sep}} \rangle \sim e^{\beta\Delta/2}$. The dashed line is the maximum value of the separation, averaged over the simulation runs, which is seen to be much less than $L/2$.

We simulate the system evolving at high temperature. The decoder runs after every event is introduced to the system by the thermal evolution. At the earliest time the decoder fails we stop the simulation and record the time elapsed during the simulation. Results are obtained by averaging over 10^3 simulations runs. We find average anyon numbers $\langle N \rangle$ which confirm that the anyon density at the time the decoder fails scales like $\rho \sim e^{-\beta\Delta}$. These numbers are also seen to satisfy $\langle N \rangle \gg 1$, indicating that our data is taken from the high temperature regime.

In Sec. III.E we argued that at high temperatures, in contrast to the low temperature case, the important size scale would not be the system size L rather it would be a new length $\Lambda \sim e^{\beta\Delta/2}$. This is the typical separation between creation events. So it corresponds to the distance the average anyon will have to diffuse in order for the de-
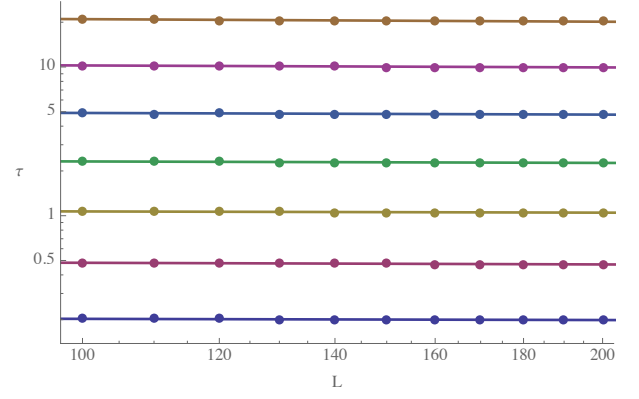

FIG. 30 Approximate system size independence of the high temperature coherence time. Plots of τ on a Log scale against L for different temperatures $\beta = 2.0, 2.5, \ldots 5.0$. Linear fits show very small negative gradients ranging from -0.03 for the lowest value of β, down to -0.06 for the highest β. However, zero gradient is well within the 95% confidence interval of each fit.

coder to no longer be able to reliably identify which other anyon it was created with. In order to test that this average motion is the main decoherence mechanism at high temperature, not rare anyon pairs that move fast and separate to logical distances $L/2$, we study the distance between anyon pairs at the time the decoder fails. During the simulation anyons that are created together are marked as a member of their given creation pair. At the end of the simulation we measure the Euclidean distance between each marked pair. If two anyons from two separate pairs fuse, the remaining two unpaired anyons on the lattice are marked as members of the same pair. As one might expect, we find that extended pairs created from a fusion will typically achieve a greater separation than pairs that are initialized by creation from vacuum. However, its effect is small with respect to the average data. Our numerical results show that the average separation between all anyon pairs grows like $e^{\beta\Delta/2}$, as predicted. In addition we find that the maximum separation between any pair is always much less than $L/2$. The scaling of the average and maximum separations are shown in Fig. 29. These observations confirm that the decoherence results from the average motion of anyons in local regions.

The scaling of coherence time with β is shown in Fig. 7, presented in Subsec. III.E. We see that the data reproduces the exponential dependence on $\beta\Delta$ predicted in Eqn. (34). Another prediction of the model was that τ_{high} would be independent of system size. Fig. 30 plots the numerical values of coherence times against L showing that the data is consistent with this idea.

References

Aharonov, D., and M. Ben-Or, 1997, in *STOC '97 Proceedings of the twenty-ninth annual ACM symposium on Theory of computing*, p. 176.

Al-Shimary, A., J. R. Wootton, and J. K. Pachos, 2013, New J. Phys. **15**, 025027.

Alicki, R., and M. Fannes, 2009, Phys. Rev. A **79**, 012316.

Alicki, R., M. Fannes, and M. Horodecki, 2009, J. Phys. A: Math. Theor. **42**, 065303.

Alicki, R., M. Horodecki, P. Horodecki, and R. Horodecki, 2010, Open Syst. Inf. Dyn. **17**, 1.

Alicki, R., and K. Lendi, 2007, *Quantum Dynamical Semigroups and Applications* (Springer).

Aliferis, P., and A. W. Cross, 2007, Phys. Rev. Lett. **98**, 220502.

Aliferis, P., D. Gottesman, and J. Preskill, 2006, Quant. Inf. Comp. **6**, 97.

Anderson, J. T., G. Duclos-Cianci, and D. Poulin, 2014, Phys. Rev. Lett. **113**, 080501.

Anderson, J. T., and T. Jochym-O'Connor, 2014, arXiv:1409.8320 .

Anderson, P. W., 1958, Phys. Rev. **109**, 1492.

Andrist, R. S., J. R. Wootton, and H. G. Katzgraber, 2014, arXiv:1406.5974 .

Anwar, H., B. J. Brown, E. T. Campbell, and D. E. Browne, 2014, New J. Phys. **16**, 063038.

Bacon, D., 2006, Phys. Rev. A **73**, 012340.

Bacon, D., and A. Casaccino, 2006, arXiv:quant-ph/0610088 .

Bacon, D., S. T. Flammia, A. W. Harrow, and J. Shi, 2014, arXiv:1411.3334 .

Barends, R., J. Kelly, A. Megrant, A. Veitia, D. Sank, E. Jeffry, T. C. White, J. Mutus, A. G. Fowler, B. Campbell, Y. Chen, Z. Chen, *et al.*, 2014, arXiv:1402.4848 .

Barkeshli, M., P. Bonderson, M. Cheng, and Z. Wang, 2014, arXiv:1410.4540 .

Barkeshli, M., C.-M. Jian, and X.-L. Qi, 2013, Phys. Rev. B **87**, 045130.

Becker, D., T. Tanamoto, A. Hutter, and F. L. P. D. Loss, 2013, Phys. Rev. A **87**, 042340.

Beige, A., D. Braun, B. Tregenna, and P. L. Knight, 2000, Phys. Rev. Lett. **85**, 1762.

Bombin, H., 2010a, Phys. Rev. Lett. **105**, 030403.

Bombin, H., 2010b, Phys. Rev. A **81**, 032301.

Bombin, H., 2013, arXiv:1311.0879 .

Bombin, H., 2014, arXiv:1404.5504 .

Bombin, H., R. S. Andrist, M. Ohzeki, H. G. Katzgraber, and M. A. Martin-Delgado, 2012, Phys. Rev. X **2**, 021004.

Bombin, H., R. W. Chhajlany, M. Horodecki, and M. A. Martin-Delagado, 2013, New J. Phys. **15**, 055023.

Bombin, H., and M. A. Martin-Delgado, 2006, Phys. Rev. Lett. **97**, 180501.

Bombin, H., and M. A. Martin-Delgado, 2007a, Phys. Rev. B **75**, 075103.

Bombin, H., and M. A. Martin-Delgado, 2007b, Phys. Rev. Lett. **98**, 160502.

Bombin, H., and M. A. Martin-Delgado, 2009, J. Phys. A: Math. Theor. **42**, 095302.

Bonati, C., 2014, Eur. J. Phys. **35**, 035002.

Bortz, A. B., M. H. Kalos, and J. L. Lebowitz, 1975, J. Comp. Phys. **17**, 10.

Bravyi, S., 2006, Phys. Rev. A **73**, 042313.

Bravyi, S., 2011, Phys. Rev. A **83**, 012320.

Bravyi, S., D. P. DiVincenzo, and D. Loss, 2011a, Ann. Phys. **326**, 2793.

Bravyi, S., D. P. DiVincenzo, D. Loss, and B. M. Terhal, 2008, Phys. Rev. Lett. **101**, 070503.

Bravyi, S., G. Duclos-Cianci, D. Poulin, and M. Suchara, 2013, Quant. Inf. Comp. **13**, 0963.

Bravyi, S., and J. Haah, 2011a, arXiv:1112.3252 .

Bravyi, S., and J. Haah, 2011b, Phys. Rev. Lett. **107**, 150504.

Bravyi, S., and J. Haah, 2013, Phys. Rev. Lett. **111**, 200501.

Bravyi, S., and M. B. Hastings, 2013, arXiv:1311.0885 .

Bravyi, S., M. B. Hastings, and S. Michalakis, 2010a, J. Math. Phys. **51**, 093512.

Bravyi, S., and A. Kitaev, 2005, Phys. Rev. A **71**, 022316.

Bravyi, S., and R. König, 2012, Commun. Math. Phys. **316**, 641.

Bravyi, S., and R. König, 2013, Phys. Rev. Lett. **110**, 170503.

Bravyi, S., B. Leemhuis, and B. M. Terhal, 2011b, Ann. Phys. **326**, 839.

Bravyi, S., D. Poulin, and B. Terhal, 2010b, Phys. Rev. Lett. **104**, 050503.

Bravyi, S., and B. Terhal, 2009, New J. Phys. **11**, 043029.

Bravyi, S. B., and A. Y. Kitaev, 1998, arXiv:quant-ph/9811052 .

Brell, C. G., 2014, A proposal for self-correcting stabilizer quantum memories in 3 dimensions (or slightly less), in preparation.

Brell, C. G., S. Burton, G. Dauphinais, S. T. Flammia, and D. Poulin, 2014, Phys. Rev. X **4**, 031058.

Brell, C. G., S. T. Flammia, S. D. Bartlett, and A. C. Doherty, 2011, New J. Phys. **13**, 053039.

Brennen, G. K., and J. K. Pachos, 2007, Proc. R. Soc. A **10**, 1098.

Brown, B. J., A. Al-Shimary, and J. K. Pachos, 2014, Phys. Rev. Lett. **112**, 120503.

Campari, R., and D. Cassi, 2010, Phys. Rev. E **81**, 021108.

Castelnovo, C., and C. Chamon, 2007, Phys. Rev. B **76**, 184442.

Castelnovo, C., and C. Chamon, 2008, Phys. Rev. B **78**, 155120.

Castelnovo, C., and C. Chamon, 2011, Phil. Mag. **92**, 1.

Chamon, C., 2005, Phys. Rev. Lett. **94**, 040402.

Chesi, S., D. Loss, S. Bravyi, and B. M. Terhal, 2010a, New J. Phys. **12**, 025013.

Chesi, S., B. Röthlisberger, and D. Loss, 2010b, Phys. Rev. A **82**, 022305.

Cirillo, E., and J. Lebowitz, 1998, J. Stat. Phys. **90**, 211.

Davies, E. B., 1974, Commun. Math. Phys. **39**, 91.

Day, F. V., and S. D. Barrett, 2012, arXiv:1201.0390 .

Dennis, E., A. Kitaev, A. Landahl, and J. Preskill, 2002, J. Math. Phys. **43**, 4452.

Deutsch, D., 1985, Proc. R. Soc. Lond. A **400**, 97.

Devoret, M. H., and R. J. Scoelkopf, 2013, Science **339**, 1169.

DiVincenzo, D. P., and D. Loss, 2005, Phys. Rev. B **71**, 035318.

Dorier, J., F. Becca, and F. Mila, 2005, Phys. Rev. B **72**, 024448.

Douçot, B., M. V. Feigel'man, and L. B. Ioffe, 2003, Phys. Rev. Lett. **90**, 107003.

Duan, L.-M., and G.-C. Guo, 1997, Phys. Rev. Lett. **79**, 1953.

Duclos-Cianci, G., and D. Poulin, 2010, Phys. Rev. Lett. **104**, 050504.

Duclos-Cianci, G., and D. Poulin, 2013, Phys. Rev. A **87**, 062338.

Dusuel, S., M. Kamfor, R. Orús, K. P. Schmidt, and J. Vidal, 2011, Phys. Rev. Lett. **106**, 107203.

Eastin, B., and E. Knill, 2009, Phys. Rev. Lett. **102**, 110502.

Einarsson, T., 1990, Phys. Rev. Lett. **64**, 1995.

Farrow, T., and V. Vedral, 2014, arXiv:1406.0659 .

Feynman, R. P., 1982, Int. J. Theo. Phys. **21**, 467.

Freedman, M. H., and M. B. Hastings, 2014, Quant. Inf. Comp. **14**, 144.

Freedman, M. H., M. Larsen, and Z. Wang, 2002, Commun. Math. Phys. **227**, 605.

Freeman, C. D., C. M. Herdman, D. J. Gorman, and K. B. Whaley, 2014, Phys. Rev. B **90**, 134302.

Fuchs, G. D., G. Burkard, P. V. Klimov, and D. D. Awschalom, 2011, Nat. Phys. **7**, 789.

Garrahan, J. P., and M. E. J. Newman, 2000, Phys. Rev. E **62**, 7670.

Gottesman, D., 2001, *Stabilizer Codes and Quantum Error Correction*, Ph.D. thesis, California Institute of Technology.

Griffiths, R. B., 1964, Phys. Rev. **136**, 437.

Grinstein, G., 2004, IBM J. Res. Dev. **48**, 5.

Haah, J., 2011, Phys. Rev. A **83**, 042330.

Haah, J., 2013, Commun. Math. Phys. **324**, 351.

Haah, J., 2014, Phys. Rev. B **89**, 075119.

Haah, J., and J. Preskill, 2012, Phys. Rev. A **86**, 032308.

Hamma, A., C. Castelnovo, and C. Chamon, 2009, Phys. Rev. B **79**, 245122.

Hamma, A., R. Ionicioiu, and P. Zanardi, 2005a, Phys. Rev. A **71**, 022315.

Hamma, A., R. Ionicioiu, and P. Zanardi, 2005b, Phys. Lett. A **337**, 22.

Hamma, A., P. Zanardi, and X.-G. Wen, 2005c, Phys. Rev. B **72**, 035307.

Harrington, J. W., 2004, *Analysis of quantum error-correcting codes: sympletic lattice codes and toric codes*, Ph.D. thesis, California Institute of Technology.

Harty, T. P., D. T. C. Allcock, C. J. Ballance, L. Guidoni, H. A. Janacek, N. M. Linke, D. N. Stacey, and D. M. Lucas, 2014, arXiv:1403.1524 .

Hastings, M. B., 2011, Phys. Rev. Lett. **107**, 210501.

Hastings, M. B., G. H. Watson, and R. G. Melko, 2014a, Phys. Rev. Lett. **112**, 070501.

Hastings, M. B., D. Wecker, B. Bauer, and M. Troyer, 2014b, arXiv:1403.1439 .

Herold, M., E. T. Campbell, J. Eisert, and M. J. Kastoryano, 2014, arxIV:1406.2338 .

Herrera-Martí, D. A., Y. Li, and L. C. Kwek, 2014, Quant. Inf. Comp. **14**, 1136.

Huang, K., 1987, *Statistical Mechanics* (New York: John Wiley & Sons).

Hutter, A., and D. Loss, 2014, Phys. Rev. A **89**, 042334.

Hutter, A., D. Loss, and J. R. Wootton, 2014a, arXiv:1410.4478 .

Hutter, A., F. L. Pedrocchi, J. R. Wootton, and D. Loss, 2012a, arXiv:1209.5289 .

Hutter, A., J. R. Wootton, and D. Loss, 2014b, Phys. Rev. A **89**, 022326.

Hutter, A., J. R. Wootton, B. Röthlisberger, and D. Loss, 2012b, Phys. Rev. A **86**, 052340.

Iblisdir, S., D. Pérez-García, M. Aguardo, and J. K. Pachos, 2009, Phys. Rev. B **79**, 134303.

Iblisdir, S., D. Pérez-García, M. Aguardo, and J. K. Pachos, 2010, Nucl. Phys. B **829**, 401.

Ising, E., 1925, Z. Phys. **31**, 253.

Kapit, E., J. T. Chalker, and S. H. Simon, 2014, arXiv:1408.0959 .

Kay, A., 2009, Phys. Rev. Lett. **102**, 070503.

Kay, A., 2011, Phys. Rev. Lett. **107**, 270502.

Kay, A., and R. Colbeck, 2008, arXiv:0810.3557v1 .

Kempe, J., D. Bacon, D. A. Lidar, and K. B. Whaley, 2001, Phys. Rev. A **63**, 042307.

Kim, I. H., 2012, arXiv:1202.0052 .

Kitaev, A., 2006, Ann. Phys. **321**, 2.

Kitaev, A., and L. Kong, 2012, Commun. Math. Phys. **313**, 351.

Kitaev, A., and J. Preskill, 2006, Phys. Rev. Lett. **96**, 110404.

Kitaev, A. Y., 1997, Russian Math. Surveys **52**, 1191.

Kitaev, A. Y., 2003, Ann. Phys. **303**, 2.

Knill, E., R. Laflamme, and L. Viola, 2000, Phys. Rev. Lett. **84**, 2525.

Knill, E., R. Laflamme, and W. Zurek, 1996, arXiv:quant-ph/9610011 .

Knill, E., R. Laflamme, and W. H. Zurek, 1998, Proc. R. Soc. Lond. A **454**, 365.

Kogut, J. B., 1979, Rev. Mod. Phys. **51**, 659.

Kribs, D., R. Laflamme, and D. Poulin, 2005, Phys. Rev. Lett. **94**, 180501.

Kribs, D. W., R. Laflamme, D. Poulin, and M. Lesosky, 2006, Quant. Inf. Comp. **6**, 382.

Kubica, A., and M. E. Beverland, 2014, arXiv:1410.0069 .

Kugel, K. I., and D. I. Khomskii, 1973, Sov. Phys. JETP **37**, 725.

Laidler, K. J., 1972, J. Chem. Ed. **49**, 343.

Landon-Cardinal, O., and D. Poulin, 2013, Phys. Rev. Lett. **110**, 090502.

Lebowitz, J. L., and A. E. Mazel, 1998, J. Stat. Phys. **90**, 1051.

Leggett, A. J., S. Chakravarty, A. T. Dorsey, M. P. A. Fisher, A. Garg, and W. Zwerger, 1987, Rev. Mod. Phys. **59**, 1.

Leinaas, J. M., and J. Myrheim, 1977, Il Nuovo Cimento **37 B**, 1.

Levin, M., and X.-G. Wen, 2006, Phys. Rev. Lett. **96**(110405).

Lidar, D. A., and T. A. Brun (eds.), 2013, *Quantum Error Correction* (Cambridge University Press).

Lidar, D. A., I. L. Chuang, and K. B. Whaley, 1998, Phys. Rev. Lett. **81**, 2594.

Mazáč, D., and A. Hamma, 2012, Ann. Phys. **327**, 2096.

Michnicki, K. P., 2012, arXiv:1208.3496 .

Michnicki, K. P., 2014, Phys. Rev. Lett. **113**, 130501.

Nakahara, M., 2003, *Geometry, Topology and Physics* (Institute of Physics).

Nayak, C., S. H. Simon, A. Stern, M. Freedman, and S. D. Sarma, 2008, Rev. Mod. Phys. **80**, 1083.

Nigg, D., M. M. E. A. Martinez, P. Schindler, M. Hennrich, T. Monz, M. A. Martin-Delagado, and R. Blatt, 2014, arXiv:1403.5426 .

Nussinov, Z., 2013, arXiv:1303.5922 .

Nussinov, Z., and G. Ortiz, 2008, Phys. Rev. B **77**, 064302.

Nussinov, Z., and G. Ortiz, 2009a, Proc. Natl. Acad. Sci. USA **106**, 16944.

Nussinov, Z., and G. Ortiz, 2009b, Ann. Phys. **324**, 977.

Nussinov, Z., G. Ortiz, and E. Cobanera, 2012, Ann. Phys. **327**, 2491.

Onsager, L., 1944, Phys. Rev. **65**, 117.

Pachos, J. K., 2012, *Introduction to Topological Quantum Computation* (Cambridge University Press).

Pachos, J. K., and A. Beige, 2004, Phys. Rev. A **69**, 033817.

Paetznick, A., and B. W. Reichardt, 2013, Phys. Rev. Lett. **111**, 090505.

Palma, G. M., K.-A. Suominen, and A. K. Ekert, 1996, Proc. R. Soc. Lond. A **452**, 567.

Pastawski, F., A. Kay, N. Schuch, and I. Cirac, 2010, Quant. Inf. Comp. **10**, 0580.

Pastawski, F., and B. Yoshida, 2014, arXiv:1408.1720 .

Pedrocchi, F. L., S. Chesi, and D. Loss, 2011, Phys. Rev. B **83**, 115415.

Pedrocchi, F. L., A. Hutter, J. R. Wootton, and D. Loss, 2013, Phys. Rev. A **88**, 062313.

Peierls, R., 1936, Proc. Cam. Phil. Soc. **32**, 477.

Poulin, D., 2005, Phys. Rev. Lett. **95**, 230504.

Poulin, D., M. B. Hastings, D. Wecker, N. Wiebe, A. C. Doherty, and M. Troyer, 2014, arXiv:1406.4920 .

Preskill, J., 1998, Proc. R. Soc. Lond. A **454**, 385.

Preskill, J., 2004, Lecture notes on quantum computation.

Raussendorf, R., J. Harrington, and K. Goyal, 2006, Ann. Phys. **321**, 2242.

Reed, M. D., L. DiCarlo, S. E. Nigg, L. Sun, L. Frunzio, S. M. Girvin, and R. J. Schoelkopf, 2012, Nature **482**, 382.

Richards, L. H., S. W. Sides, M. A. Novotny, and P. A. Rikvold, 1995, J. Magn. Magn. Mater. **150**, 37.

Robert, C. P., and G. Casella, 2004, *Monte Carlo Statistical Methods* (Springer).

Röthlisberger, B., J. R. Wootton, R. M. Heath, J. K. Pachos, and D. Loss, 2012, Phys. Rev. A **85**, 022313.

Saeedi, K., S. Simmons, J. Z. Salvail, P. Dluhy, H. Riemann, N. V. Abrosimov, P. Becker, H.-J. Pohl, J. J. L. Morton, and M. L. W. Thewalt, 2013, Science **342**, 830.

Sarvepalli, P., and K. R. Brown, 2012, Phys. Rev. A **86**, 042336.

Schoelkopf, R. J., and S. M. Girvin, 2008, Nature **451**, 664.

Shinoda, M., 2002, J. Appl. Prob. **39**, 1.

Shor, P. W., 1994, SIAM J. Sci. Comp. **26**, 1484.

Shor, P. W., 1996, in *the Proceedings of the 37th Annual Symposium on Foundations of Computer Science*.

Stark, C., lode Pollet, A. Imamoğlu, and R. Renner, 2011, Phys. Rev. Lett. **107**, 030504.

Steane, A. M., 1996, Phys. Rev. Lett. **77**, 793.

Suchara, M., S. Bravyi, and B. Terhal, 2011, J. Phys. A: Math. Theor. **44**, 155301.

Terhal, B. M., 2013, arXiv:1302.3428 .

Terhal, B. M., and G. Burkard, 2005, Phys. Rev. A **71**, 012336.

Trebst, S., P. Werner, M. Troyer, K. Shtengel, and C. Nayak, 2007, Phys. Rev. Lett. **98**, 070602.

Tsomokos, D. I., T. J. Osborne, and C. Castelnovo, 2011, Phys. Rev. B **83**, 075124.

Tupitsyn, I. S., A. Kitaev, N. V. Prokof'ev, and P. C. E. Stamp, 2010, Phys. Rev. B **82**, 085114.

Vezzani, A., 2003, J. Phys. A: Math. Gen. **26**, 1593.

Vidal, J., S. Dusuel, and K. P. Schmidt, 2009, Phys. Rev. B **79**, 033109.

Viyuela, O., A. Rivas, and M. A. Martin-Delagado, 2012, New J. Phys. **14**, 033044.

Walker, K., and Z. Wang, 2012, Front. Phys. **7**, 150.

Wang, C., J. Harrington, and J. Preskill, 2003, Ann. Phys. **303**, 31.

Wecker, D., B. Bauer, B. K. Clark, M. B. Hastings, and M. Troyer, 2014, Phys. Rev. A **90**, 022305.

Wegner, F. J., 1971, J. Math. Phys. **12**, 2259.

Weiss, U., 2012, *Quantum Dissipative Systems*, volume 2 (World Scientific Publishing Co. Pte. Ltd.).

Wen, X.-G., 2003, Phys. Rev. Lett. **90**, 016803.

Wen, X.-G., 2004, *Quantum Field Theory of Many-Body Systems* (Oxford Graduate Texts).

Wilczek, F., 1982, Phys. Rev. Lett. **49**, 957.

Witten, E., 1988, Commun. Math. Phys. **117**, 353.

Wootton, J. R., 2012, Journal of Modern Optics **59**(20), 1717.

Wootton, J. R., 2013, Phys. Rev. A **88**, 062312.

Wootton, J. R., J. Burri, S. Iblisdir, and D. Loss, 2014, Phys. Rev. X **4**, 011051.

Wootton, J. R., V. Lahtinen, and J. K. Pachos, 2009, LNCS **5906**, 56.

Wootton, J. R., and D. Loss, 2012, Phys. Rev. Lett. **109**, 160503.

Wootton, J. R., and J. K. Pachos, 2011a, Phys. Rev. Lett. **107**, 030503.

Wootton, J. R., and J. K. Pachos, 2011b, ENTCS **270**, 209.

Yeomans, J. M., 1992, *Statistical Mechanics of Phase Transitions* (Oxford University Press).

Yoshida, B., 2011, Ann. Phys. **326**, 2566.

Yoshida, B., 2013, Phys. Rev. B **88**, 125122.

Yoshida, B., 2014, arXiv:1404.0457 .

Yoshida, B., and I. L. Chuang, 2010, Phys. Rev. A **81**, 052302.

Zanardi, P., 2000, Phys. Rev. A **63**, 012301.

Zanardi, P., and M. Rasetti, 1997, Phys. Rev. Lett. **79**, 3306.

Zeng, B., A. Cross, and I. L. Chuang, 2011, IEEE Trans. Inf. Theo. **57**, 6272.

Zilberberg, O., B. Braunecker, and D. Loss, 2008, Phys. Rev. A **77**, 012327.